DESIGN OF EJECTOR FOR A SOLAR THERMAL AIR-CONDITIONING WITH STORAGE SYSTEM

CHAKRI SRIPANOM

A Thesis Submitted to the Graduate School of Naresuan University

In Partial Fulfillment of the Requirements

for the Doctor of Philosophy Degree in Renewable Energy

July 2015

Copyright 2015 by Naresuan University

Thesis entitled "Design of ejector for a solar thermal air-conditioning with storage system"

by Mr. Chakri Sripanom

has been approved by the Graduate School as partial fulfillment of the requirements for the Doctor of Philosophy Degree in Renewable Energy of Naresuan University.

Oral Defense Committee

Wirungrong S. ..... Chair

(Wirungrong Sangarunlerd, Ph.D.)

..... Advisor

(Assistant Professor Sarayooth Vaivudh, Ph.D.)

P. Thanarak ..... Internal Examiner

(Assistant Professor Prapita Thanarak, Ph.D.)

Approved

.....

(Panu Putthawong, Ph.D.)

Associate Dean for Administration and Planning

for Dean of the Graduate School

29 JUL 2015

ACKNOWLEDGEMENT

The author is grateful thank to Assist. Prof. Dr.Sarayooth Vaivudh and Dr. Sukruedee Sukchai for invaluable advices and kindly inspiration.

I would like to thank staff of School of Renewable Energy Technology (SERT), Naresuan University for suggestion and a helping hand.

I would like to thank all my friends for their warm support, kind advice and friendship.

I would like to thank Naresuan University Research Funds to support for this research. And promote energy conservation fund for the scholarships.

Finally, special thanks my father, my mother and my family for their support, love and encouragement throughout this study.

Chakri Sripanom

Title	DESIGN OF EJECTOR FOR A SOLAR THERMAL AIR-CONDITIONING WITH STORAGE SYSTEM
Author	Chakri Sripanom
Advisor	Assistant Professor Sarayooth Vaivudh, Ph.D.
Academic Paper	Thesis Ph.D. in Renewable Energy Naresuan University, 2014
Keywords	Ejector/ Solar cooling system/ Storage system

ABSTRACT

This study investigated the effects of operating condition and ejector geometry on the R141b ejector refrigeration for achieve the high system performance. The first step to determine the operating condition and ejector geometry through computer calculation program. That found at the generator temperature is 84 °C evaporator temperature at 8 °C, diameter of nozzle throat is 2 mm. diameter of nozzle exit is 8 mm. diameter of mixing chamber inlet is 25 mm and diameter of constant area section is 8 mm. The entrainment ratio and COP of computer calculation program is 0.289 and 0.230, respectively. The second step ejector is fabricated and equipped to solar ejector refrigeration system, it is found that average COP is 0.231.

The economics analysis of solar ejector cooling system with storage system are investigated. The investment cost of the system and payback period were 158,158 baht and 7.75 years, respectively. The return value on a net present value (NPV) was 60,872.63 baht, internal rate of return (IRR) is 13.57%.

LIST OF CONTENTS

LIST OF CONTENTS (CONT.)

LIST OF TABLES

LIST OF FIGURES

LIST OF FIGURES (CONT.)

LIST OF FIGURES (CONT.)

CHAPTER I

INTRODUCTION

Rationale of the study and statement of the problem

Currently, global warming has been causing an increase in global temperature. As a result, there has been an increase in air conditioning demand as well, which can be observed from the worldwide growth of air conditioning market. The growth rate assessment is at about 17%. In figure 1, the sales rates of room air-conditioners (RAC units) are shown in various regions of the world. The expected increase in 1998 was about 26 million units while it was more than 40 million units in 2006. [1].

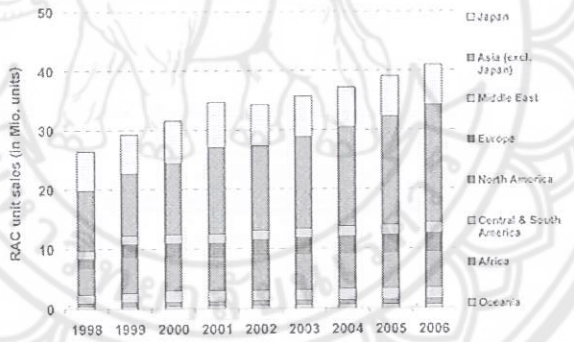

Figure 1 Annual sale of small room air conditioners (RAC units) [1]

Approximately 15% of electronic products worldwide are mostly air conditioning and refrigeration systems [2]. In Thailand, electricity consumption can be categorized into 3 main parts: 40% consumed by industry sector, 35% consumed by business sector, and 25% consumed by residential sector. Over 50% (approximately $50x10^3$ GWh/year) of electricity cost is consumed by air conditioning systems, due to the climate of Thailand that is located along the equator line causing a tropical climate. Nowadays, most of office buildings and houses are primarily designed to be dependent to an air conditioning system. It leads to an increase in the air conditioning demand

every year, at about 400,000 machines per year. Electronic productions from power plant thusly have to support the air conditioning system at about 600 MW each year [3]. According to the steadily increasing cooling system demand, the energy price trend is rising all the time. Therefore, it is necessary to seek for energy from different sources, for instance, solar energy, as a replacement of fossil energy. Solar energy is clean, it has no impact to the environment, and it can produce both electricity and thermal energy. The solar thermal can be used for cooling system and to reduce CO_2 emission that comes from the combustion of fossil fuels used to produce electricity.

The common cooling technologies being used are vapor compressed refrigeration systems that are made to be compatible with solar energy in order to extract electricity from solar cells, which are Desiccant System, Passive Cooling System, Absorption Refrigeration System, and Ejector Refrigeration System. According to literature review conducted by many researchers, an ejector refrigeration system has been studied and developed due to many of its advantages, for example, the simplicity of the installation, design, and operation, the relatively low cost in heat operation system, the possible usage in residential sector, and it can be used as an environment-friendly refrigerator as well. However, the ejector refrigeration system is prone to be lacking in energy storage system. Therefore, the objective of this research is to develop a residential solar ejector refrigeration system with the effective energy storage system for air conditioning. The performance analysis and economic feasibility comparing to other cooling systems are studied as well.

Objectives of the study

1. To design an ejector for a solar thermal air conditioning integrated with energy storage system
2. To evaluate economic analysis of the solar thermal air conditioning with storage system

Scopes of the study

1. Cooling system with energy storage for residential sector.
2. The R141b is used as a refrigerant.

3. Economic comparison between the solar cooling system with conventional systems.

Benefits of the study

1. A prototype of the solar thermal air conditioning integrated with storage system.

2. A feasibility of implementing the system will be distributed.

CHAPTER II

LITERATURE REVIEWS

Principle of Ejector Refrigeration Cycle

Ejector refrigeration was first developed by Le Blance and Charles Parsons around 1901 using water as refrigerant [3]. It experienced a wave of popularity during the early 1930s for air conditioning systems in large buildings [34]. Ejector refrigeration cycle is similar to the conventional vapor compression system except that the compressor is replaced by a liquid circulation pump, generator and ejector [4].

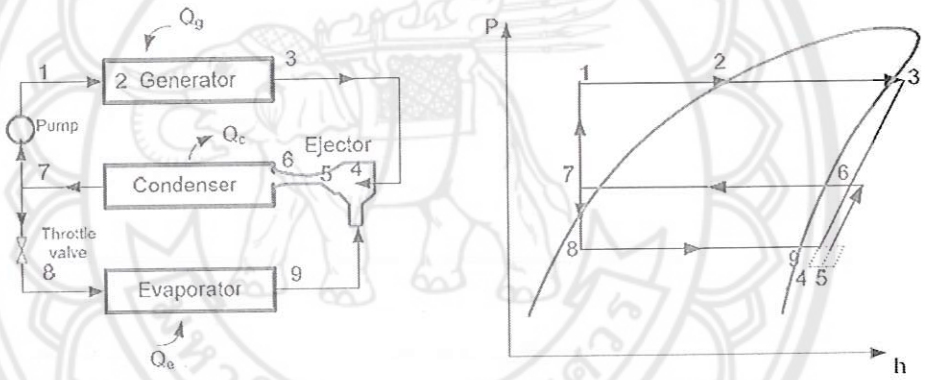

Figure 2 Schematic diagram of an Ejector Refrigeration Cycle [4]

The refrigeration cycle is shown in Figure 2, the primary vapor stream from the generator accelerates through the nozzle of the ejector, resulting in having a low pressure at the nozzle exit. The pressure is accordingly lower than the pressure in the evaporator. So, the vapor is drawn from the evaporator. The two streams are mixed in a mixing zone at the end of the converging section. After getting mixed, a combined stream becomes a transient supersonic stream. Along the constant area and the diffuse sections, a transverse shock is taking place in order to balance the pressure difference. The velocity of the combined stream becomes subsonic and decelerates in the diffuser after the shock. The vapor from the ejector then goes to the condenser, and then one

part of the fluid is pumped to the generator and the rest goes to the evaporator, resulting in reaching an evaporator pressure by the expansion device at last [5].

In Figure 2, the procedures of the ejector refrigeration system are represented in a pressure-enthalpy diagram. The model of the ejector refrigeration system is based on the thermodynamic states in each operating point according to Figure 2 and the following equations. The numbers in the subscription refer to the conditions mentioned in Figure 2 and, Energy balance at the mixing point of the ejector:

$$(\dot{m}_g + \dot{m}_e)h_5 = \dot{m}_e h_9 + \dot{m}_g h_3 \quad (1)$$

For the mass conservation law of impulse at the mixing section of the ejector,

$$\dot{m}_g c_g + \dot{m}_e c_e = (\dot{m}_g + \dot{m}_e)c_m \quad (2)$$

Assuming that the inlet area from the evaporator is large enough, c_e can be set as 0; Equation 2 can be simplified as:

$$\frac{\dot{m}_e}{\dot{m}_g} = \frac{c_g}{c_m} - 1 \quad (3)$$

The mass flow rate ratio between the streams from the evaporator and the generator in Equation 3 is as followed, ω is referred to as entrainment ratio.

$$\omega = \frac{\dot{m}_e}{\dot{m}_g} \quad (4)$$

Another important criterion for the ejector is the compression ratio, which is defined as the pressure ratio between the condenser and the ejector.

$$r_p = \frac{P_c}{P_e} \quad (5)$$

The critical condenser pressure is the name used to call the back pressure or the condenser pressure at the critical condition. The ejector refrigeration system is generally operated at the critical condenser temperature. The compression ratio at the critical condition is called the critical compression ratio, r_p^*

$$r_p^* = \frac{P_c^*}{P_e} \tag{6}$$

The efficiency of the ejector cooling system is widely expressed in terms of both an entrainment ratio and a coefficient of performance (COP_{ejc}). Neglecting the work input to the pump, the thermal COP of the ejector refrigeration system is defined as a ratio between cooling capacity and necessary heat input, as shown in the following equation.

Coefficient of performance:

$$COP_{ejc} = \frac{Q_e}{Q_g} = \frac{\dot{m}_e(h_9 - h_8)}{\dot{m}_g(h_3 - h_1)} \tag{7}$$

The cycle performance computation was carried out based on the energy conservation equations for the generator, evaporator, condenser and pump under the steady state operation conditions. These basic equations are given as followed, respectively:

$$Q_g = \dot{m}_g(h_3 - h_1) \tag{8}$$

$$Q_e = \dot{m}_e(h_9 - h_8) \tag{9}$$

$$Q_c = \dot{m}_c(h_7 - h_6) \tag{10}$$

The coefficient of performance of the cycle is given by:

$$COP = \frac{Q_e}{(Q_g + W)} \tag{11}$$

Principle of ejector

The ejectors are an essential part in refrigeration and air conditioning, desalination, petroleum refining and chemical industries [5]. Moreover, the ejectors form an integral part of distillation columns, condensers and other heat exchange processes. Even though the construction and operation principles of jet ejectors are commonly known, an ejector is a device in which a higher pressure fluid, which is also called primary fluid, is used to induce a lower pressure fluid, which is also called secondary fluid, into the ejector. Fluids from these two streams are mixed together and discharged to a pressure that lies between the pressures of these two fluids. The ejector and a pump are used instead of a compressor (in a vapor-compression system) for producing a cooling power in an ejector refrigeration cycle.

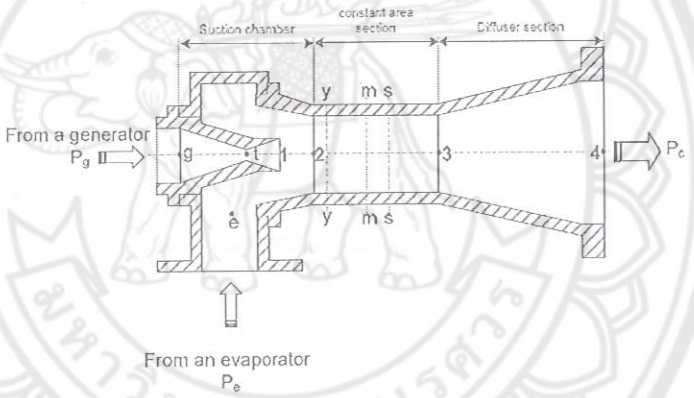

Figure 3 Ejector Geometry and Sections [4]

An ejector is consisted of 3 main parts: a suction chamber, a constant area and mixing chamber, and a diffuser. A schematic of ejector geometry is shown in Figure 3. Vapor is drawn from the evaporator when the primary flow goes through a converging-diverging nozzle in the ejector. The secondary flow is accelerated to a high velocity vapor stream and eventually reaches the subsonic velocity. Mixing starts at the onset of the constant-area section (section y-y, hypothetical throat, in Figure 3). In section y-y, both streams develop uniform pressure; the choking of the secondary flow occurs then. A mixed stream develops into a transient supersonic stream and shocks at section s-s. The velocity of the mixing fluid must be high enough in order to

increase the pressure after the deceleration in the diffuser into an appropriate condensing pressure.

Normally, different ejectors have contrasting characteristics, resulting in various performances. Ejector performance is primarily dependent on design and operating conditions. Double choking should be taken into account for the best performance. The design principle of the steam ejector can be used as a guideline for other working fluids, but it cannot be wholly applied for all cases. There is no unique solution for every single ejector. When operating the ejector in a critical mode, the hypothetical throat analysis can be used as a key to calculate performance and dimensioning the ejector.

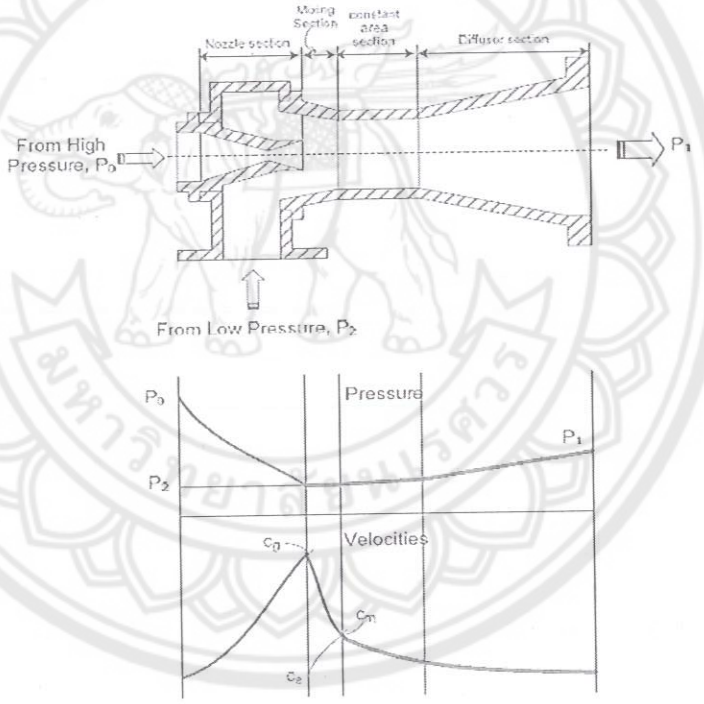

Figure 4 The Geometric, Pressure and Velocity Diagram in an Ejector [4]

The design of the ejector can be commonly categorized into two types, depending on the position of the nozzle, as followed.

1. "Constant-Area Mixing Ejector": the exit of the nozzle is within the constant area of the ejector. Primary and secondary fluids are mixed in this area.

2. "Constant-Pressure Mixing Ejector": the exit of the nozzle is in the suction chamber, which lies ahead of the constant area. At a specific pressure, primary and secondary flows are mixed in the suction chamber. Pressure of the mixing streams remains constant along the chamber from the nozzle exit to the inlet of the constant area section.

The constant-pressure mixing ejector is more promising than the constant-area mixing ejector due to its better generating performance with the design concept that mixing occurs in the constant-area section [6, 25]. Choking phenomena can be observed in 2 places: the primary flow through the nozzle and the secondary flow. The acceleration of the flow from the stagnant state has a significant effect on the chocking in the secondary flow. This happens in the suction chamber at the inlet of the supersonic flow to the constant-area section. As described previously, performance of the ejector is normally measured by a mass flow ratio between the streams from the evaporator and generator, which is called the entrainment ratio (ω).

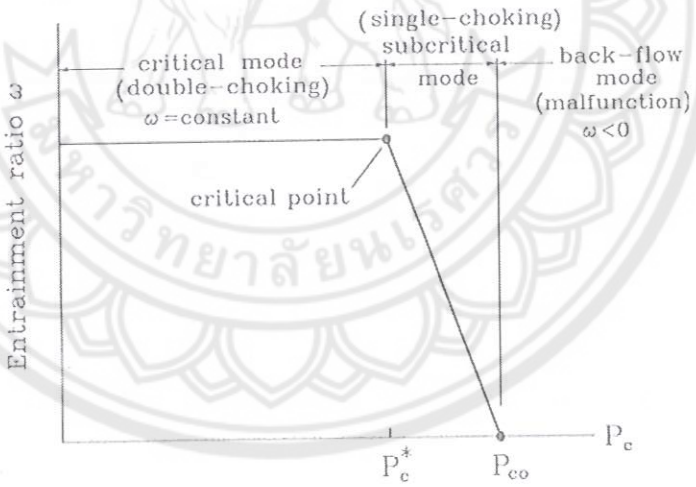

Figure 5 Operational modes of ejector [4]

The entrainment ratio depends on a back pressure (also called condenser pressure, P_c) at a specific primary pressure (P_g) and secondary pressure P_e. According to the back pressure, there are 3 operation modes that best performance can be obtained at the critical mode, where the back pressure is lower than the critical pressure. During this state, the entrainment ratio is constant and choking phenomenon

occurs both in the primary and entrained flow. The entrainment ratio decreases when the back pressure is higher than the critical pressure; and the choking only exists in the primary flow, not in the secondary flow. If the back pressure is higher than P_{co}, as shown in Figure 5, there will be no choking phenomena in either flow. P_{co} is considered as the limiting pressure of ejector operational mode. The operation would subsequently fail thusly.

The following analysis starts with the expansion process of the primary flow through the nozzle, and is followed by the analysis of secondary flow and mixed flow at different cross sections, and the flow through the diffuser at the end. The analysis has an assumption that the process in the ejector is adiabatic. Kinetic energy of the inlet and outlet flows is not considered. Friction and mixing loss is counted as the form of isentropic efficiency. The flow within the ejector is assumed to be steady and the working fluid has constant properties along the ejector.

1. The expansion process of the primary flow through the nozzle

Vapor from the generator expands irreversibly in the primary nozzle, resulting in a partial vacuum at the nozzle exit. The first law of thermodynamics is applied to the energy balance equation as followed:

$$Q = \varepsilon_t + h_B - H_A + \frac{c_B^2 - c_A^2}{2} + g(z_B - z_A) \qquad (12)$$

The velocity of the stream at the nozzle exit (c_g) can be expressed with the assumption of adiabatic condition (q = 0), no work (ε_t = 0), and no influence of elevation change$(z_B = z_A)$, as followed;

$$c_g = \sqrt{2(h_g - h_m)} \qquad (13)$$

$$= \sqrt{2\eta_N(h_g - h_{gm,is})} \qquad (14)$$

Where a nozzle's isentropic efficiency (η_N) can be defined as,

$$\eta_N = \frac{h_g - h_m}{h_g - h_{gm,is}} \tag{15}$$

where

h_m is enthalpy of the mixing fluid at mixing point

h_g is enthalpy of the driving (primary) fluid from the generator

$h_{gm,is}$ is enthalpy of the driving fluid (primary) from the generator expanded isentropically to the mixing pressure.

The mass flow from the generator through the nozzle at choking condition can be expressed as,

$$\dot{m}_g = P_g A_t \sqrt{\frac{\eta_N \gamma}{T_g R}\left(\frac{2}{\gamma+1}\right)^{\gamma+1/\gamma-1}} \tag{16}$$

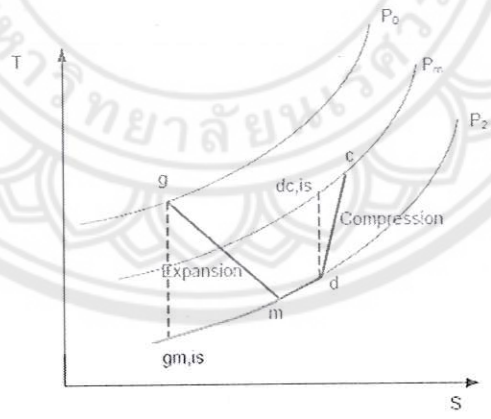

Figure 6 The T-S Diagram for Expansion and Compression Process [4]

The Mach number of the fluid from the generator ($Ma_{g,1}$), which expands through the nozzle can be depicted as,

The Mach number of the fluid from the generator ($Ma_{g,1}$) that expands through the nozzle can be illustrated as,

$$Ma_{g,1} = \sqrt{\frac{2\eta_N}{\gamma - 1}\left[1 - \left(\frac{p_1}{p_g}\right)^{\gamma-1/\gamma}\right]} \tag{17}$$

The relation between the Mach number and the cross sectional area can be illustrated as,

$$\left(\frac{A_{g1}}{A_t}\right)^2 \approx \frac{1}{Ma_{g1}^2}\left[\frac{2}{\gamma+1}\left(1 + \frac{\gamma-1}{2}Ma_{g1}^2\right)\right]^{\gamma+1/\gamma-1} \tag{18}$$

$$\frac{P_g}{P_{g1}} \approx \left(1 + \frac{(\gamma-1)}{2}Ma_{g1}^2\right)^{\gamma/\gamma-1} \tag{19}$$

The Mach number of the primary flow at cross section y-y can be calculated from the following equation

$$\frac{P_{gy}}{P_{g1}} \approx \left[\frac{1 + \left(\frac{\gamma-1}{2}\right)Ma_{g1}^2}{1 + \left(\frac{\gamma-1}{2}\right)Ma_{gy}^2}\right]^{\gamma/\gamma-1} \tag{20}$$

The area of the primary flow core at the y-y section is calculated by using the isentropic relation that includes an arbitrary coefficient, $\emptyset$, which signifies in the loss in the flow from section 1-1 to y-y.

$$\frac{A_{gy}}{A_{g1}} \approx \frac{\emptyset_g/Ma_{gy}}{1/Ma_{g1}}\left(\frac{\frac{2}{\gamma+1}\left(1 + \left(\frac{\gamma-1}{2}\right)Ma_{gy}^2\right)}{\frac{2}{\gamma+1}\left(1 + \left(\frac{\gamma-1}{2}\right)Ma_{g1}^2\right)}\right)^{(\gamma+1)/2(\gamma-1)} \tag{21}$$

The arbitrary coefficient for the primary flow $(\emptyset_g)$ that leaves the nozzle is assumed to be around 0.88, according to [25].

Importantly, the throat area of the primary flow can be calculated by assuming the throated pressure at first and later calculating the mass flux through this throat. Calculations will be continually done until the maximum mass flux through this throat is conveyed. The first assumed throated pressure could be the throated pressure, which generates the unity Mach number.

$$P_t = P_g\left(1+\frac{(\gamma-1)}{2}\right)^{\gamma-1/\gamma} \tag{22}$$

2. The Secondary Flow

The secondary flow rate at choking condition (section y-y) is illustrated as,

$$\dot{m}_e = \frac{P_e A_{ey}}{\sqrt{T_e}}\sqrt{\frac{\gamma}{R}\left(\frac{2}{\gamma-1}\right)^{\gamma+1/\gamma-1}}\sqrt{\eta_{Ne}} \tag{23}$$

Assuming that the entrained flow has obtained the choking conditions, the Mach number of the secondary flow at section y-y is approximately one,

$$Ma_{ey} = \sqrt{\frac{2}{\gamma-1}\left[1-\left(\frac{P_e}{P_{ey}}\right)^{\gamma-1/\gamma}\right]} \tag{24}$$

The area at from the entrance of the secondary flow to the mixing zone can be calculated in a similar way by calculating the throat diameter of the nozzle.

3. Cross-sectional area at section y-y (A_3)

A cross-sectional area at y-y is the summation of the area for primary flow A_{gy} and entrained flow A_{ey},

$$A_3 = A_{ey} + A_{gy} \tag{25}$$

4. Mixing Section

The energy balance at the mixing point can be defined as,

$$(\dot{m}_g + \dot{m}_e) \cdot h_m = \dot{m}_e \cdot h_e + \dot{m}_g \cdot h_{g,exp} \quad (26)$$

where: h_m is enthalpy of the mixing fluid at the mixing point

h_e is enthalpy of the entrained refrigerant (secondary fluid) from the evaporator

$h_{g,exp}$ is enthalpy of the driving fluid from the generator after the expansion through the nozzle.

The temperature and the Mach number of the streams at section y-y can be written as,

$$\frac{T_g}{T_{gy}} = 1 + \frac{\gamma - 1}{2} Ma_{gy}^2 \quad (27)$$

$$\frac{T_e}{T_{ey}} = 1 + \frac{\gamma - 1}{2} Ma_{ey}^2 \quad (28)$$

A vacuum takes place at the exit of the nozzle, thus the stream from the evaporator is absorbed in to the ejector. The entrained stream then mixes perfectly with the higher-pressure stream from the generator. To make it simpler, it can be assumed that the mixing pressure is constant. Pressure remains unchanged while the mixing of the two streams occurs.

The mass conservation law of impulse can be written as:

$$\emptyset_m(\dot{m}_g \cdot c_{g,exp} + \dot{m}_e \cdot c_e) = (\dot{m}_g + \dot{m}_e) \cdot c_m \quad (29)$$

where: $\dot{m}_g$ is mass flow of driving (primary) fluid from generator

$\dot{m}_e$ is mass flow of the entrained (secondary) refrigerant from the evaporator

$c_{g,exp}$ is velocity of driving (primary) fluid from the generator after expansion in the nozzle entering the mixing section

c_e is velocity of entrained (secondary) refrigerant from the evaporator

c_m is velocity of mixing fluid leaving the mixing section

An arbitrary coefficient accounting for friction loss $\emptyset_m$, varies with the ejector area ratio (A_3/A_t). [25], it is reported that

$$\emptyset_m = 0.80 \; for \; \frac{A_3}{A_t} > 8.3 \tag{30}$$

$$\emptyset_m = 0.82 \; for \; 6.9 \leq \frac{A_3}{A_t} \leq 8.3 \tag{31}$$

$$\emptyset_m = 0.84 \; for \; \frac{A_3}{A_t} < 6.9 \tag{32}$$

It can also be expressed as in the following equation:

$$\emptyset_m = 1.037 - 0.02857 \cdot \frac{A_3}{A_t} \tag{33}$$

The length of the mixing section is generally defined in terms of the throat diameters. There are various recommendations for the lengths of the steam jet ejectors, depending on the research groups. However, all of them are in the range of 6-10 times of the throated diameter [7].

$$L_{mix} = 6 \cdot D_3 \tag{34}$$

Another important issue is the angle of the mixing section. Ejector efficiency will be reduced if the angle is too large. On the contrary, if the angle is too small, the ejector will be unable to compress the vapor flow to design the condensing

pressure. Angles of the mixing section cone are about 7-10 degrees for the first portion and 3 to 4 degrees for the second portion.

The velocities of the primary and secondary flows at section y-y can be expressed as:

$$c_{gy} = Ma_{gy} \cdot \sqrt{\gamma \cdot R} \cdot T_{gy} \quad (35)$$

$$c_{ey} = Ma_{ey} \cdot \sqrt{\gamma \cdot R} \cdot T_{ey} \quad (36)$$

5. Constant Area Section

In the constant area section, supersonic shock occurs around section s-s, as shown in Figure 3. Complex oblique shock patterns are included in the shock that happens here; this is due to a thick boundary layer and a very peak velocity profile.

To make the ejector effective, it is recommended that the length of the constant-area throat section should be three to five throat diameters long. In this case, this length is suggested to be five throat diameters long.

Assuming that the mixed flow after the shock undergoes an isentropic process, the pressure of the mixed flow from m-m to 3-3 is constant at P_3.

$$P_3 = P_m \left[1 + \frac{2\gamma}{\gamma+1}(Ma_m^2 - 1)\right] \quad (37)$$

$$Ma_3^2 = \frac{1 + \frac{\gamma-1}{2} Ma_m^2}{\gamma Ma_3^2 - \frac{\gamma-1}{2}} \quad (38)$$

The Mach number of the stream after the shock flow is,

$$Ma_3 = \sqrt{\frac{Ma_2^2 + \frac{2}{\gamma-1}}{\left(\frac{2\gamma}{\gamma-1}\right) Ma_2^2 - 1}} \quad (39)$$

It is mentioned that the constant-area section diameter is a critical design parameter. There are several methods to calculate this dimension in the literature; however, none is accurate. The only way to determine this is by experiment or, if possible, an analysis of manufacturer data.

6. Diffuser

After going through the mix, the mixing stream will form a single supersonic stream and then move forward through a constant-area section with transverse shock to the diffuser. In the diffuser section, the stream will be compressed into condensing pressure and the velocity of the stream will decrease.

The subsonic diffuser is in a conical shape. For the steam ejector, the angle varies between 5 to 12 degrees with an axial length of 4 to 12 throat diameters. It is recommended that the axial length should be 6 times the throat diameter.

From the energy conservation equation, the velocity of the mixing stream can be written as followed,

$$c_m = \sqrt{2 \cdot (h_c - h_d)} = \sqrt{2 \cdot (1/\eta_D) \cdot (h_{da,is} - h_d)} \qquad (40)$$

The nomenclature 'c, d and dc, is' here refers to the point in Figure 7.

A diffuser isentropic efficiency η_D is defined as,

$$\eta_D = \frac{h_{dc,is} - h_d}{h_c - h_d} \qquad (41)$$

The stream is compressed to a higher pressure, based on an assumption of a reversible adiabatic process in the subsonic flow. The velocity at the exit is believed to be zero, the pressure lifted in the diffuser can thus be estimated as followed:

$$\frac{P_4}{P_3} = \left(\frac{\eta_D(\gamma - 1)}{2} Ma_3^2 + 1\right)^{\gamma/\gamma - 1} \qquad (42)$$

7. Performance

The performance of an ejector can be generally defined in terms of the mass flow rate ratio between the streams from the evaporator and generator. It can be called as the entrainment ratio (ω). The following equations of the entrainment ratio are repeated below for the convenience in referring.

$$\omega = \frac{\dot{m}_e}{\dot{m}_g} \tag{43}$$

From the mass conservation law of impulse Equation (20) and the velocity equations;

$$\omega = \frac{c_g}{c_m} - 1 \tag{44}$$

$$\omega = \sqrt{\frac{h_g - h_m}{h_c - h_d}} - 1 \tag{45}$$

$$\omega = \sqrt{(\eta_N \cdot \eta_D)\frac{h_g - h_{gm,is}}{h_{dc,is} - h_d}} - 1 \tag{46}$$

In addition, the entrainment ratio can be described by the ratio of the Mach number between the streams of the evaporator and generator [8] as followed.

$$\omega = \frac{Ma_e}{Ma_g} \tag{47}$$

One of the important parameters is the nozzle position. The distance between the nozzle exit and constant area (section x-x) is suggested by [25] to be about 1.5 times of the constant-area chamber diameter.

Energy Storage System

[9] Energy storage (ES) is storing some forms of energy that can be drawn upon to perform some useful operations at a later time are stored. A device that stores energy is sometimes called an accumulator. All forms of energy are potential energy (e.g. chemical or gravitational), kinetic energy, electrical energy or thermal energy. All these forms of energy could be stored using an appropriate method, system or technology. Figure 7 shows a large variety of energy storage systems that are under development.

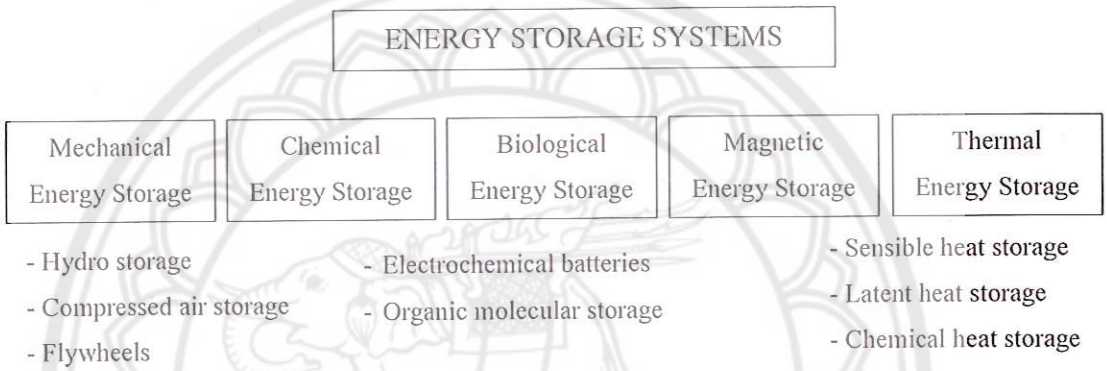

Figure 7 Classification of the energy storage systems [9]

ES is critically important to the success of any intermittent energy source in any meeting demand. ES systems can be significantly contributed to meet a society's needs for a more efficient, environmentally benign energy use in the building of heating and cooling system, aerospace power, and utility applications. The use of ES systems often results in such significant benefits, such as the reduction in energy costs; the reduction in energy consumption; the improvement of the indoor air quality; an increase in the flexibility of the operation and the reduction initial and maintenance costs.

ES can also improve energy system performances by smoothing the supply and increasing the reliability. For example, storage would improve the performance of a power generating plant by load leveling. The higher efficiency would lead to the energy conservation and would improve cost effectiveness. Some of the renewable energy sources can only provide energy intermittently.

Thermal Energy Storage

Thermal energy storage (TES) systems have a potential in increasing the efficiency of the use of thermal energy equipment and of facilitating a large-scale switching. They are normally useful for correcting the mismatch between the supply and the demand of energy. [10] The TES is not a relatively new concept, in fact, it has been used for centuries. Energy storage can reduce time or rate mismatch between energy supply and energy demand, and it significantly plays a role in energy conservation. Large TES systems have been employed in a more recent history for numerous applications, ranging from solar hot water storage to the founding of air conditioning systems.

The length of time during which energy can be kept stored with acceptable losses is one of the important characteristics of a storage system. If solar energy is converted into a fuel, such as hydrogen, there will be no such a time limit. The storage in form of thermal energy may last for a very short time because of the loss by radiation, convection and conduction. Another important characteristic of a storage system is its volumetric energy capacity, or the amount of energy stored per unit volume. The smaller the volume, the better the storage system is. Therefore, a good system should have a long storage time and a small volume per unit of stored energy. If a mass specific heat capacity is not small, denser materials that have smaller volumes would correspondingly advantage the larger energy capacity per unit volume. The space available is limited both in transportation and in habitat applications. The volume occupied by the present available storage systems is considerable and may be an important factor in limiting the size of provided storage. The amount of energy storage provided is dictated by the cost. The cost of floor space or volumetric space should be one of the parameters in optimizing the size of storage.

TES have three basic methods for storing thermal energy as followed. [11]

1. Sensible heat storage is when a liquid or a solid is heated without changing a phase. The amount of energy stored is dependent on the temperature change of the material.

2. Latent heat storage is when a material is heated while undergoing a phase change (usually melting). The amount of energy stored in this case depends on the mass and latent heat of fusion of the material. The storage operates isothermally at the

melting point of the material. If isothermal operation at the phase change temperature is difficult, the system would be operated over a range of temperatures, including the melting point. The sensible heat contributions and the amount of energy stored have to be considered as well.

3. Chemical energy storage is when the heat is used in order to induce a certain chemical reaction and then to store the products. The heat is released when the reverse reaction occurs. In this case, the storage essentially operates isothermally during the chemical reactions as well. However, the temperature at which heat flows from the heat supply is usually different.

The selection of a TES system method depends on the storage period required, for example, diurnal or seasonal, economic viability, operating conditions, and so on. Many research and development activities on energy have concentrated on the efficient energy use and the energy conservation, and TES appears to be one of the more attractive thermal technologies that has been developed.

1. Sensible heat storage system

Energy is stored or extracted by heating or cooling a liquid or solid that does not change its phase during the process. [11] One of the most attractive features of the sensible heat storage systems is that the charging and discharging operations can be expected to be completely reversible for an unlimited number of cycles. Effectiveness of the sensible heat storage system is dependent on the specific heat and if volume is taken into account, on the density of the storage media. [12]

The sensible heat Q_s gained or lost by a material in changing in temperature from T_1, to T_2, is

$$Q_s = M \int_{T_1}^{T_2} C_p dt = V \int_{T_1}^{T_2} C_p dt \qquad (48)$$

Where: M is the mass, kg

C_p is the specific heat, J/kgK

ρ is density of material, kg/m^3 (if the volume V is constant)

V is the volume of material, m^3

T_1 and T_2 are the operating temperature limits, K.

It is observed from this equation that the higher the specific heat and density of material is, the greater the quantity of energy that will be stored in a given volume of the material. However, there are several other parameters that have an effect on the performance of system, for instance, the temperature of operation, thermal conductivity, thermal diffusivity, vapor pressure, compatibility between the storage material and the container, stability of material at the highest temperature of cyclic operation, and of course, the cost of the system.

For certain types of applications, it is important that the thermal energy is supplied at a temperature that is equivalent to or above a certain threshold temperature (lowest operating temperature). Sensible heat storage has some inherent drawbacks for such applications because the temperature of the storage material has to rise above this threshold temperature when thermal energy is stored. The temperature of the storage declines during the discharge period until it reaches an equivalent temperature to the threshold temperature, assuming there is no temperature drops across the heat exchanger at the load end. During the charging, the temperature of the sensible heat storage material continually increases. The charging reaches termination at a certain storage temperature, T_{max}. The energy source has to supply thermal energy at temperature varying from $T_{threshold}$ to T_{max}

Certain applications require energy at steadily increasing temperatures, not at constant temperature. When the load consists of a fluid or solid that is to be sensibly heated, the heat transfer to the fluid has to be at monotonically increasing temperatures. Examples of such loads are solar air heating system for drying or space healing, and solar thermal power Plant.

The following are the conclusions about the drawbacks of sensible heat storage for such applications: [13]

1.1 Mean temperature of storage is higher than the threshold temperature. Higher temperatures of storage result in higher heat losses from the storage.

1.2 Temperature of the storage material continually rises during heat deposition, which results in steadily decreasing heat flux deliveries

1.3 Heat storage occurs at temperatures that are higher than ambient. Hence, the insulation is required to prevent heat loss and is added to the system cost.

One of the most attractive features of sensible heat storage system is that the charging and the discharging operations can be expected to be completely reversible for an unlimited number of cycles, i.e., over the life span of the storage.

The quantities of material that is required for the storage tank and the heat losses are approximately proportional to the surface area of the tank. The storage capacity is proportional to the volume of the tank. Larger tanks have a smaller surface area to volume ratio and therefore are less expensive and have less energy stored per unit.

The efficiency of thermal storage can be defined as the ratio of heat output to heat input, heat output being lower than the input by the amount of heat losses. This definition of efficiency only considers the energy balance from the point of view of the first law of thermodynamics. However, in the case of sensible heat storage, the temperature of stored medium drops due to heat losses and therefore energy is available at a lower temperature. Lower temperature of the fluid leads to lower rates of energy transfer to the load, or to requirement of larger heat exchangers. In case the stored thermal energy has to be converted into mechanical energy or other high quality forms of energy, not only the quantity but also the quality of energy charge and discharge must be taken into consideration. Thus the definition of efficiency taking into account, the second law of thermodynamics would be the ratio of availability of the energy discharged to the availability of the energy charged.

2. Well-nixed liquid storage and sensible heat storage media

The most widely used method of sensible heat storage is a well-mixed liquid storage. The transient energy balance equation for a hot liquid storage tank can be considerably simplified if the temperature in the storage tank is assumed to be uniform, which is called well-mixed storage.

Sensible heat storage media may be classified according to the basis of the heat storage media as liquid, solid and dual media. An example of liquid media storage is water, being inexpensive and widely available. For the storage of hot water; steel, concrete, fiberglass, fiberglass reinforced plastic, or vinyl lined wooden tanks may be employed. If the tank is cylindrical, vertical mounting is generally preferred when comparing to the horizontal due to the requirement of the latter that is has to be

resistant beam bending or buckling. Fiberglass or fiberglass reinforced plastic tanks have the major advantage that they are corrosion resistance.

Since sensible heat storage media may be classified on the basis of the heat storage media as liquid, solid, and dual media, the thermophysical properties of selected liquid for sensible heat storage, liquids, which are plentiful and economically competitive, are shown in Table 1

Table 1 Liquid media for sensible heat storage [11]

Medium	Type	Temperature range (°C)	Density (kg/m^3)	Heat Capacity (J/kg K)	Heat Conductivity (W/m^2k)
Water	-	0 to 100	1000	4190	0.63 at 38 °C
Caloria HT 43	oil	-10 to 315	-	2300	-
Dowtherm A	oil	12 to 260	867	2200	0.112 at 260 °C
Therminol55	oil	-18 to 315	-	2400	
Therminol66	oil	-9 to 343	750	2100	0.106 at 343 °C
Hitec	Molten salt	141 to 540	1680	1560	0.61
Draw Salt	Molten salt	220 to 540	1733	1550	0.57
Ethanol	Organic liquid	Up to 78	790	2400	-

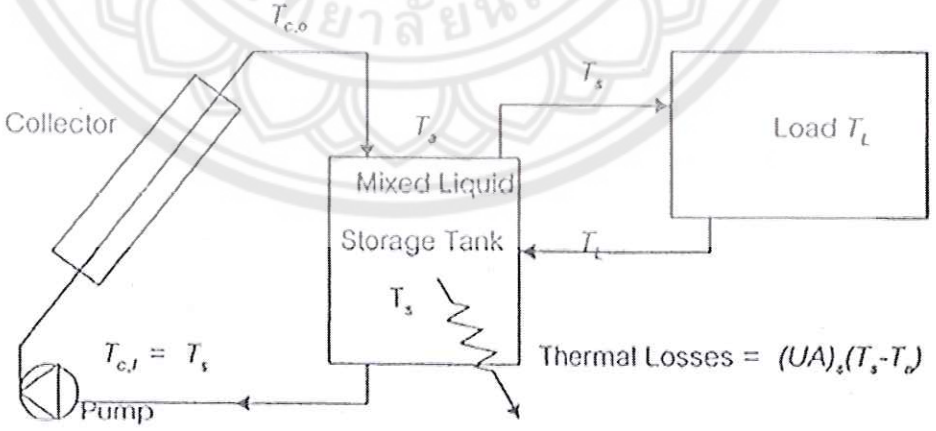

Figure 8 Essentials of mixed liquid storage systems. [13]

Assuming that the storage tank has a uniform temperature T_s, energy balance on a storage tank can then be expressed as:

$$(MC_p)_s \frac{dT_s}{dt} = Q_c - Q_L - (UA)_s(T_s - T_a) \quad (49)$$

Where: M is the mass of media in storage tank, kg

Q_c is the rate of heat addition by the collector, J/s

Q_L is the rate of heat removal by the load, J/s

U is the overall heat transfer collection between media in the tank, Wm^2K

T_a is the ambient at temperature, K and

A is the surface area of the storage tank, m^2.

For a reasonable time period Δt, the rates of heat additional and removal are assumed to be constant, and then Equation (50) can be written for each time interval as

$$T_{s,new} = T_{s,old} + \frac{\Delta t}{(MC_p)_s}\left[Q_c - Q_L - (UA)_s(T_{s,old} - T_a)\right] \quad (50)$$

Equation 50 can be used to estimate the hourly storage water temperature, provided that hourly heat addition and heat withdrawal are known. In the case of solar thermal energy, it is used for charging the storage. This method gives successful results when one hour intervals are taken.

Thermal storage tank without heat exchanger

This type, the liquid flows directly in and out of storage, the solar collector inlet temperature, T_{ci} is as same as temperature in the storage T_s, and the energy rate is given as

$$Q_c = A_c F_R[(\tau\alpha)G_T(t)_e - (UA)_s(T_s - T_a)] \quad (51)$$

Where F_R is heat removal factor,

A_c is area of collector, m^2

$\tau\alpha$ is transmissivity and absorptivity respectively

It is assumed that there is no drop in temperature of the fluid between the collector and the tank.

The rate of heat addition Q_c by the collector can be written as

$$Q_c = (\dot{m}C_p)_c(T_{c,o} - T_s) \quad (52)$$

Where $\dot{m}$ is the flow rate in kg/s, and C_p is the specific heat of HTF flowing through the collector. In writing the equation 52, it is assumed that there is no temperature drop of the fluid between the collector and the tank.

Similarly, the rate of heat removal by the load $\dot{Q}_L$ can be written as:

$$Q_L = (\dot{m}C_p)_L(T_s - T_L) \quad (53)$$

Where $\dot{m}_L$ is the flow rate of load stream and it is again assumed that there is no temperature drop between the tank and the load.

Cold Thermal Energy Storage [14]

Cold thermal energy storage (CTES) is the storage of cool energy produced during sunshine hours in a cool thermal storage tank, either in a sensible heat form or in a latent heat form is yet another option for storing the energy. CTES has recently increasingly attracted interest in industrial refrigeration applications, such as process cooling, food preservation and building air conditioning systems. CTES appears to be one of the most appropriate methods to correct the mismatch that occurs between the supply and the demand of energy. Cool energy storage requires a better insulation tank, as the energy available in the cool state is expensive, comparing to the heat available in a hot storage tank.

Sensible heat chilled water storage systems have pointed out that the percent cold recoverable in a discharge cycle increases with an increase in the initial temperature difference, aspect ratio and flow rate. It is indicated that partial discharging in one discharge cycle involves in a relatively longer residence time of cool water in storage, leading to a significant decrease in thermal efficiency, as the temperature of the chilled water in the tank increases because of the heat conduction through the walls. Hence, for any practical requirements, the storage system should be designed with several tanks so that it is based on the cooling requirement, and the required number of tanks can be charged and discharged.

[15] Cool storage technology is an effective means of shifting peak electrical loads. It is considered as a part of the strategy for energy management in buildings. There are three principal types of cool storage system that are being developed, chilled water storage, ice storage and eutectic salt.

Chilled water storage system requires the largest storage tanks. However, it is compatible with existing chiller systems. A tank is charged with water at 4–6 °C during the charging mode. During the discharging mode, chilled water is supplied from the bottom of the tank and is then returned to the top of the tank. The sensible heat capacity of water to store cooling capacity is used by chilled-water CTES systems.

The net rate of energy transfer to or from the storage tank due to water flow through the inlet and outlet is considered to be instantaneous capacity. For charging and discharging, instantaneous capacity may be described as,

$$Q = \dot{m} c_p (T_h - T_l) \tag{54}$$

Where $\dot{m}$, T_h and T_l all could be the function of time. During charging period, T_h depends on the temperature distribution in the tank at the start of charging and T_l is determined by the chiller outlet temperature. During discharging, T_h depends on the temperature distribution in the tank at the start of discharging and T_h is determined by the cooling coils outlet water temperature. Integrated capacity is the total energy flow to or from the storage due to water flow through the tank during some period of time. It can be mathematically expressed as

$$Q = \int_0^{t_f} q dt \tag{55}$$

Substituting Equation 55 and noting that mass flow rate can be determined at either the inlet or outlet port by $\dot{m} = \rho AV$ gives:

$$Q = \int_0^{t_f} \rho c_p (T_h - T_l) AV dt \tag{56}$$

where AV is the volume flow rate through the storage. Now, the incremental volume flow, dv, in any time increment dt can be written as:

$$dv = AV dt \tag{57}$$

Hence equation 57 can be rewritten as:

$$Q = \int_0^{v_f} \rho c_p (T_h - T_t) dv \tag{58}$$

where v_f is the total flow volume during the period of interest.

Storage efficiency is defined as the ratio of the cooling effect that is removed from the storage during a single and complete discharge cycle to the cooling effect deposited during the immediately preceding complete charge cycle [16]. It can be expressed as:

$$\eta_{st} = \frac{Q_d}{Q_c} \tag{59}$$

Solar Collector

Solar energy collectors are the special kind of heat exchangers that transform solar radiation energy to internal energy of the transport medium. [17] The solar collector is the major component of any solar system. Using this device, the incoming solar radiation is absorbed, converted into heat, and transferred into a fluid (usually air, water, or oil) flowing through the collector. The solar energy that is being collected is then carried from the circulating fluid either directly to the hot water or space conditioning equipment or to a thermal energy storage tank, from which it can be drawn to be used at nights or on cloudy days. Basically, there are two types of solar collectors. [18]

1. Non-concentrating or stationary collector: The area for the interception and absorption of the solar radiation are shared on the same space, whereas a sun-tracking concentrating solar collector usually has concave reflecting surfaces to intercept and focus the sun's beam radiation to a smaller receiving area, thereby it causes an increase the radiation flux, such as Flat plate collector, Stationary compound parabolic collectors, and Evacuated tube collector.

2. Concentrating collector: it is suitable for high-temperature applications. Solar collectors can also be distinguished by the type of heat transfer liquid used (water, non-freezing liquid, air, or heat transfer oil) and that whether they are covered or uncovered, such as parabolic trough, power tower, central receiver concentrator.

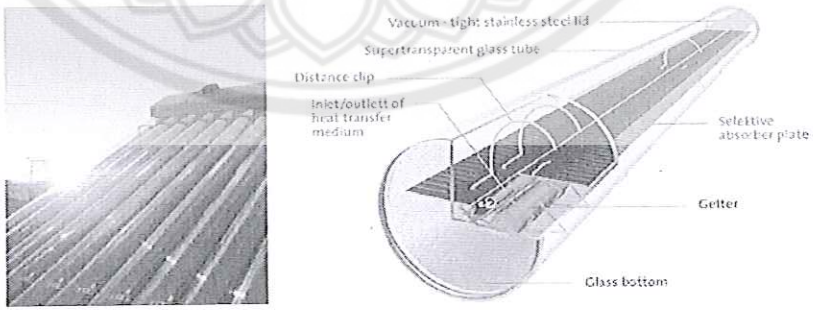

Figure 9 Evacuated tube collector

Evacuated Tube Collectors

The conventional simple flat plate solar collectors were developed to be used in sunny, warm climates. Those advantages, however, are greatly reduced when conditions become unfavorable during the cold, cloudy, and windy days. Furthermore, weathering influences such as condensation and moisture, have caused early deterioration of internal materials, resulting in a reduced performance and system failure. Evacuated heat pipe solar collectors (tubes) differently operate from the other collectors available on the market. These solar collectors consist of a heat pipe inside a vacuum-sealed tube, in an actual installation; many tubes are connected to the same manifold. [17]

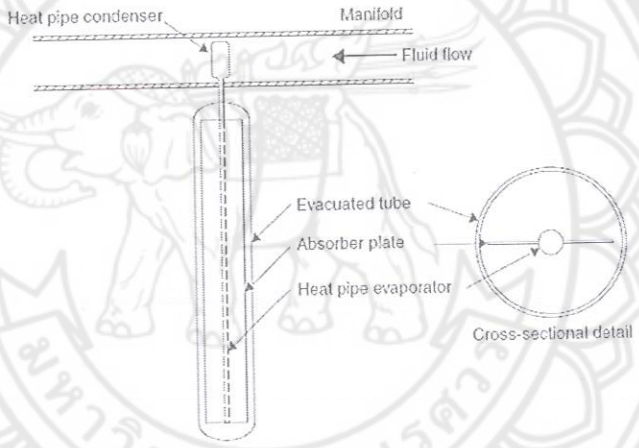

Figure 10 Schematic diagram of an evacuated tube collector [18]

Evacuated tube collectors (ETCs) have demonstrated that the combination of a selective surface and an effective convection suppressor has greatly resulted in a good performance at high temperatures. The vacuum envelope reduces convection and conduction losses, so the collectors can be operated at higher temperatures than flat-plate collectors. Like flat-plate collectors, they collect both direct and diffuse radiation. However, they have higher efficiency at the low incidence angles. This effect tends to be advantageous for evacuated tube collectors rather than flat-plate collectors in terms of daylong performance.

Evacuated tube collectors use liquid-vapor phase change materials to transfer heat at high efficiency. These collectors feature a heat pipe (a highly efficient thermal conductor) placed inside a vacuum-sealed tube. The pipe, which is a sealed copper pipe, is then attached to a black copper fin that fills the tube (absorber plate). Protruding from the top of each tube is a metal tip attached to the sealed pipe (condenser). The heat pipe contains a small amount of fluid (e.g., methanol) that undergoes an evaporating-condensing cycle. In this cycle, solar heat evaporates the liquid and the vapor travels to the heat sink region, where it condenses and releases its latent heat. The condensed fluid returns to the solar collector and the process is repeated. Water or glycol flows through the manifold and picks up the heat from the tubes. The heated liquid circulates through another heat exchanger and gives off its heat to a process or water stored in a solar storage tank. Another possibility is to use the ETC connected directly to a hot water storage tank.

Due to the fact that it is impossible for the evaporation or condensation above the phase-change temperature to happen, the heat pipe offers inherent protection from freezing and overheating. This self-limiting temperature control is a unique feature of the evacuated heat pipe collector.

Within steady-state conditions, the useful heat delivered by a solar collector equals to the energy absorbed by the heat transfer fluid minus the direct or indirect heat losses from the surface to the surroundings. The useful energy collected from a collector can be obtained from the following formula:

$$Q_u = A_{sc}[G_T\tau\alpha - U_L(T_P - T_a)] = \dot{m}C_p(T_o - T_i) \qquad (60)$$

If a suitable correction factor is included, equation 49 can be modified by substituting inlet fluid temperature (T_i) for the average plate temperature (T_P). The result from the equation is as followed

$$Q_u = A_{sc}F_R[G_T(\tau\alpha) - U_L(T_i - T_a)] \qquad (61)$$

where F_R is collector heat removal factor

U_L is heat loss coefficient

It is defined that the solar collector efficiency is the ratio of the useful heat gained over any time period to the incident solar radiation over the same period. The instantaneous energy efficiency of the solar collector can also be expressed in the form of the average Bliss coefficient $(F_R(\tau\alpha)=0.80)$ and the heat loss coefficient $((F_R U_L)=1.5)$, [4] as shown in equation 51

$$\eta_{sc} = \frac{Q_u}{A_{sc} G_T} = F_R(\tau\alpha) - \frac{F_R U_L (T_i - T_a)}{G_T} \qquad (62)$$

Heat Exchanger [19]

Heat exchangers are used to transfer heat between two or more streams of fluid that flow through the apparatus. A major characteristic of heat exchanger design is the relative flow configuration, which is the set of geometric relationships between the streams. It must be emphasized that the configurations described represent the ideal; it is never possible, in practice, to make the flow patterns conform to the ideal.

Counter flow: In a counter-flow heat exchanger, the two fluids flow parallel to each other in the opposite directions. In Figure 11, a configuration schematically is represented, by showing a single smaller-diameter tube coaxially placed within a tube of larger diameter. The two fluids respectively flow within the inner tube and through the annular space that separates the two tubes. In practice, a large number of tubes can be inserted within a single surrounding tube, of much larger diameter, known as the shell. Here the symbol T is used for temperature; subscript 1 denotes the first stream, and subscript 2 the second stream; the subscript *.in.* denotes the entry conditions, whereas *out*. Denote the leaving condition.

Counter-flow exchangers are the most effective. Due to the fact that they make the best use of the available temperature difference, and they can obtain the highest change of temperature of each fluid. This remark is further described below.

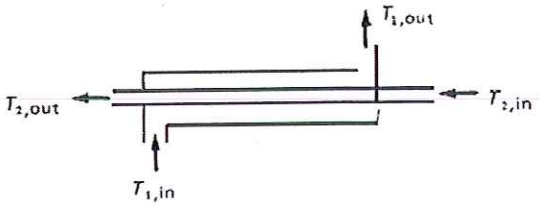

Figure 11 Schematic representation of a counter-flow heat exchanger [19]

Plate Heat Exchanger

The plate heat exchangers (PHEs) are compact and efficient, and are widely used in a large number of industrial applications. Their types, structures and scopes of application are still going through more developments. The core components of the PHE are plates, which not only facilitate heat transfer between the cold and hot fluids, but also bear the pressure difference on both sides. Many kinds of corrugated plates and fluid flow channels between the plates have been studied in pursuit of high efficiency with small flow resistance, high heat transfer and large bearing pressure capacity. [20]

Normally, the main parameters in an evaluation of the performance of corrugated PHEs are the efficiency of heat transfer, flow resistance, and the pressure capacity.

A number of characteristics attractive among these are as followed: [21]

1. Superior thermal performance.

Plate heat exchangers are capable of nominal approach temperatures of 5 °C, comparing to a nominal 10°C for shell and tube units. In addition, overall heat transfer coefficients (U) for plate type exchangers are three to four times of those of shell and tube units.

2. Availability of a wide variety of corrosion resistant alloys.

Since the heat transfer area is constructed from thin plates, stainless steel and any other high alloy construction costs significantly less than for a shell and tube exchanger of similar material.

3. Ease of maintenance.

The construction of the heat exchanger is such that, upon disassemblage, all heat transfer areas are available for inspection and cleaning. Disassemblage consists only of loosening a small number of tie bolts.

4. Expandability and multiplex capability.

The nature of the plate heat exchanger construction permits expansion of the unit should heat transfer requirements increase after installation. In addition, two or more heat exchangers can be housed in a single frame, in order to reduce space requirements and capital costs.

5. Compact design.

The superior thermal performance of the plate heat exchanger and the space efficient design of the plate arrangement have resulted in a very compact piece of equipment. Space requirements for the plate heat exchanger generally run from 10% to 50% that of a shell and tube unit for equivalent duty. In addition, tube cleaning and replacing clearances are eliminated.

In Figure 12, an introduction to the terminology of the plate heat exchanger is presented. Plate heat exchanger that is used in this section refers to the gasket plate and frame variety of heat exchanger. Other types of plate heat exchangers are available. However, among these, only the brazed plate heat exchanger has been found applicable in geothermal systems.

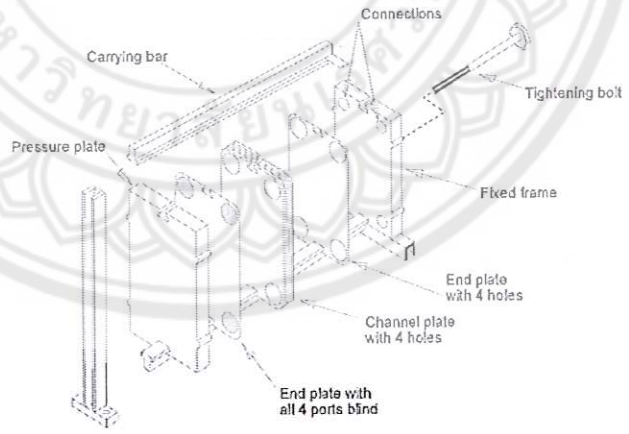

Figure 12 The plate heat exchanger [20]

As it is shown in Figure 12, the plate heat exchanger is basically a series of individual plates pressed between two heavy end covers. The entire assembly is held together by the tie bolts. Individual plates are hung from the top carrying bar and are

guided by the bottom-carrying bar. For single-pass circuiting, hot and cold side fluid connections are usually located on the fixed end cover. Multi-pass circuiting has a result in fluid connections on both fixed and moveable end covers.

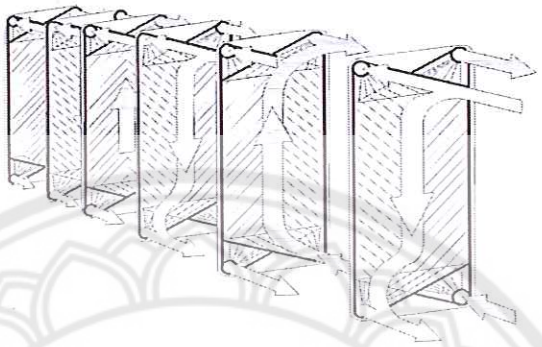

Figure 13 Nature of fluid flow through the plate heat exchanger [20]

Figure 13 illustrates the nature of fluid flow through the plate heat exchanger. The primary and secondary fluids flow in opposite directions on either side of the plates. Water flow and circuit are controlled by the plate gaskets placement. By having various positions of the gasket, water can be channeled over a plate or past it. Gaskets are installed in such a way that a gasket failure cannot result in a mixing of the fluids. In addition, the outer circumference of all gaskets is exposed to the atmosphere. As a result, if a leak ever occurs, a visual indication is sufficiently provided.

Since heat exchangers are used in many applications in various industries, the improvement of the performance of heat exchangers plays an important role in the efficient energy utilization. Heat exchanger design and analysis can be commonly conducted by the LMTD (logarithmic mean temperature difference) [22, 23] method or the effectiveness–number of transfer units method. For the LMTD method, heat transfer equation can be written as followed:

$$Q = UN_{plate}A_pF\Delta T_{lm} \quad (63)$$

where: Q is heat transfer

U is overall heat transfer coefficient

N_{plate} is number of plate that contact with two fluid inside PHE except the cover plates.

A_p is surface area for heat transfer

F is the factor that used to solve log mean temperature difference ΔT_{lm} is log mean temperature difference

The log mean temperature difference is calculated with the use of the difference between the entering and leaving temperatures of the two fluids, according to the following equation

$$\Delta T_{lm} = \frac{\Delta T_1 - \Delta T_2}{lm(\Delta T_1/\Delta T_2)} \quad (64)$$

The thermal model of ideal countercurrent flow exchanger is shown. The efficiency of the PHE is never greater than one of the ideal countercurrent flow cases. Hence, if $\varepsilon_{cc} < \varepsilon^{min}$ is verified, it is unnecessary to solve the thermal model of the PHE since ε_{cc} represents a rigorous upper bound for e and thus the constraint is not satisfied. [24]

$$\varepsilon_{cc} = \begin{cases} \dfrac{1 - e^{-NTU.(1-C^*)}}{1 - C^*.e^{-NTU.(1-C^*)}} & if\ C^* < 1 \\ \dfrac{NTU}{NTU + 1} & if\ C^* = 1 \end{cases} \quad (65)$$

$$NTU = \frac{U.(N_c - 1).A_{plate}}{min(W_h\,.Cp_h, W_c.Cp_c)} \quad (66)$$

$$C^* = \frac{min(W_h\,.Cp_h, W_c.Cp_c)}{max(W_h\,.Cp_h, W_c.Cp_c)} \quad (67)$$

Where N_C is number of channels

The overall heat transfer coefficient can be selected from Figure 14. For a good quality of geothermal fluid in applications, where competent operating personnel maintain the system, there is no reason to specify fouling factors that are any higher than 0.00015. In fact, some designers use no fouling allowances. For systems that are less carefully maintained, a value of 0.0002 may be used.

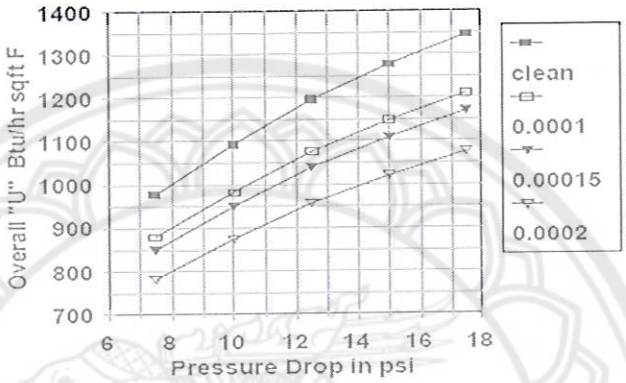

Figure 14 Performance of plate heat exchangers [20]

Literature Review

Huang, BJ., et al. [25] In the present study, the A 1-D analysis for the prediction of ejector performance at critical-mode operation is carried out. It is assumed that the constant-pressure mixing occurs inside the constant-area section of the ejector and the entrained flow at choking condition is analyzed. An experiment using 11 ejectors and R141b as the working fluid to verify the analytical results is also taken place. To determine the coefficients, the test results are used, η_p, η_s, ϕ_p, and ϕ_m defined in the 1-D model by matching the test data with the analytical results. It is shown that the 1-D analysis, with the use of the empirical coefficients, can predict the performance of the ejectors accurately. A new concept, such as a constant pressure ejector in which mixing of the primary and secondary flows occur with the constant area section, it also introduced. The prediction of the ejector performance at critical mode operation is accomplished with the use of the one-dimensional ejector flow model. They also conducted experiments using the ejectors in different dimensions and R141b as the working fluid to compare the analytical results with experimental

results. The authors concluded that the one-dimensional model, using empirical coefficients taking into the losses in the ejector account, could accurately predict the performance of the ejectors.

Huang, BJ. and Chang, JM. [26] show the two empirical correlations from the test results of 15 ejectors that are derived for the performance prediction of ejectors with the use of R141b as the working fluid. To correlate the performance of the ejector, the ratio of the hypothetical throat area of the entrained flow to the nozzle throat area A_e/A_t, the geometric design parameter of the ejector A_3/A_t, and the pressure ratios P_g/P_e and P_c^*/P_e are used. It is predicted that the entrainment ratio v using the correlations is within $\pm$ 10% error. A method of calculation for the ejector design using the correlations is also developed. R141b is shown in the present study to be an effective working fluid for an ejector. The measured v for the ejectors used in the present study can reach as high as 0.54 at P_g = 0.465 MPa (84°C), P_c^* = 0.087 MPa (28°C) and P_e = 0.040 MPa (8°C). For P_g = 0.538 MPa (90°C), Pc* = 0.101 MPa (32°C) and P_e = 0.040 MPa (8°C), ω reaches 0.45

Yapıcı, R., et al. [27] has studied the performance of the ejector refrigeration system using ejectors with cylindrical mixing chamber at operating conditions with choking in the mixing chamber. The reason for choosing the condenser pressure is that the secondary flow choking can occur even in the ejector with the smallest area ratio. In the present study, the performance of the constructed system is determined by using six configurations of ejector and R-123 as working fluid in the system. The study is performed over a range of the ejector area ratio from 6.5 to 11.5 at the compression ratio 2.47. In the mentioned range, the experimental coefficient of performance of the system rises from 0.29 to 0.41, as the optimum generator temperature increases from 83 to 103 °C. In the parametric study, similar experimental results was also found when the efficiencies of the nozzle and diffuser are taken as 0.90.

Selvaraju, A. and Mani, A. [28]. It is found that vapor ejector refrigeration system yields better performance when the ejector operates at choking-mode. To carry out a study on performance of the system, a computer-code based on existing one dimensional ejector theory has been developed. When operating conditions are changed, the critical performance parameters of the system are changed to different critical values. Effects of change in a specific heat of the working fluid and friction at

the constant-area mixing chamber besides internal irreversibility of the ejector are included in the code. The simulated performance results are to be compared with the available experimental data from the literature for validation. The effects of operational parameters and ejector configurations of the system on critical performance are studied. Moreover, the comparison of performance of the system with environment friendly refrigerants, R134a, R152a, R290, R600a and R717 is made.

Guo, J. and Shen, H.G. [29] used a lumped method combined with dynamic model as a proposal for the use in the investigation of the performance and solar fraction of a solar-driven ejector refrigeration system (SERS) using R134a, for office air conditioning application for buildings in Shanghai, China. Classical hourly outdoors temperature and solar radiation model were used to provide basic data for the accurate system performance analysis. The results indicate that during the office working-time (from 9:00 to 17:00), the average COP and the average solar fraction of the system were 0.48 and 0.82, respectively, when the operating conditions were: generator temperature (85 °C), evaporator temperature (8 °C) and condenser temperature varying with ambient temperature. This is to be compared with traditional compressor based air conditioner; the system can save up to 80% electric energy when providing the same cooling capacity for office buildings. Hence, the system provides a good energy conservation method for office buildings.

Wimolsiri Pridasawas and Per Lundqvist [30] speak about the performance of the solar-driven ejector refrigeration system with iso-butane (R600a) as the refrigerant in their study. The effects that both the operating conditions and the solar collector types have on the system's performance are also examined by dynamic simulation. To model and analyze the performance of a solar-driven ejector refrigeration system, the TRNSYS and EES simulation tools are used. The whole system is modelled under the TRNSYS environment, but the model of the ejector refrigeration subsystem is developed in the Engineering Equations Solver (EES) program. 75% of a solar fraction is obtained when using the evacuated tube solar collector. The system requires relatively high generator temperature in the very hot environment, thus a flat plate solar collector is not economically competitive because of the high amount of auxiliary heat that are needed in order to boost up the generator temperature. The results from the simulation indicate that an efficient ejector system can only work in a

region with decent solar radiation and in a place with a sufficiently low condenser temperature. The average yearly system thermal ratio (STR) is about 0.22, the COP of the cooling subsystem is about 0.48, and the solar collector efficiency is about 0.47 at T_e 15 °C, T_e 5 °C above the ambient temperature, evacuated collector area 50 m^2 and hot storage tank volume 2 m^3.

Aphornratana, S. and Eams, I. W. [31] conduct an experimental study of a steam-ejector refrigerator using an ejector with a primary nozzle that could be axially moved within the mixing chamber section. They studied the effects on coefficient of performance and cooling capacity that is produced by adjusting the position of the nozzle as well. The experimental rig and method are described and results show that there is a clear benefit of using such a primary nozzle.

Alexis, GK. and Katsanis, JS. [32] discuss about the behavior of methanol through an ejector operating in a refrigeration system with a medium temperature thermal source. A method has been developed for detailed calculation of the proposed system, which employs analytical functions describing the thermodynamic properties of methanol. The proposed cycle has been compared with a Carnot cycle working at the same temperature levels. They have discussed the influences of three major parameters, generator, condenser and evaporator temperatures, on ejector efficiency and coefficient of performance as well. In addition, the maximum value of COP was estimated by the correlation of the above three temperatures for constant superheated temperature 150 °C, and it was 0.139–0.467. The generator temperature 117.7–132.5 °C, condenser temperature 42–50 °C and evaporator temperature –10 –5 °C were all the designed conditions.

Yinhai, Zhu and Yanzhong, Li [33] proposed a novel ejector model for the performance evaluation on ejectors with both dry and wet vapor working fluids at critical operating mode. In order to approach the real velocity distribution inside the ejecto, a simple linear function is defined. By integrating the velocity function at the inlet section of the mixing chamber, the mass flow rates of the primary flow and secondary flow are derived. By considering the flow characteristics of the critical mode-operating ejector, the developed model contains only one energy conservation equation and is independent from the flow in the mixing chamber and the diffuser. In order to verify the effectiveness of the new model, the experimental data from

different ejector geometries and various operation conditions reported earlier are used. It has been found that the model has a good performance in the prediction of the mass flow rates and the entrainment ratio for both dry and wet vapor ejectors.

Da-Wen Sun [34] composes an analysis on the effect of ejector geometries on performance. For a 5 kW steam-jet refrigerator, technical data including flow rates, entrainment ratio and ejector geometry are provided. These data can be served as guides in designing ejector-cycle refrigerators with other cooling capacities.

Da-Wen Sun [35] According to the results, it is shown that this program can predict the performance of an ejector refrigeration system and provide optimum ejector design data for the system. The program can be used to compare the performance of various refrigerants that are being used in an ejector refrigeration system. Eleven refrigerants were tested using the program in the current study. These refrigerants include water (R718), halocarbon compounds, for instance, CFCs (R11, R12, R113), HCFCs (R21, R123, R142b) and HFCs (R134a, R152a), a cyclic organic compound (RC318), and an azeotrope (R500). According to the result, a steam jet refrigeration cycle has the lowest COP value. For CFCs, R12 gives better performance; for HCFCs, R142b gives high COP value; the HFC refrigerants tested have comparative performance, with R152a giving the best performance among all the other refrigerants. Using HFC refrigerants, which cause no ozone depletion, also produces extra environmental benefits. The system that uses azeotrope R500 as refrigerant also performs well. This pattern of performance variation for various refrigerants is mostly independent from the system operating conditions. An ejector refrigeration cycle using a refrigerant with large latent heat can make the full use of the ejector performance characteristics. A steam jet system is prone to be suitable for experimental studies, since small steam jet refrigeration units require comparatively large ejectors that are easier to be manufactured.

Huang, BJ., et al. [36] developed a high-performance solar ejector cooling system using R141b as the working fluid. It was experimentally obtained a COP of 0.5 for a single-stage ejector cooling system at a generating temperature of 90°C, condensing temperature of 28°C, and an evaporating temperature 8°C. For solar cooling application, an optimum overall COP can be obtained at around 0.22 at a

generating temperature of 95°C, evaporating temperature of 8°C and solar radiation at 700 W/m^2.

Huang, BJ., et al. [37] study the performance of a solar ejector cooling system that is simulated using three different collectors: a conventional flat plate collector, a high efficiency flat plate collector and a vacuum-tube collector. It is shown that with the appropriate selection of the generating temperature, an optimum COP can be easily achieved. The solar ejector cooling system using the single-glazed solar collector with selective surface and an enhanced air insulating layer can be the most economical when it is operated at the optimum generating temperature of the ejector cooling machine. In this case, the solar system cost is around 1 USD per watt for the cooling capacity for air conditioning applications.

Latra Boumaraf and André Lallemand [38] describe a whole simulation program that is useful for the evaluation of the performance and the characteristics of the operating cycle of an ejector refrigerating system with the working fluids R142b and R600a. The cycle is determined by using the temperatures of the three thermal sources and local heat transfer coefficients for the boiler, the condenser and the evaporator. Moreover, a correlation of the ejector entrainment ratio established in different operating conditions at critical point from the conservation equations of the 1-D model available in the literature included in the simulation program. Earlier, all the components of the system were dimensioned for a refrigerating power of 10 kW, the hot source temperature is equivalent to 120 and 130 °C, whereas those of the intermediate and the cold sources are fixed at 35 and 10 °C, respectively (dimensioning conditions). Then, the system performance is investigated in dimensioning conditions and in off-dimensioning conditions using the simulation program. Particularly, according to the analysis of the results, it is shown that at fixed cold source temperature, the intermediate temperature corresponding to the critical mode with ($P_c <= P_c^*$), the system COP tends to decrease when the hot source temperature is higher than that of its dimensioning. Consequently, it is suggested that dimension the system components is at the highest possible temperature in order to affirm the better performance in the case of an operating at lower temperature of the hot source. Also, it is noted that R142b tends to give a better performance of the system in all cases. This is because the R142b is a heavier fluid than R600a.

Alexis, GK. and Karayiannis, EK. [39] describe the performance of an ejector cooling system driven by solar energy and R134a as working fluid. The system operating in a correlation with the intermediate temperature of solar collector in Athens, in the present solar ejector cooling system with R134a as working fluid is presented and is analyzed. During the 21st day of 5 months (May–September) in Athens, the solar ejector cooling system can be operated with coefficient of the performance of 0.011 – 0.101 and the solar collector efficiency can be varied from 0.319 to 0.507 for generator temperature (82–92°C), condenser temperature (32 – 40°C) and evaporator temperature (-10 – 0°C). The maximum COPs is obtained on July (T_g = 92°C, T_c = 32°C, T_e = 0°C) and the minimum on May (T_g = 82°C, T_c = 40°C, T_e = -10°C). The coefficient of performance may be relatively low but the solar energy is available in Athens. Also, this study showed that the COP of ejector cooling system is an exponential function of generator, condenser and evaporator temperature.

Rafet Yapıcı [40] study a novel ejector that was designed based on a constant area ejector model and manufactured in order to investigate the performance of an ejector refrigeration system in a wider operating range. The ejector, with movable primary nozzle, was mounted on the system that was previously constructed for low-pressure refrigerants. The modified refrigeration system has been tested using hot water as driving fluid and R123 as working fluid. The effects of the operating temperatures on the cooling capacity and performance coefficient of the system were experimentally investigated when the primary nozzle position at its optimum at the ejector area ratio of 9.97. As a result, a performance coefficient of 0.39 was obtained at the vapor generator temperature 98 °C, the evaporator temperature 10 °C and critical condenser pressure 129 kPa.

Hisham El-Dessouky, et al. [41] conduct a study on semi-empirical models that are developed for design and rating of steam jet ejectors. The model gives the entrainment ratio as a function of the expansion ratio and the pressures of the entrained vapor, motive steam and compressed vapor. Also, correlations are developed for the motive steam pressure at the nozzle exit as a function of the evaporator and condenser pressures and the area ratios as a function of the entrainment ratio and the stream pressures. This allows the full design of the ejector, where defining the ejector load

and the pressures of the motive steam, evaporator and condenser gives the entrainment ratio, the motive steam pressure at the nozzle outlet and the cross section areas of the diffuser and the nozzle. The developed correlations are based mainly on large database that manufacturer design data and experimental data are all included. The model includes correlations for the choked flow with compression ratios above 1.8. In addition, a correlation is provided for the non-choked flow with compression ratios below 1.8. The values of the coefficient of determination (R^2) are 0.85 and 0.78 for the choked and non-choked flow correlations, respectively. As for the correlations for the motive steam pressure at the nozzle outlet and the area ratios, they all have R^2 values above 0.99.

Ouzzane, M. and Aidoun, Z. [42] The main purpose of the study was to develop a mathematical model and computer programs for ejector studies in refrigeration cycles. Version A of the program was written for optimal ejector design while Version B, with more built-in flexibility, was intended for the simulation. The study is a one-dimensional analysis of compressible refrigerant flow, based on a forward marching technique of solution for the conservation equations. Refrigerant properties were evaluated using NIST [NIST Standard Reference Database 23, NIST Thermodynamics and Transport Properties of Refrigerants and Refrigerant Mixtures, 1998, REFPROP, Version 6.01] subroutines for equations of state solutions. The approach assesses the flow locally and provides the flexibility of returning upstream for correcting adjustments. Model validation against the R141b data of Huang, et al. [Int. J. Refrig. 22 (1999) 354] has shown a very good agreement under all conditions. An analysis with refrigerant R142b was performed for typical refrigeration conditions. The entrainment ratio x, the compression ratio P_6/P_2 and geometric parameters such as diameters and axial dimensions were used to assess performance. Local distributions of pressure, temperature and Mach number were obtained for typical conditions and the mixing chamber was found to greatly impact operation and performance, by controlling the shock wave occurrence and intensity.

Yongprayun, S., et al. [43] study the Life Cycle Cost Analysis (LCCA) of solar absorption cooling system at School of Renewable Energy Technology (SERT), Naresuan University, Phitsanulok, Thailand, which is at a variety of chiller Coefficient of Performance (COP) and Solar Fractions ($SOLF_{the}$). The analysis used LCCA

method base on assumption of the life time is 20 years, the operation period is 8 hour per day, the maintenance cost is 1% of the overall capital cost, the energy consumption consists of the auxiliary heat by LPG and the electricity and inflation rate is 3%. The final result has shown the increasing of the COP effect on the energy cost when the highest COP is 0.7, the lowest energy cost is 3.00 Baht per kWh.

From literature review, it is found that there was widespread use of the ejector. Also, many researchers have developed an improved ejector performance. The ejector can be used with the cooling system and it can increase system performance, but not inclusive with energy storage system, and no ejector cooling system to a residential. So the integration should be investigated for the improvement.

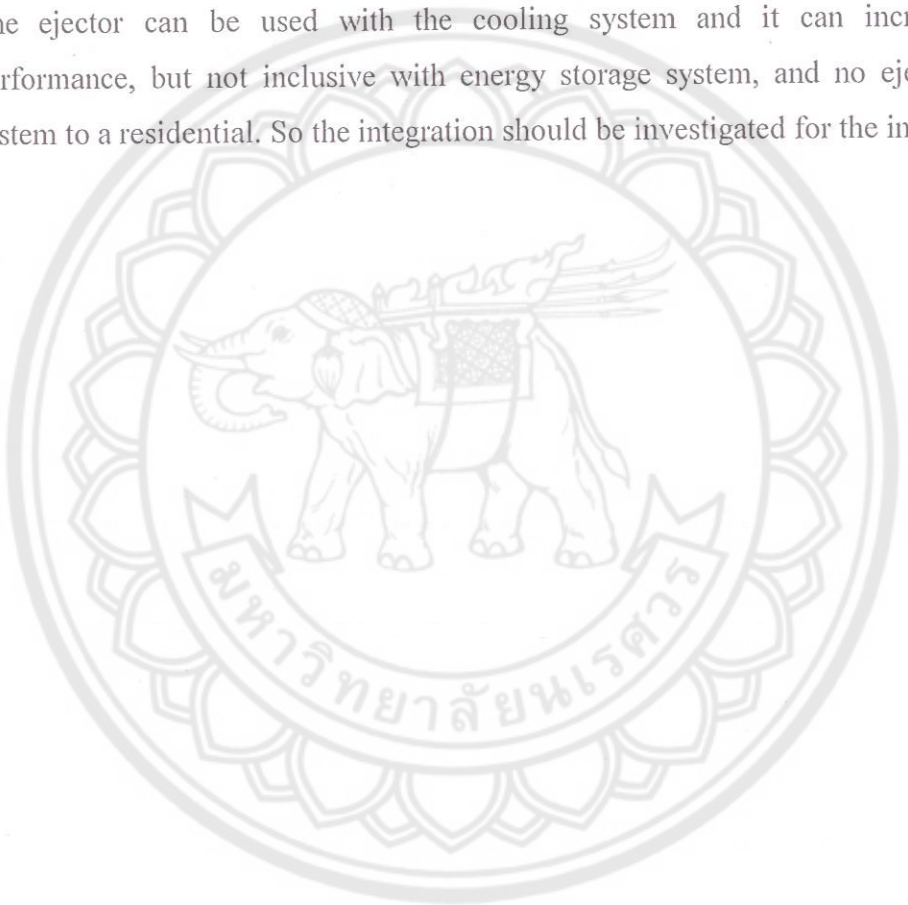

CHAPTER III

RESEARCH METHODOLOGY

The methodology of this research is presented in this chapter. The methodologies are the design of the system; the fabrication ejector and the setup and testing of the solar thermal system; the evaluation of the performance of analytical prototype; the economic analysis. For each of the methodology, details are to be described as followed.

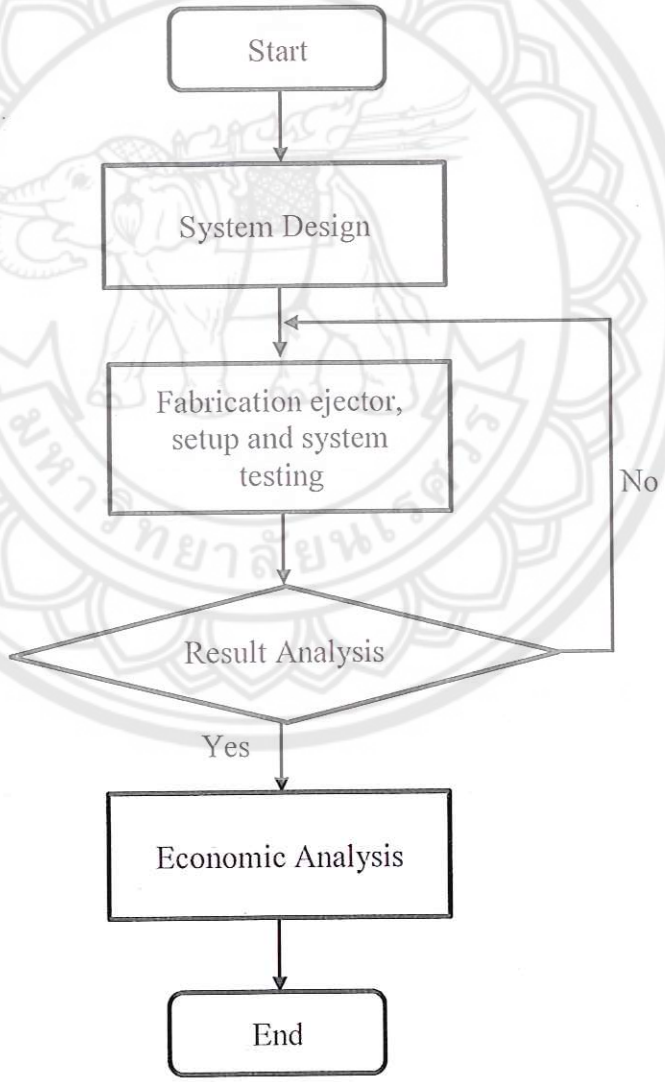

Figure 15 Flow chart of the dissertation methodology

Experimental apparatus

The schematic diagram of the experimental apparatus is shown in Figure 16. The systems consist of three main parts: solar system unit, ejector cooling unit, and cooling load unit

Solar System Unit

A solar system unit is designed to supply heat to the generator as a major source of energy for the ejector cooling system. Hot water is used in this research to conduct the experiment for the system

1. Storage tank is used to store hot water to keep the generator constantly supplied for the stability of the system. In this research, the well-mixed thermal storage.

2. Water pump is used in the system to deliver water from the storage tank back to the evacuated tube solar collector for water heating. In this research, the centrifugal pumps (Pedrollo: Model CPm 130) are used. The pump is driven by a 0.5 hp electric motor in order to supply the maximum the flow rate of 10-80 L/min and the pressure of 6 bars.

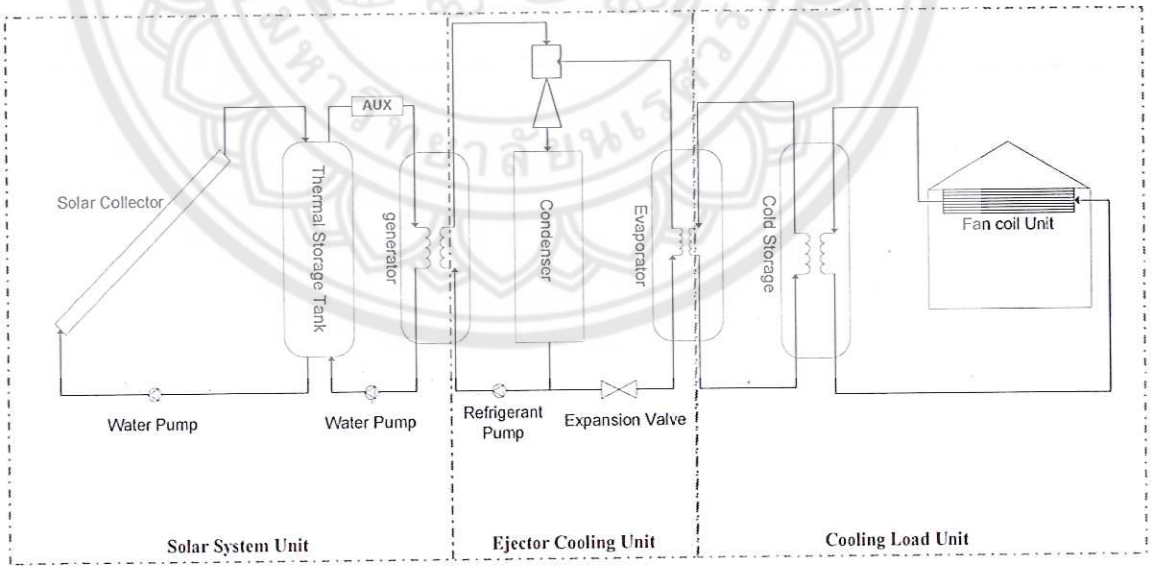

Figure 16 Schematic diagram of the system

Ejector Cooling Unit

Ejector cooling unit is a component that delivers cool water to the cooling load unit as a supplement to be used in air conditioning system. There are devices used in the system as followed.

1. Ejector

Ejector is a device that is used to increase fluid pressure and send the high-pressure fluid to the condenser to produce cooling power. After that, the ejector is used to replace the compressor in vapor compression cooling unit.

2. Generator

Generator is a device that is used to generate the saturated vapor that is the primary fluid needed for the ejector by using the heat exchange between hot water from the storage tank and a working fluid. In this research, the plate heat exchanger (Ranotech model BL 26/42) was used as a generator.

3. Condenser

Condenser is a device that is used to get a high-pressure steam from the ejector and cool it in order to remove the superheat and the latent heat respectively, so that the refrigerant will be condensed back into liquid form. In addition, the liquid is normally slightly sub cooled. In almost all cases, the cooling medium is either air or water. In this research, the plate heat exchanger (Ranotech model BL 26/24) was used as a condenser.

4. Evaporator

Evaporator is a device with a purpose of receiving low-pressure, low temperature fluid from the expansion valve in order to bring it to closely contact thermal with the load. The refrigerant takes up its latent heat from the load and leaves the evaporator as a dry gas. In this research, the plate heat exchanger (Ranotech model BL 26/18) was used as an evaporator.

5. Receiver tank

Receiver tank is a device that is used to store the working fluid from the condenser tank and to supply it to the evaporator tank to generate secondary fluid.

6. Refrigeration pump

Refrigeration pump is a device that is used to transport a working fluid from the condenser to exchange heat with hot water at a generator in order to produce saturated vapor that is sent to the ejector. In this research, the Multi-stage centrifugal pumps (Pedrollo: Model 4CRm 80) were used. The pump was driven by 0.85 hp electric motor to supply maximum flow rate of 120 l/min and a pressure of 6 bars.

Cooling Load Unit

Cooling load unit that contains cold thermal storage and chilled water fan coil unit which served to keep the cool water produced by the solar ejector refrigerated unit and supply the cool air in any desired area.

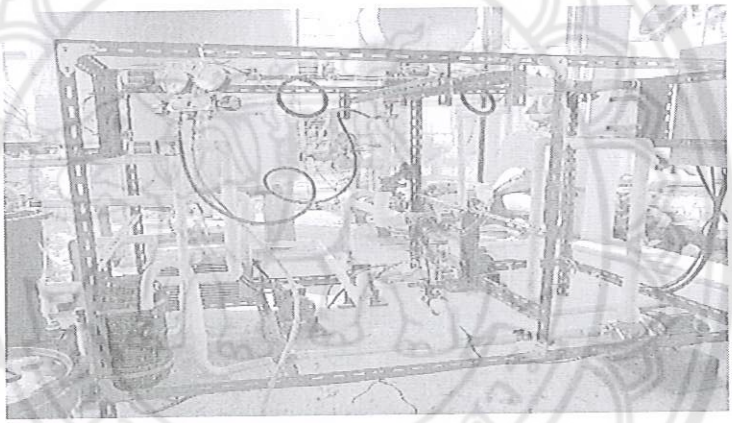

Figure 17 Experimental apparatus

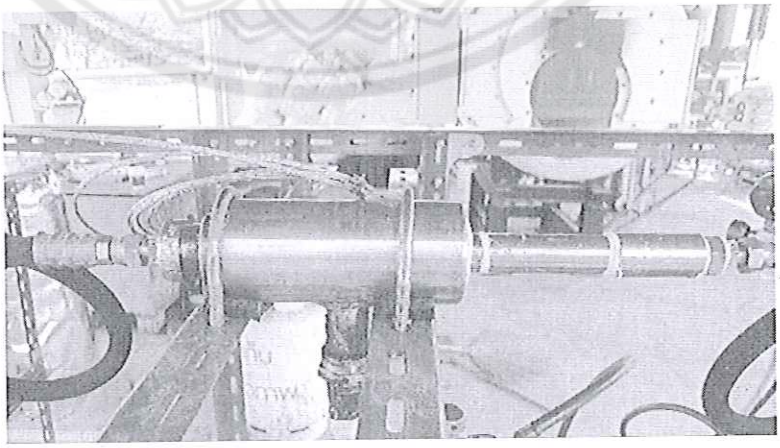

Figure 18 Ejector

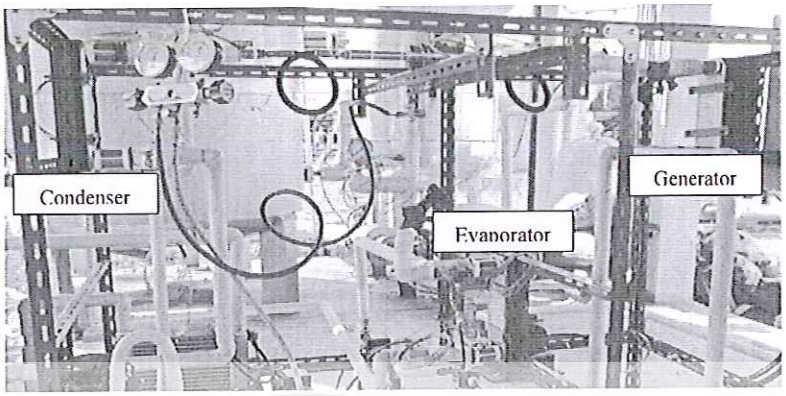

Figure 19 Plate heat exchangers that are being used as system components such as generator, condenser and the evaporator

Figure 20 Storage tank

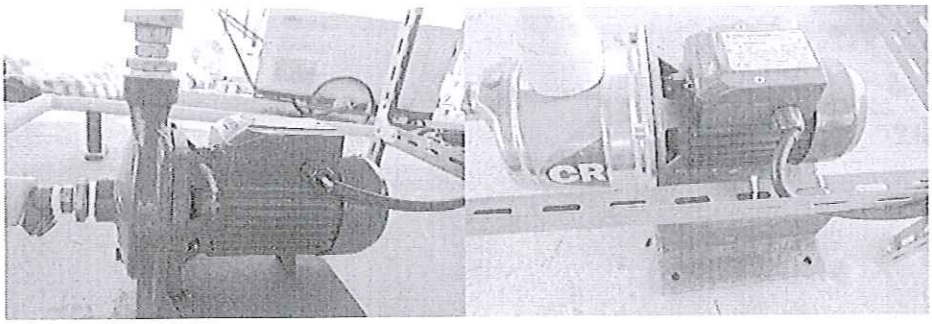

Figure 21 Hot water and refrigeration pump

Instruments

In this research, the parameters that will be used to collect data to analyze the results are determined as followed.

Temperature: Thermocouples type K is used to detect the change in temperature of the incrassated position as shown in figure 22.

Pressure: Using the pressure gauge to detect the pressure. At the generator, condenser, thermal storage tank, cold thermal storage, the pressure used was all the same at 0-6 bars, and using vacuum gauge at the evaporator that show in Figure 23.

Flow rate: The manual-balancing valve (Oventrop Hydrocontrol-R series) is used to control the flow rate for primary motive, and secondary suction that show in Figure 24.

Data logger: in this research used wisco model AI 210 and EX 210 expansion module for temperature recording that show in Figure 25

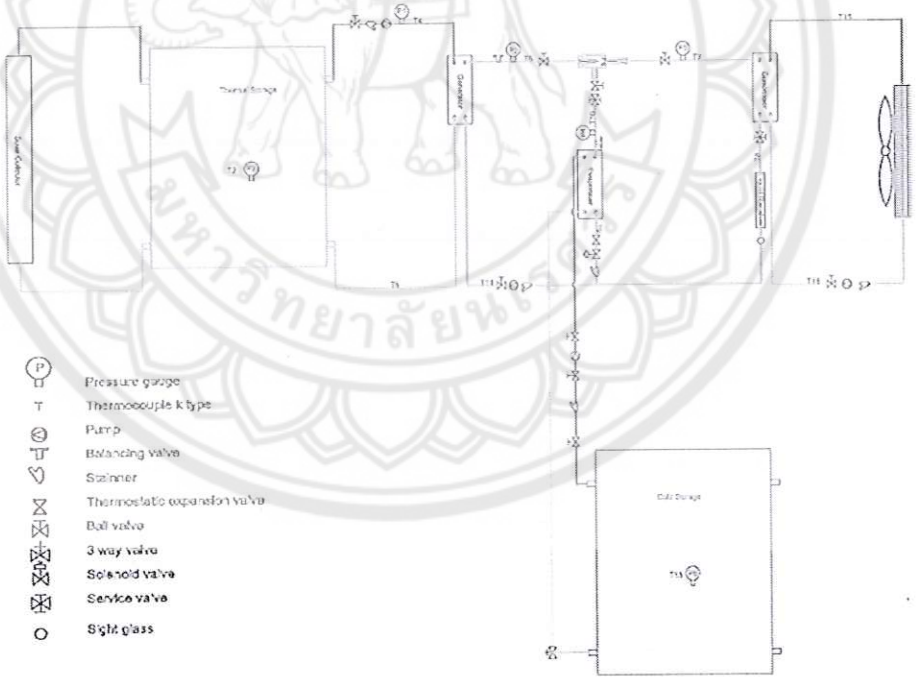

Figure 22 Schematic diagram of experimental apparatus

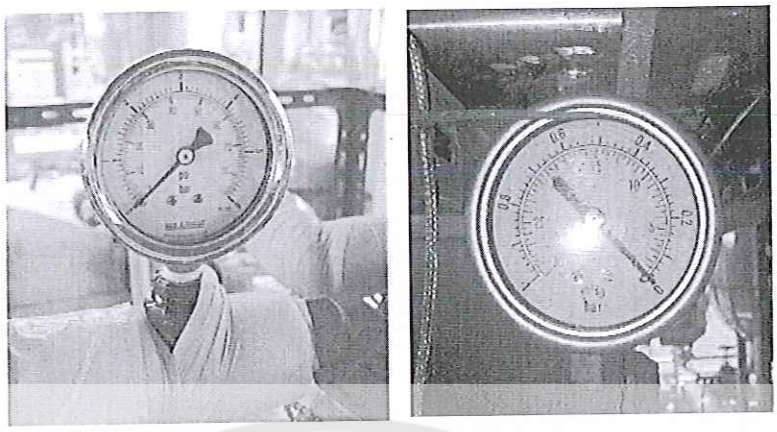

Figure 23 Pressure gauge and vacuum gauge

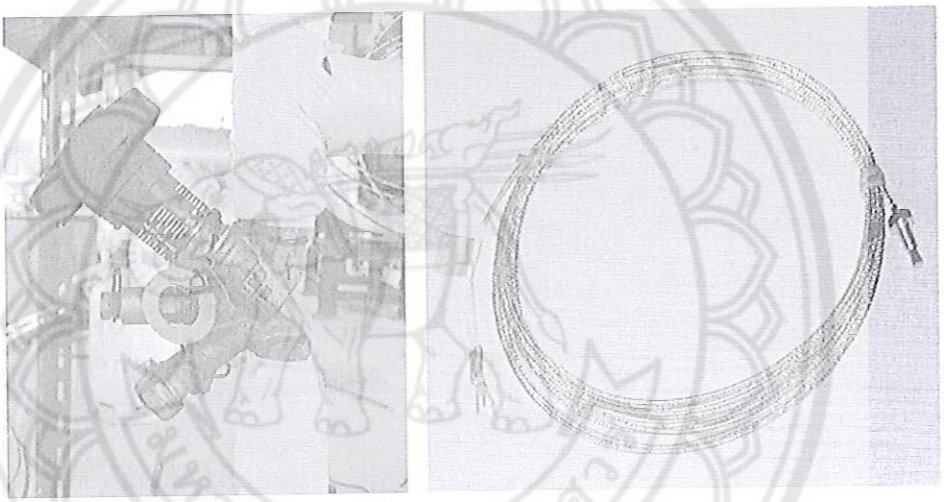

Figure 24 Manual balancing valve and Thermocouples type K

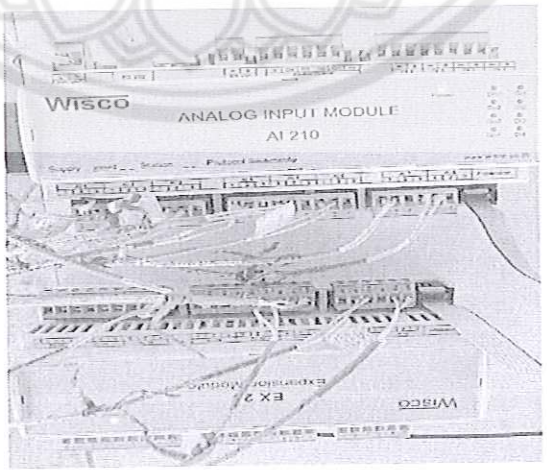

Figure 25 Data logger

System Design

In this research, Matlab® Program was used to calculate the equation of ejector refrigeration system. For the calculation, thermodynamics properties of R141b [50] is used for database of program.

Although the refrigerant R141b used in the experiment although has good performance, it still needs to be replaced with a low ODP working fluid. This requires modification of the ejector design in order to maintain a high COP.

Table 2 R141b properties

Property	Values
Chemical formula	$CCL_2F\text{-}CH_3$
Boiling point at 1 atm (°C)	32.05
Specific heat ratio of vapor	1.135
Specific heat of R141b at 25 °C (kJ/kg-k)	1.16
Molecular Weight (kg/kmol)	116.95
Liquid density at 25 °C (kg/m^3)	1234

The ejector calculation programing

The simulation of R141b ejector is mathematically applied.[36] The assumptions for computer simulation program are as followed.

1. Efficiency of nozzle (η_n) = 0.85
2. Efficiency of suction (η_s) = 0.85
3. Efficiency of diffuser (η_d) = 0.85
4. The temperature of generator (Tg) = 84 °C
5. The temperature condenser (Tc) = 28 °C
6. The temperature evaporator (Te) = 8 °C

The calculation of the primary nozzle geometrics

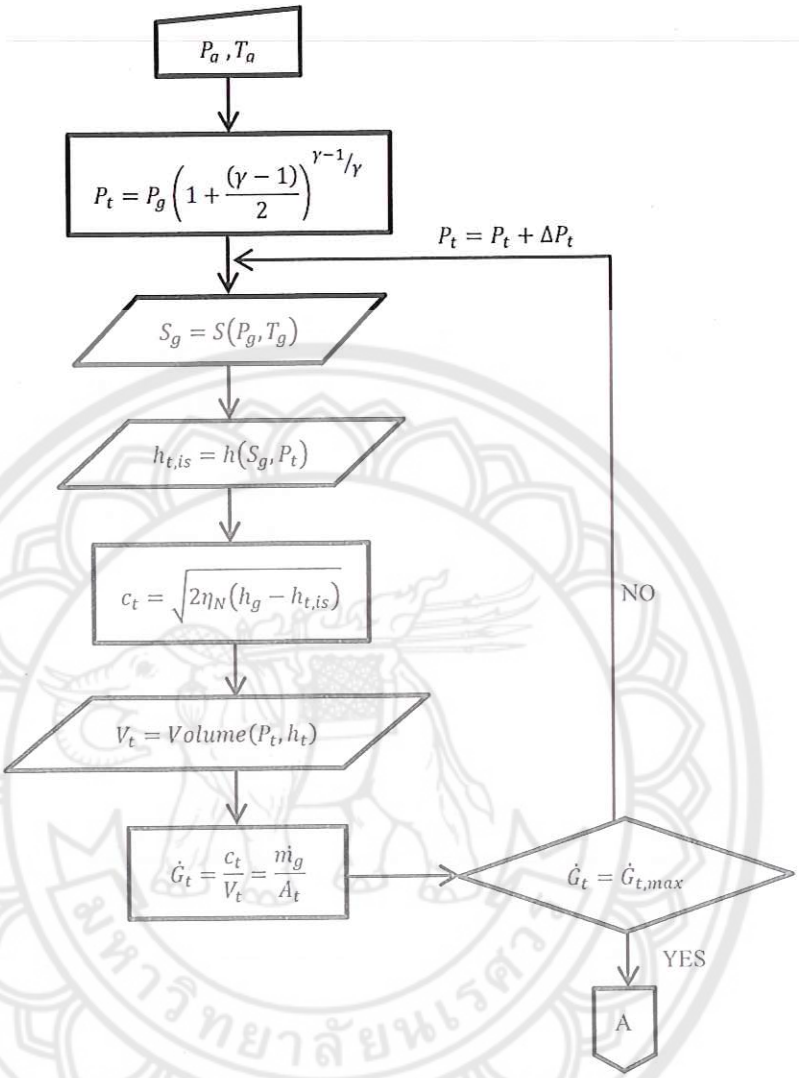

Figure 26 Flow chart of calculating nozzle throat diameter

The calculation of the throat diameter of the secondary flow.

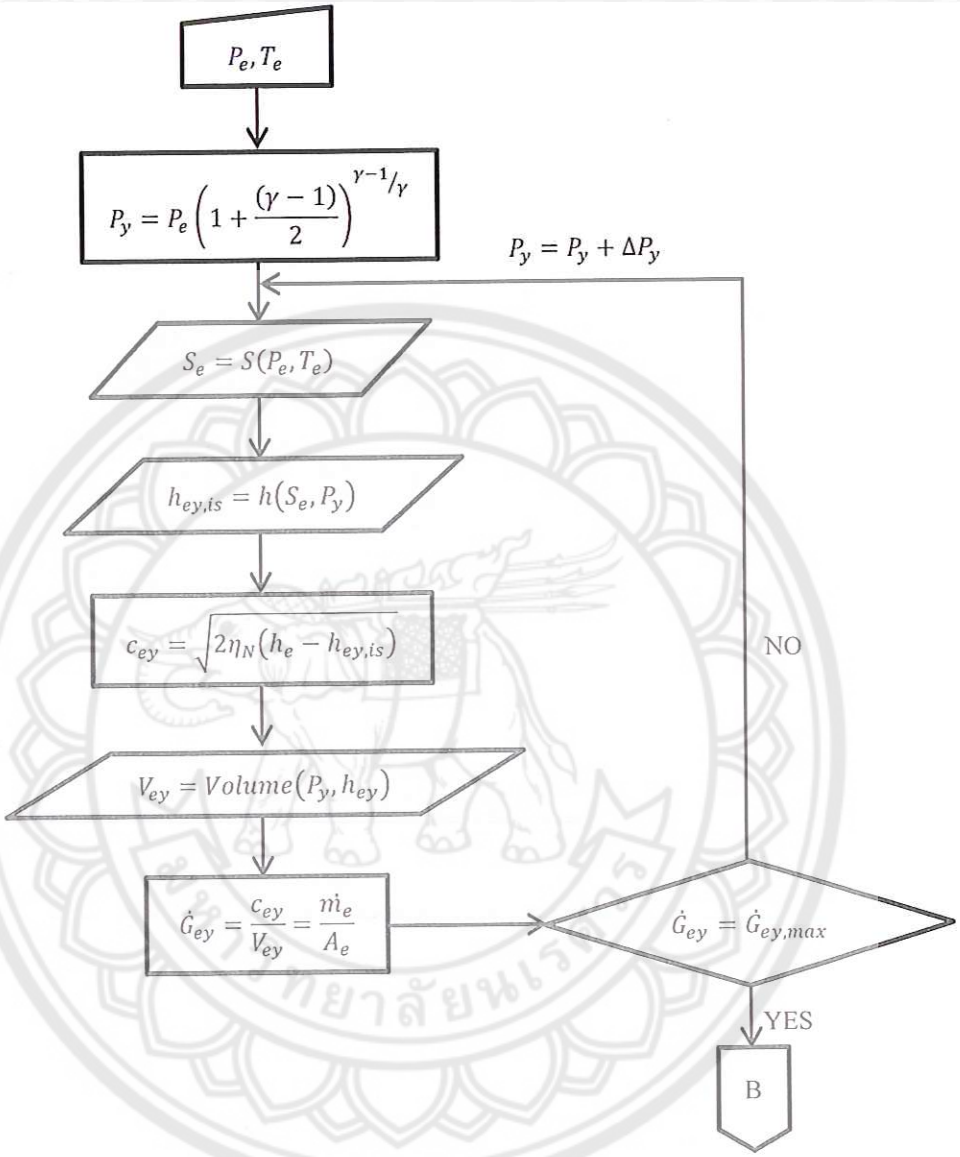

Figure 27 Flow chart of the calculating throat diameter of the secondary flow

The calculation of the ejector dimension

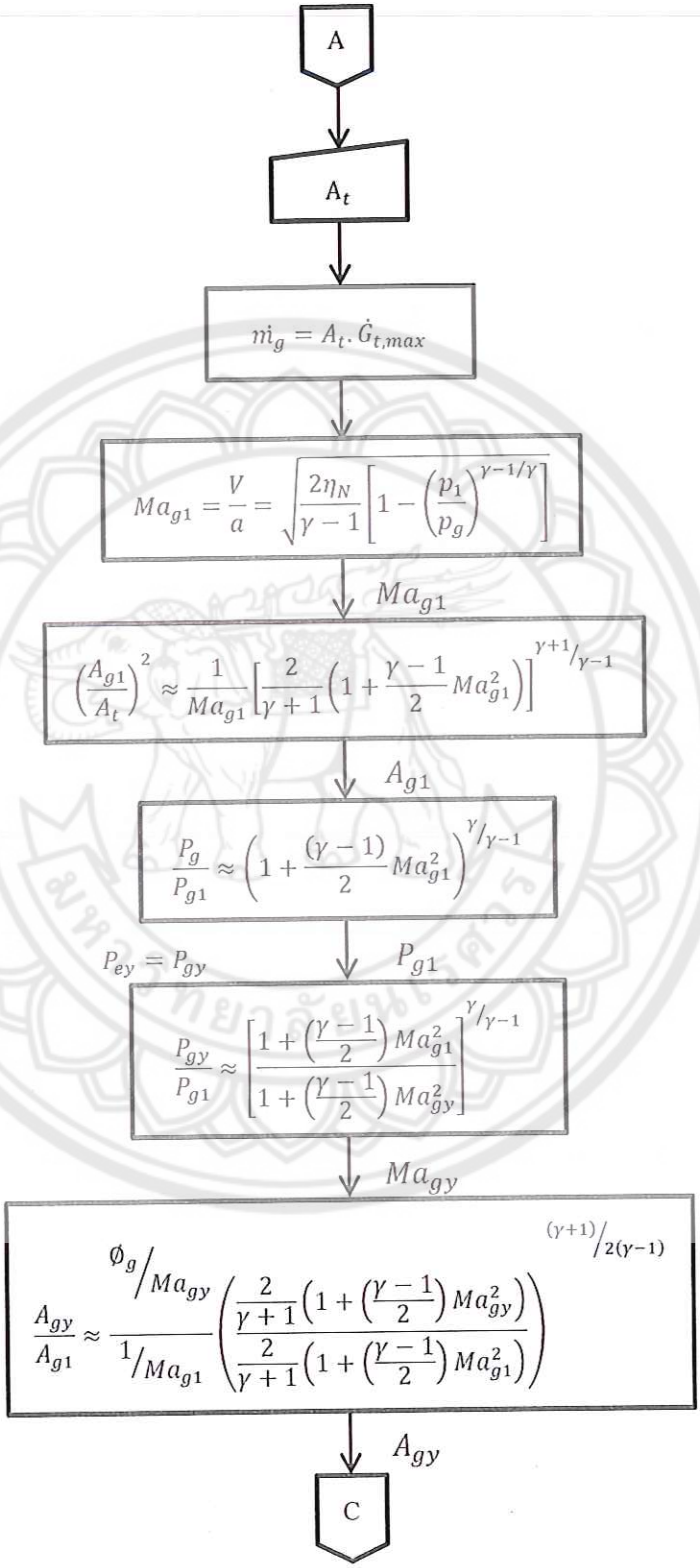

Figure 28 Flow chart of the calculation of the ejector dimension

The calculation of the ejector performance.

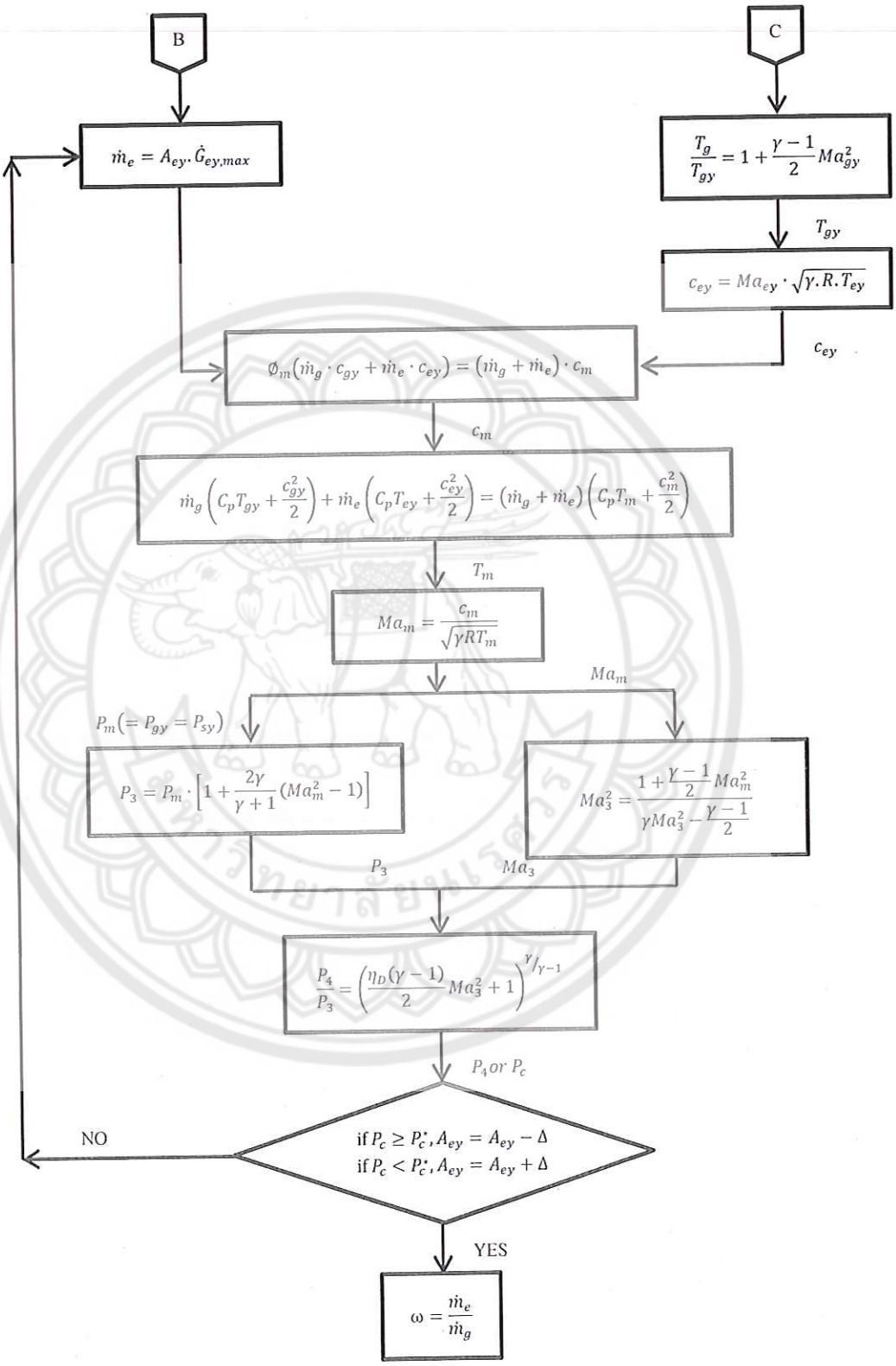

Figure 29 Flow chart of for the calculation of the ejector performance

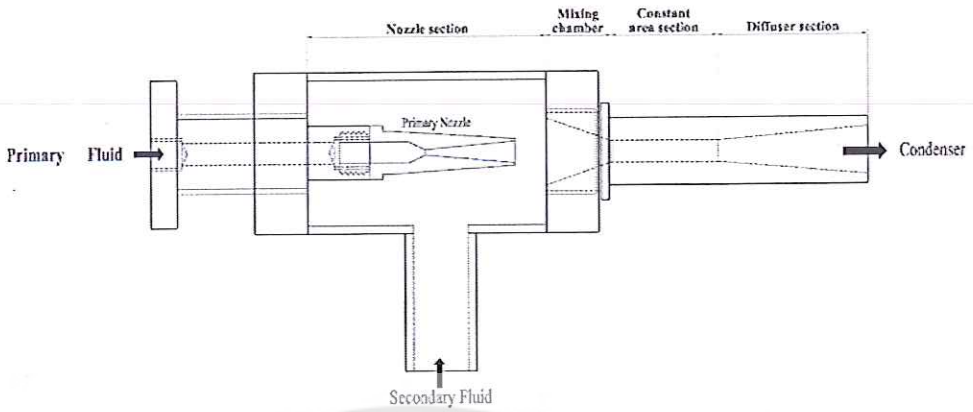

Figure 30 Ejector assembly

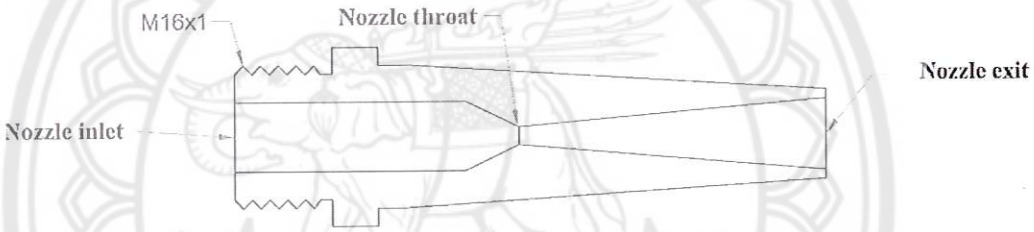

Figure 31 Primary nozzle assembly

Thermal Energy Storage calculation.

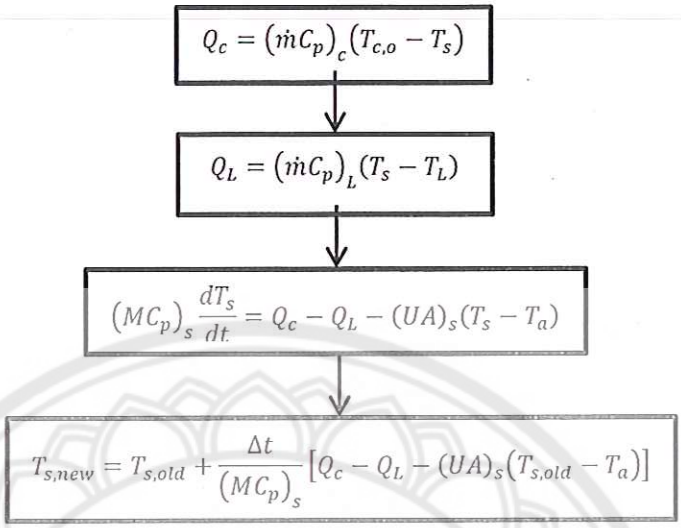

Plate heat exchanger calculation.

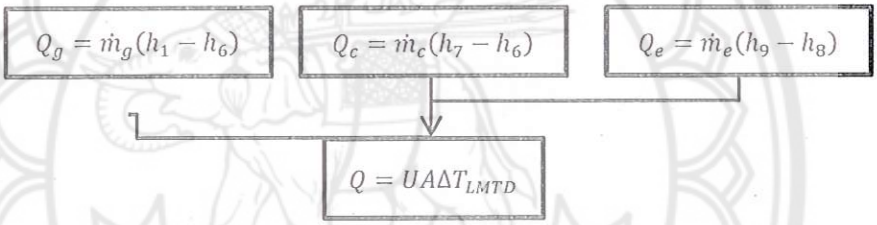

Figure 33 Flow chart of the generator condenser and evaporator calculation

Solar collector calculation.

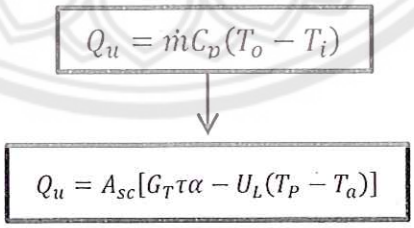

Figure 34 Flow chart of the solar collector calculation

Experimental setup

The experimental practice of the R141b ejector refrigeration system uses the operating condition and ejector geometry via the result of the simulation program. The experiment was tested from 09.00 am to 16.00 pm at the School of Renewable Energy Technology, Naresuan University, Thailand.

To start a test, the hot water should be generated from LPG water heater in order to enhance the refrigerant temperature, and then it should be stored in the hot water storage tank. After that, turn on the hot water pump for it to circulate to the generator to exchange with R141b. Then, turn on the water pump by opening cooling water valve to let water flow through the condenser. After the R141b is increased to the set point, the vapor enters to the primary nozzle of the ejector by opening the balancing valve manually when the R141b vapor reaches the temperature of 84°C pressure at 4-5.5 bars. After the temperature of generator is steady, by opening balancing valve, the secondary flow is entrained to ejector suction and mixed with the primary flow at mixing chamber.

In order to continuously make the system operate, the refrigeration pump should be turned on to feed the refrigerant from the receiver tank to the generator.

Economic analysis

The economics of solar energy systems are particularly complex with many inevitable uncertainties due to several factors. The principal reason to use the solar energy for heating or cooling is the cost reduction. Therefore, an economic analysis must be carried out to determine whether a particular solar system is economically advantageous for a particular project. [43]

In order to decide the acceptable project, economic analysis is set as Net Present Value (NPV), Internal Rate of Return (IRR), and Payback Period (PB)

Net Present Value (NPV)

It is the difference between the present value of the future cash flows from an investment and the amount of investment. Present value of the expected cash flows is computed by discounting them at the required rate of return. A zero net present value means the project repays the original investment, plus the required rate of return.

A positive net present value means a better return, and a negative net present value means a worse return. The formula of NPV is shown as followed

$$NPV = \sum_{t=1}^{n} \frac{R_t}{(1+i)^t} - I_0 \tag{68}$$

Where R_t is Net Revenue

I_0 is Initial Investment

i is discount Rate

n is the total number of periods n

t is to the time periods

Internal Rate of Return (IRR)

The rate of return that would make the present value of future cash flows plus the final market value of an investment or business opportunity equals to the current market price of the investment or opportunity. The internal rate of return is an important calculation that is frequently used to determine whether a given investment is worthwhile. An investment is generally considered worthwhile if the internal rate of return is greater than the return of an average similar investment opportunity, or if it is greater than the cost of capital of the opportunity.

$$-I_0 + \sum_{t=1}^{n} \frac{CF_t}{(1+IRR)^t} = 0 \tag{69}$$

Where n is the total number of periods n

CF_t is cash flow at time

I_o is Initial Investment

IRR is internal rate of return

Payback Period (PB)

Payback period, in capital budgeting, is the length of time needed to recoup the cost of the capital investment. The payback period is the ratio between the initial investment (cash outlay, regardless of the source of the cash) and the annual cash inflows for the recovery period.

$$PB = \frac{Cost\ of\ project}{Annual\ cash\ revenues} \tag{70}$$

CHAPTER IV

RESULTS AND DISCUSSION

In his chapter, the results of the research are presented in three parts: The system design, the system performance, and the economic analysis. The details in each part are described as followed.

System design

Ejector geometrics

Due to the designing of the R141b ejector to produce air conditioning with 3.5 kW spec using Matlab® to calculate the ejector geometrics, given that the generator temperature is 84 °C, condenser temperature is 28 °C, the evaporator temperature is 8 °C, the generator pressure is 0.46 Mpa, the condenser pressure is 0.087 Mpa, and the evaporator pressure is 0.040 Mpa [26], used the thermodynamic property of R141b in calculation, it is found that the nozzle throat diameter is 2 mm, the nozzle inlet diameter is 7.75 mm, the nozzle exit diameter is 8 mm, as shown in Figure 35. Table 3 shows detail of ejector geometry, mixing chamber inlet diameter is 25 mm, Constant area diameter is 8 mm, Diffuser outlet diameter is 17.8 mm, Diffuser chamber length is 56 mm. and other parts details are described in Table 3, and Figure 36 shows the ejector drawing.

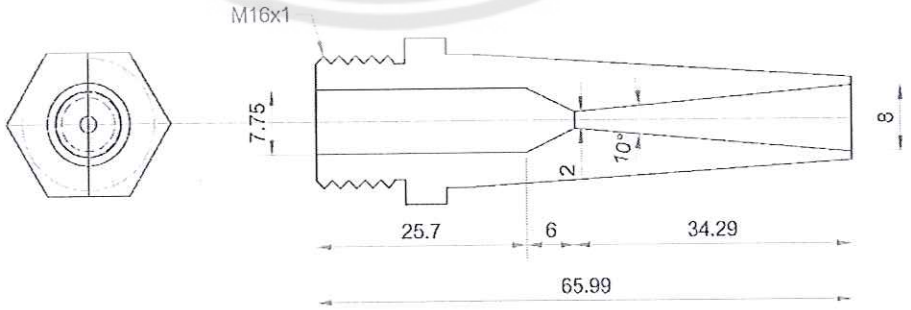

Figure 35 Detail of primary nozzle geometrics

Table 3 Design results of Ejector geometrics.

Parts	Dimension (mm.)
Secondary Inlet	
Inlet of the secondary flow	21
Secondary flow to the mixing chamber area	412.5 mm^2
Mixing Section	
Mixing chamber inlet diameter	25
Mixing chamber outlet diameter	8
Mixing chamber length	25
Mixing chamber angle	37.6°
Constant Area Section	
Constant area diameter	8
Constant area length	40
Diffuser Section	
Diffuser inlet diameter	8
Diffuser outlet diameter	17.8
Diffuser chamber length	56
Diffuser angle	10°

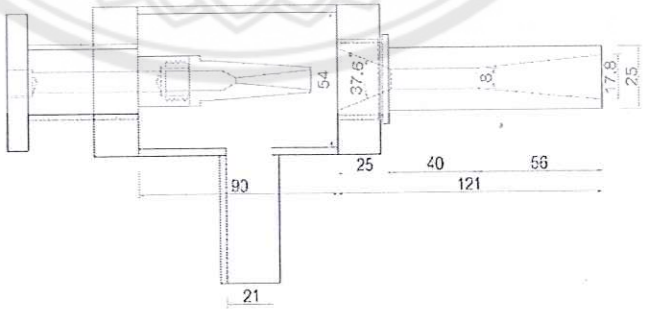

Figure 36 Ejector geometrics

Evacuated Tube solar collectors

In this research, it is given that the solar radiation is averagely 692.20 W/m^2 that data from School of Renewable Energy Technology 23 to 26 December 2014, the thermal energy demand for the air conditioning system is 3.5 kW, the collector heat removal facter ($F_R\tau\alpha$) is 0.80, the heat loss coefficient (U_L) is 1.5 W/m^2 k [4], the efficiency of evacuated Tube solar collector is 0.5, the inlet fluid temperature (T_i) is 80 °C. Accordingly, the area of solar collector can be obtained from the equation 62 as show as below:

$$\eta_{sc} = \frac{Q_u}{A_{sc}G_T} = F_R(\tau\alpha) - \frac{F_R U_L(T_i - T_a)}{G_T}$$

$$A_{sc} = \frac{Q_u}{\eta_{sc}G_T} = \frac{3{,}500}{0.5 \times 692.20} \quad \frac{w}{w/m^2}$$

$$A_{sc} = 10.11\ m^2$$

Storage system

1. Thermal storage

The calculation of the size of thermal storage tank, the storage temperature, the collector temperature is 84 C. The energy demand for the air conditioning system to continually be operated all day (Q_u), and the volume of water (V_w) to run the system can be calculated from the following equation.

$$E_g = Q_u \times t = 3{,}500 \times 6 \times 3{,}600 = 75{,}600\ kJ/day$$

The volume of water in the system can be calculated from the following equation

$$V_w = \frac{E_g}{C_p \times \Delta T} = \frac{75{,}600}{4.186 \times 55} = 321.16\ Liter$$

Then the storage tank size is 0.33 m^3

For charging and discharging, instantaneous capacity of the thermal storage tank may be described from equation 52 and 53 respectively.

$$Q_c = (\dot{m}C_p)_c(T_{c,0} - T_s)$$

$$Q_L = (\dot{m}C_p)_L(T_s - T_L)$$

For the startup, the thermal storage is heated from the initial temperature to reach 84 °C, having a completed the startup procedure, and with constancy, the first charging experiment was commenced, as shown in Figure 37.

During the tests, the inlet temperature that is put to the storage tank was manually increased to reach about 84 °C and then it was maintained at an almost constant level of about 84 °C for most of the charging process.

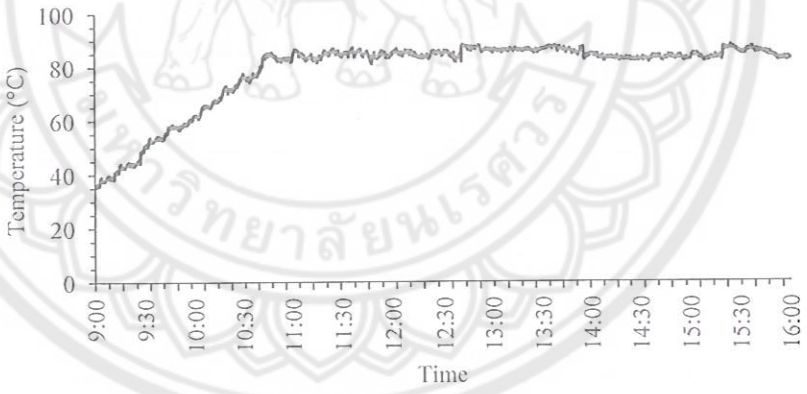

Figure 37 Experiment result temperature of water in thermal storage tank

2. Cold storage

In the calculation of the cold thermal storage tank, it is given that the room temperature at the start is 30 C, the desired air conditioned room temperature is at 25 C, the difference in water inlet and outlet temperature is at 8 C Cp is 4,189 kg/s, and the cold water flow rate can be calculated as followed

$$Q_w = \dot{m}_w C_{pcw}(T_o - T_i)$$

$$\dot{m}_w = \frac{Q_w}{C_p(T_0 - T_i)} = \frac{3{,}500}{4189 \times 8}$$

$$\dot{m}_w = 0.104\ kg/s$$

The size of the storage tank can be obtained from the following equation

$$\dot{m}_w = \frac{Q_w}{C_p(T_0 - T_i)} = \frac{3{,}500}{4{,}189 \times 6}$$

$$\dot{m}_w = 0.104 \times 6{,}300 = 2255.90\ Kg/day$$

Hence, the size of the cold thermal storage tank is 2.3 m^3

The cold water in the storage tank was produced by the evaporator, the procedures were to remove the heat from the initial temperature to 8 °C, to have a completed startup procedure, and with constancy, the first charging experiment was commenced, as shown in Figure 38,

During the tests, the inlet temperature to the storage tank was manually decreased to be at about 8 °C and then it was maintained at an almost constant level at about 8 °C for most of the charging process.

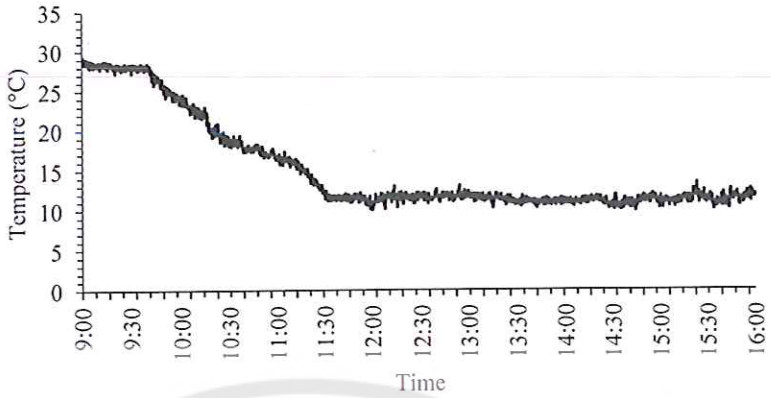

Figure 38 Experimental result temperature of water in cold storage tank

Ejector performance

For the given ejector, the performance was based on the mathematical model mentioned on 1-D model. With validation, the results were compared to the experimental values. The result comparison are shown in Table 4

Table 4 Validation of the calculated COP with experimental result.

Generator	Evaporator	COP		
(°C)	(°C)	Calculate	Experimental	Error (%)
80	8	0.262	0.254	3.204
81	8	0.255	0.254	0.287
82	8	0.249	0.255	-2.512
83	8	0.241	0.256	-5.520
84	8	0.235	0.235	0.282
85	8	0.229	0.258	-11.009
86	8	0.223	0.238	-6.184
87	8	0.217	0.216	0.790
88	8	0.213	0.215	-0.822
89	8	0.207	0.194	6.759
90	8	0.201	0.173	16.723
		Average		0.182

Table 4 shows the results of the calculating program and experiment by various operating condition at generator temperature that were in a range of 80 ºC to 90 °C and a fixed evaporator temperature of 8 °C. The system performance was shown and compared the results to the experimental result. The deviation of COP has an average of 0.182 %.

Table 5 showed the variation the design results, the generator temperature (Tg) that has an operated range from 80 ºC to 90 °C and a fixed evaporator temperature at 8 °C, secondary fluid (mie), which has an effect to the mass flow rate of primary fluid (mig), entrainment ratio (ω) and COP

Table 5 Variation of design results.

Tg (°C)	Te (°C)	mig (kg/s)	mie (kg/s)	ω	COP
80	8	0.005	0.0016	0.3245	0.2619
81	8	0.0051	0.0016	0.3168	0.255
82	8	0.0053	0.0016	0.3096	0.2485
83	8	0.0054	0.0016	0.3016	0.2415
84	8	0.0055	0.0016	0.2947	0.2354
85	8	0.0057	0.0016	0.2877	0.2292
86	8	0.0058	0.0016	0.2809	0.2232
87	8	0.0059	0.0016	0.2743	0.2174
88	8	0.0061	0.0016	0.2681	0.213
89	8	0.0062	0.0016	0.2621	0.2067
90	8	0.0064	0.0016	0.256	0.2014

Figure 39, it is found that the increasing generator temperature ranges from 80 ºC to 90 ºC and fixed evaporator temperature is at 8 ºC. The results showed that the increase in generator temperature does not affect the improvement in COP of the system. When generator temperature ranges from 80 ºC to 90 ºC, the ejector refrigeration system has the COP at 0.2619 and 0.2104, respectively. This results show that the generator temperature has an effect on COP system.

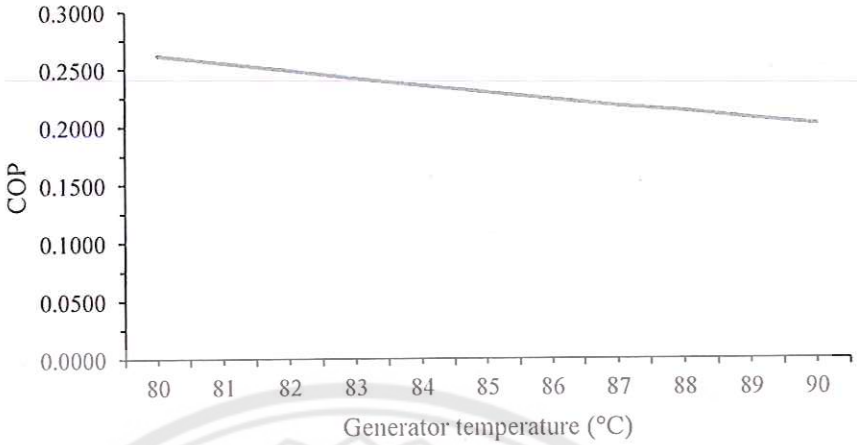

Figure 39 Variation in the performance with the generator temperature

Design result of the entrainment ratio when increasing the generator temperature ranges from 80 °C to 90 °C and the evaporator temperature is at 8 °C the results shows that the generator temperature affecting the entrainment ratio is similar to COP. According to the use of computer program to predict the ejector performance, it is found that the raising the generator temperature does not improve entrainment ratio. That shows in Figure 40.

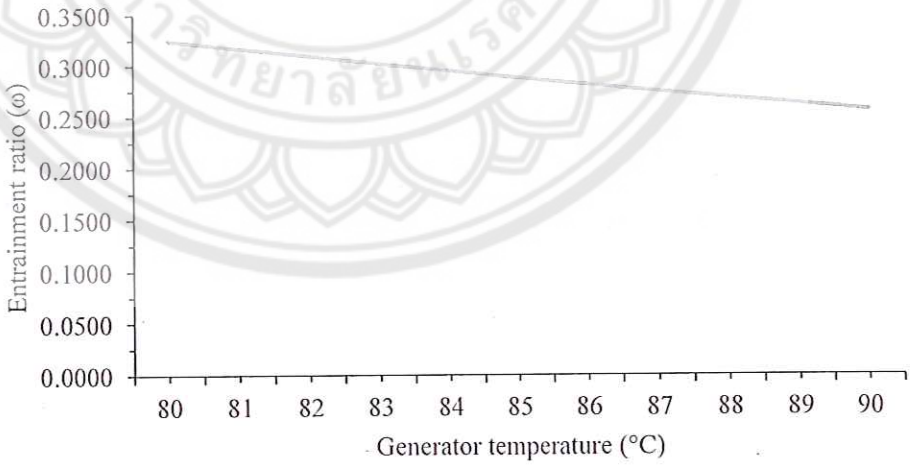

Figure 40 Variation in entrainment ratio with generator temperature

Figure 41 showed that at a constant evaporator temperature and a varied generator temperature ranging from 80 ºC to 90 ºC, the mass flow rate of primary fluid is increased from 0.0051 kg/s to 0.0064 kg/s, while mass flow rate of secondary fluid is 0.0016 kg/s, since it leads to the reduction in the entrainment ratio and COP, In addition to the high generator temperature that leads to a higher angle of expansion of primary fluid from primary nozzle. It is found that with an increase in generator temperature, the saturated vapor primary will spread and the obstructed secondary fluid will be entrained to the mixing chamber section. With this reason, the entrainment ratio and COP is decreased.

According to the results of the computer simulation program to predict the performance of the ejector refrigeration system, the operating condition can obtain the appropriate COP and can be a continuous experiment as temperature of generator for generated saturated primary vapor is 84 ºC, Although the lower temperature of 84 ºC can obtain a higher COP and the critical pressure is 0.464 MPa, at the lower generator temperature, the system is operated at low critical pressure, which is difficult to control the condenser pressure.

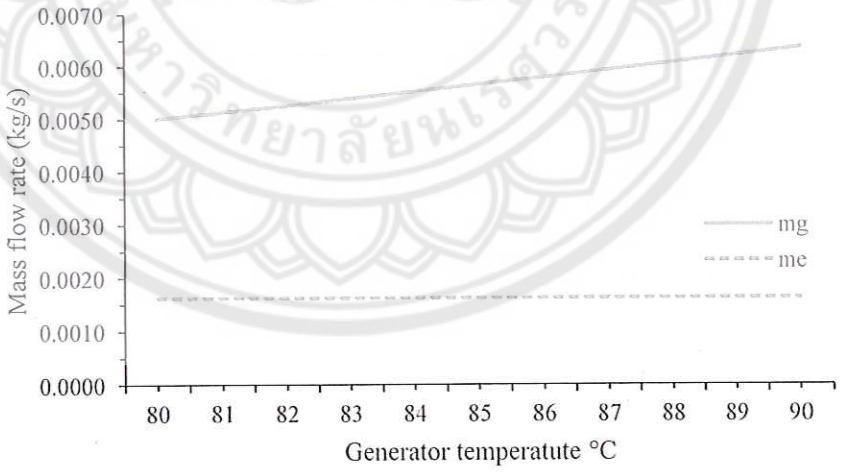

Figure 41 Variation in mass flow rate with the generator temperature

Table 6 showed the variation the experimental results, the generator temperature (T_g) operated ranging from 80 ℃ to 90 °C and the fixed evaporator temperature is at 8 ℃, which have an effect to the mass flow rate of primary fluid (mig), secondary fluid (mie), entrainment ratio (ω) and COP

Table 6 Variation of experimental results.

Tg (°C)	Te (°C)	mig (kg/s)	mie (kg/s)	ω	COP
80	8	0.0233	0.0043	0.186	0.2538
81	8	0.0233	0.0043	0.186	0.2543
82	8	0.0233	0.0043	0.186	0.2549
83	8	0.0233	0.004	0.1705	0.2343
84	8	0.0233	0.0043	0.186	0.2561
85	8	0.0233	0.0043	0.186	0.2575
86	8	0.0233	0.004	0.1705	0.2379
87	8	0.0233	0.0036	0.155	0.2157
88	8	0.0233	0.0036	0.155	0.2148
89	8	0.0233	0.0033	0.1395	0.1936
90	8	0.0233	0.0029	0.124	0.1726

Figure 42 the ejector performance by the calculation with the experimental result when the generator temperature was ranged from 80 °C to 90 °C is compared. It is found that, the result of the experiment, an increase in generator temperature will cause the COP to decrease, as well as the result of design. The deviation of COP has an average of 0.182 %.

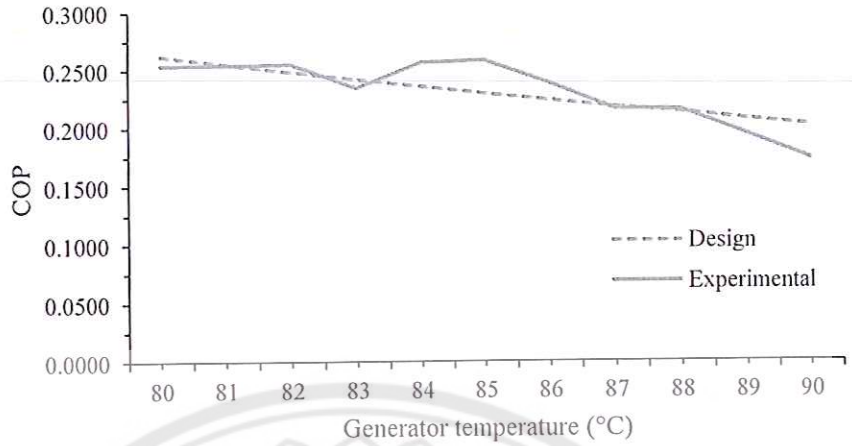

Figure 42 Comparison of the performance design result and experimental result with the generator temperature

Figure 43 showed the comparison of the entrainment ratio design result and experimental result with the generator temperature, at constant evaporator temperature and various generator temperature ranges from 80 °C to 90 °C. When the generator temperature increases, it resulted the entrainment ratio to be decreased as well, the similar design and experiment.

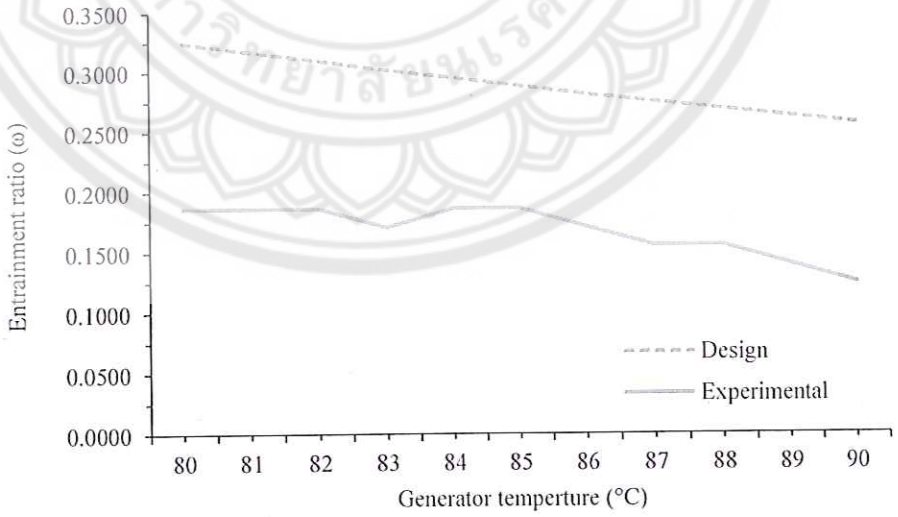

Figure 43 Comparison of the entrainment ratio design result and experimental result with the generator temperature

Figure 44 showed the comparison primary fluid mass flow rate and secondary fluid mass flow rate by calculate the result with experimental result and various generator temperature range from 80 °C to 90 °C. For study affect solar ejector cooling performance from secondary mass flow rate by fixed the primary mass flow rate. That found mass flow rate of secondary fluid decrease when generator temperature increase. As a result, COP decreased due to less secondary fluid into the mix less.

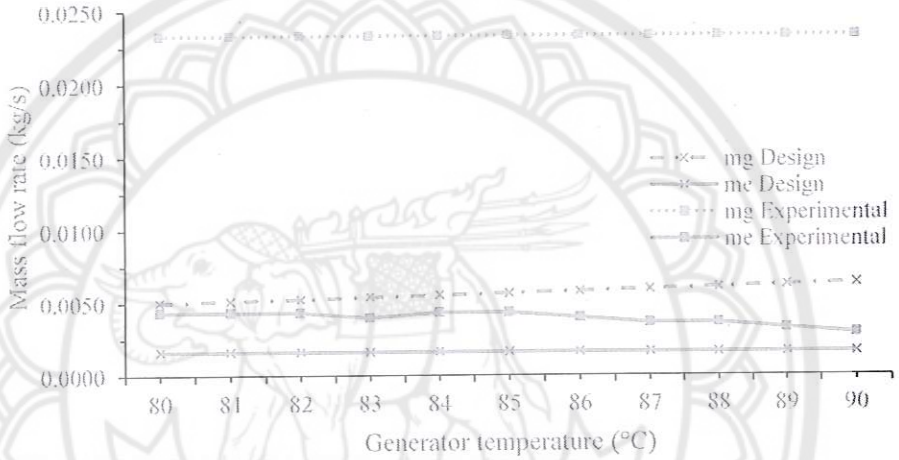

Figure 44 Comparison of the mass flow rate design result and experimental result with the generator temperature

The results of experimental practice.

The experimental practice of the ejector refrigeration system uses the operating condition and the ejector geometry via the results of simulation program. Ejector geometry is selected and shown by table 4 and the operating condition is operated at 84 °C of the generator temperature and at 8 °C for the evaporator temperature. The experiment was tested during 09.00 AM to 16.00 PM at Naresuan University, Thailand.

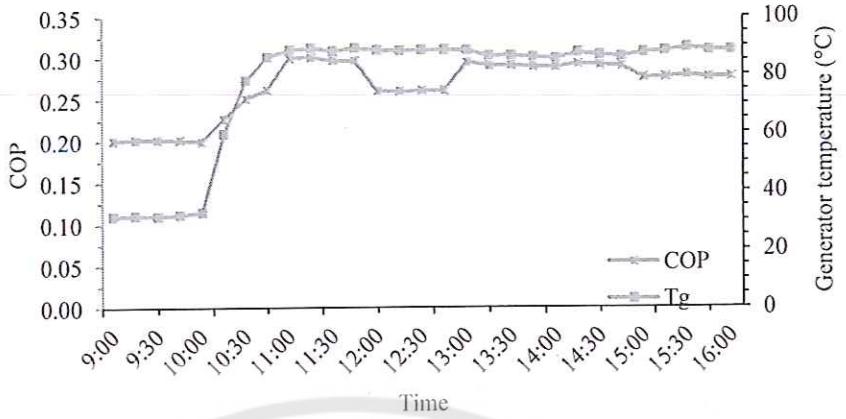

Figure 45 The relationship between COP and the generator temperature

The Figure 45 shows relationship between the COP, the generator temperature plotted with time. The average COP obtained is 0.265 and the refrigeration system performance yields the highest COP of 0.301 at 11.15 am, and COP is reduced to be 0.277 at 16.00 pm. The figure 46 shows the result of the evaporator temperature that decreases to 9.56 °C at 11:45 AM.

The change of COP can be explained as the change in the evaporator temperature. COP is higher in the first period as there is a higher evaporator temperature and COP decreases as there is a lower evaporator temperature at longer time. Furthermore, the results show that the condenser temperature significantly affects COP as well. That is, as condenser temperature decreases, COP increases.

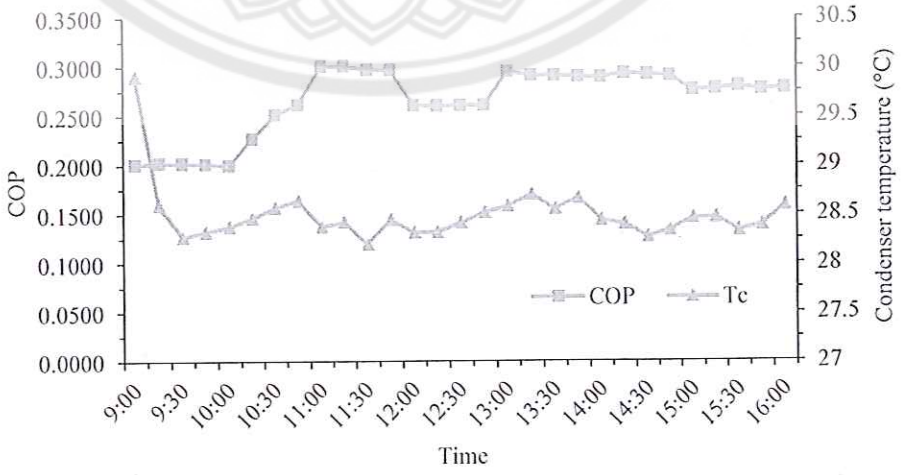

Figure 46 The relationship between COP and condenser temperature

The Figure 47 shows the relationship among the temperature of the condenser evaporator and cold water. The temperature of evaporator and cold water have similar trend, when the system begins, the temperature is reduced from 28 ℃ to 9 ℃ and with constancy, while the condenser temperature slightly increases in the afternoon according to the temperature of higher ambient temperature. Corresponding with Yapici, et al. [44], an increase in the condenser temperature causes the optimum area ratio and COP to decrease when the energies of primary and secondary flows are kept constant. Since the same amount of vapor cannot be compressed to a high condenser pressure, mass flow ratio and, hence, COP will be decreased.

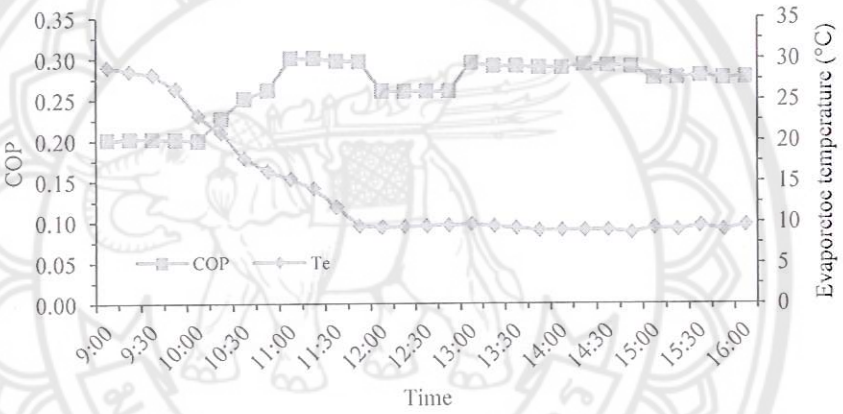

Figure 47 The relationship between the COP and the evaporator temperature

Figure 48 shows the relationship between the COP, the primary fluid and the secondary fluid mass flow rate, and the fixed primary fluid mass flow rate in order to study of effects of the secondary mass flow rate. When the mass flow of the secondary fluid is increased, it is found that the entrainment and COP are increased, but when secondary fluid mass flow rate decreases, it leads to the reduction in the entrainment and the COP due to the fact that an increase or a decrease in the mass flow of the secondary fluid that is put to be mixed with the primary effect has a direct effect to the efficiency of the system.

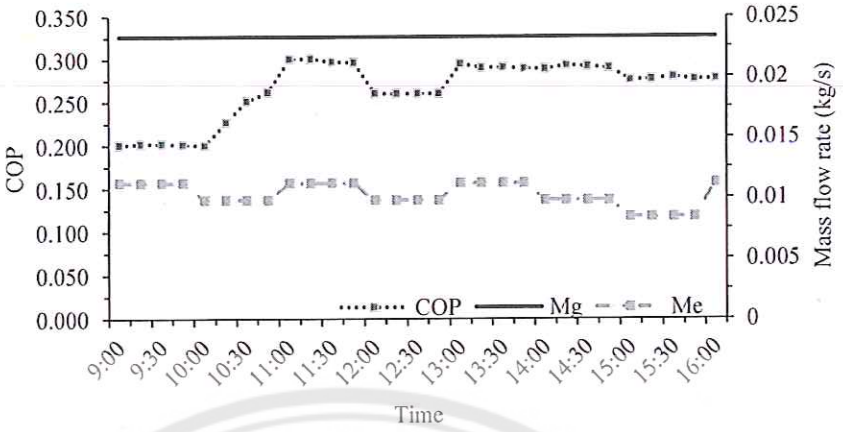

Figure 48 The relationship between the performance and the mass flow rate

The Figure 49 shows the relationship among the temperature of condenser evaporator and the chilled water. The temperature of evaporator and chilled water in cold thermal storage tank have similar trend. When the system begins, the temperature is reduced from 28 ℃ to 10 ℃ and with constancy, while the condenser temperature slightly increases in the afternoon according to the temperature of higher ambient temperature. Corresponding with Yapici, et al. [44], an increase in the condenser temperature causes the optimum area ratio and COP to decrease when the energies of primary and secondary flows are kept constant. Since the same amount of vapor cannot be compressed to high condenser pressure, mass flow ratio and, hence, COP will be decreased.

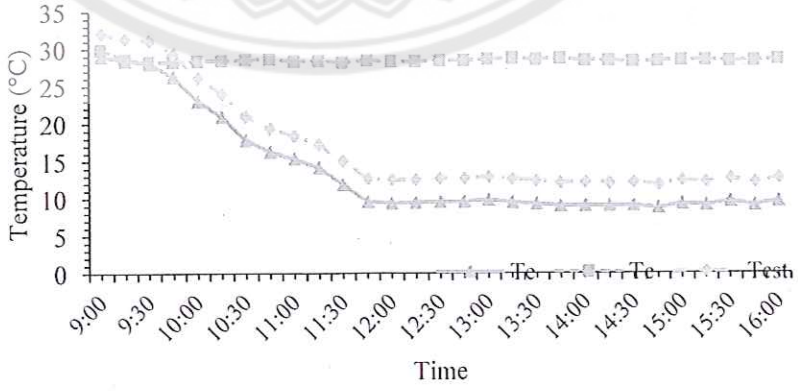

Figure 49 Temperature of condenser, evaporator and cold water in storage tank

Figure 50 shows the relationship of the COP, the condenser and the ambient temperature plotted with time. The average COP obtained is 0.265 and the refrigeration system performance yields the highest COP of 0.301 at 11.15 AM and COP reduces to be 0.277 at 16.00 PM. The change in COP can be explained as the change in the condenser temperature. COP is higher in the first period as there is a higher condenser temperature and COP decreases as there is a lower condenser temperature at longer time. This results is given as same as Pollerberg, C., et al. [45] and Yen, et al. [46] Furthermore, the results show that the condenser temperature significantly affects COP as well. That is, as condenser temperature decreases, COP will increase, thus this results is similar to Petrenko, et al. [47] and Pollerberg, C., et al. [45]

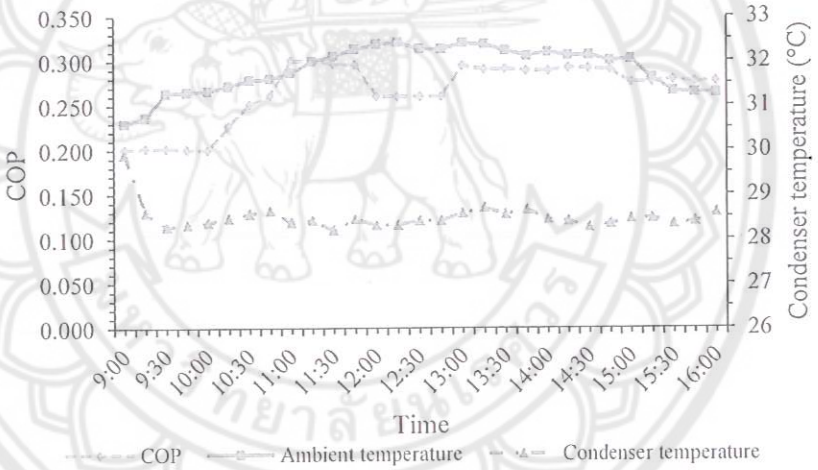

Figure 50 The COP of ejector refrigeration system, ambient temperature and condenser temperature at the various times

Economic Analysis

To evaluate the economics of the prototype and an assessment to determine the economic value for the investment decision in solar cooling system. The economic evaluation of the prototype consists of Payback Period (PB), Internal Rate of Return (IRR), and Net Present Value (NPV) are analyzed.

Table 7 shows the details of the costs that are actually incurred in establishing a system of this research. It was found that the price of the most expensive plate heat exchanger is up to 22%.

Table 7 The Capital cost structure of solar ejector cooling system

list	Cost (Baht)
Ejector	15,000
Plate heat exchanger	35,096
Storage system	3,060
Insulation	1,140
Pumping	13,898
Piping	31,638
Cooling system	12,188
Ejector	15,000
Plate heat exchanger	35,096
Storage system	3,060
Insulation	1,140
Pumping	13,898
Piping	31,638
Cooling system	12,188
Auxiliary heater	5,785
Structure	2,576
Instrument	15,725
Control	8,052
Reference (R141b)	4,000
Installation	10,000
Total	158,158

Figure 51 shows the ratio of the equipment prices. It is found that the most expensive plate heat exchanger was 22 %, Followed by the piping system, which is accounted for 20%, and insulation accounted in the lowest prices at 1 %.

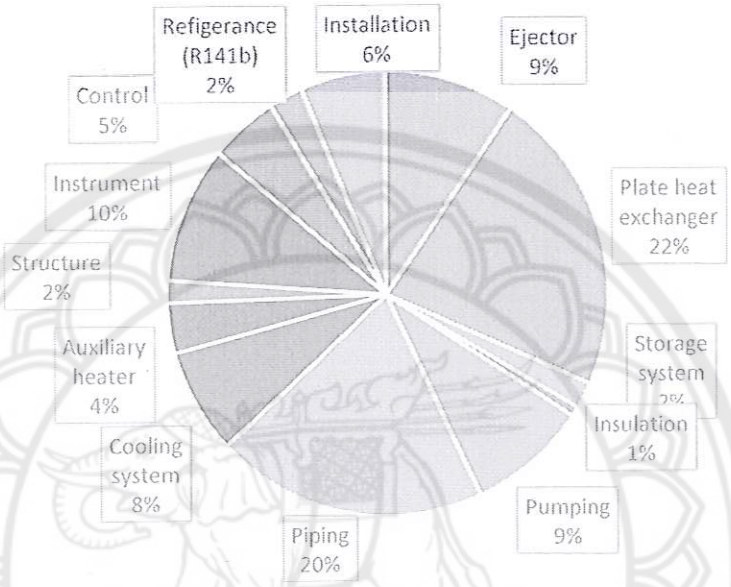

Figure 51 the ratio of equipment prices

Variation is used to calculate the economics. Investment cost was 158,158 baht, maintenance cost of about 3 % of Investment cost was 4,745 baht, savage value 5 % of Investment cost was 7,908 baht,[48] operation day was 300 days, the discount rate was 8.75 %, [49] the electricity cost was 4 Baht, [48] and Electricity saving was 25,200 as it is shown in table 8

Table 8 The variables used to calculate the economics.

Variables	Value
Investment Cost (Baht)	158,158
Maintenance cost 3 % of Investment cost (Baht)	4,745
Savage value 5 % of Investment cost (Baht)	7,908
Life time (year)	15

Table 8 (cont.)

Variables	Value
Operation time (hour/day)	6
Operation day (day/year)	300
loaning interest rate 8.75 %	8.75
Electricity cost (Baht/kWh)	4
Electricity saving (Baht/kWh)	25,200

Table 9 shows the economic analysis results, payback period (PB), internal rate of retune (IRR), Net present value (NPV)

Table 9 The result of solar ejector cooling system economic analysis

Year	Variables	Cost	Electricity saving	Time t Calculation
0	Investment		158,158	-158,158
1	Operation and maintenance	4,745	25,200	22,189
2	Operation and maintenance	4,745	25,200	19,537
3	Operation and maintenance	4,745	25,200	17,203
4	Operation and maintenance	4,745	25,200	15,147
5	Operation and maintenance	4,745	25,200	13,337
6	Operation and maintenance	4,745	25,200	11,743
7	Operation and maintenance	4,745	25,200	10,340
8	Operation and maintenance	4,745	25,200	9,104
9	Operation and maintenance	4,745	25,200	8,016
10	Operation and maintenance	4,745	25,200	7,058

Table 9 (cont.)

Year	Variables	Cost	Electricity saving	Time t Calculation
11	Operation and maintenance	4,745	25,200	6,215
12	Operation and maintenance	4,745	25,200	5,472
13	Operation and maintenance	4,745	25,200	4,818
14	Operation and maintenance	4,745	25,200	4,243
15	Operation and maintenance	4,745	25,200	3,736
Summary		71,171	378,000	(0)
Total cost				158,158
loaning interest rate				8.7%
Payback Period				7.75
IRR				13.57%
NPV				60,872.63

The economics analysis of solar ejector cooling system are invested in the investment cost of 158,158 baht. When calculating, the payback period was 7.75 years or 7 years and 9 months. The return value on a net present value (NPV) was 60,872.63 baht of lifetime of the system throughout a period of 15 years, and internal rate of return (IRR) is 13.57%.

CHAPTER V

CONCLUSION AND RECOMMENDATION

Conclusion

In this study, the lumped method combining with dynamic model for performance prediction of solar ejector refrigeration system to provide air conditioning to residential sectors was investigated. The results from the mathematical simulation have demonstrated that the solar ejector refrigeration system can be designed to meet the cooling requirements of air conditioning for residential sectors. The following conclusions are obtained:

1. For the studied case, the condenser temperature influences more on the performance of the system than on the generator temperature.

2. From 9:00 to 16:00, on typical clear sky days, an average COP of the system is 0.265, in most of the daytime it remains between 0.300 – 0.290, except at 16:00, when it drops as low as 0.277.

3. The system requires the evacuated tube solar collector with the size of 10 m^2, the thermal storage tank with the volume capacity of 0.33 m^3, and the cold thermal storage tank with the volume capacity of 2.3 m^3 in order for the air conditioning that has 12000 Btu spec to work for 6 hours

4. For the studied case, the economics analysis showed that it is a worthy investment. The Payback Period is in 7.73 years. The return value on a Net Present Value (NPV) was 60,872.62 baht, Internal Rate of Return (IRR) is 13.57%.

The ejector is fabricated and equipped to the steam ejector refrigeration system as it is driven by solar collector. The testing on the clear sky day; the evacuated tube is the type of solar collector that is used to preheat the working fluid before putting it into the storage and to raise the temperature up to 84 °C. The results of the experimental practice showed that the solar ejector refrigeration system has the COP of 0.265.

Recommendation

The vacuum is important to operate the ejector refrigeration system. Thus, the manufacture of each component should be considered.

The cooling for the condenser is important due to the fact that if the back pressure is higher than the critical pressure, the system will be stopped.

REFERENCES

REFERENCES

[1] Henning, H.M. (2007). **Solar Air-Conditioning and refrigeration, TASK 38 of the IEA solar heating and cooling programme.** Retrieved May 10, 2011, from http://lmora.free.fr/task38/pdf/matin/Henning.pdf

[2] Chunnanond, K. and Aphornratana, S. (2004). Ejectors: Applications in refrigeration technology. **Renewable and Sustainable Energy Reviews,** 8, 129-155.

[3] Sun, D. W. and Eames, I. W. (1996). Performance characteristics of HCFC-123 ejector refrigeration cycles. **International Journal of Energy Research,** 20, 871–85.

[4] Pridasawas, W. (2006). **Solar-driven refrigeration system with focus on the ejector cycle.** Doctoral dissertation, Ph.D., School of Industrial Engineering and Management, royal Institute of Technology, KTH. Stockholm.

[5] Abdulateef, J. M., Sopian, K., Alghoul, M. A. and Sulaiman, M. Y. (2009). Review on solar-driven ejector refrigeration technologies. **Renewable and Sustainable Energy Reviews,** 13, 1338-1349.

[6] Keenan, J. H., Neumann, E. P. and Lustweek, F. (1950). An investigation of ejector design by analysis and experiment. **Journal of Applied Mechanics,** 1, 299-309.

[7] Chang, Y. J. and Chen, Y. M. (2000). Enhancement of a steam-jet refrigerator using a novel application of the Petal Nozzle. **Experimental Thermal and Fluid Science,** 22, 203-211.

[8] Riffat, S. B. and Holt, A. (1998). A novel heat pipe/ejector cooler. **Applied Thermal Engineering,** 18(3-4), 93-101.

[9] Dincer, I. and Rosen, M.A. (2011). **Thermal energy storage systems and applications** (2rd ed.). New York. Wiley.

[10] Sukhatme, S.P. and Nayak, J.K. (2008). **Solar energy principles of thermal collection and storage** (3rd ed.). New Delhi.: Tata Mcgraw-Hill.

[11] Garg, H.P., Mullick, S.C. and Bhargava, A.K. (1985). **Solar thermal energy storage.** Netherlands: D.Reidel.

[13] Vaivudh, S. (2006). **System design of high thermal energy storage for solar thermal power plant.** Doctoral dissertation, Ph.D., Naresuan University, Pitsanulok.

[14] Chidambarama, L.A., Ramanab, A.S., Kamaraja, G. and Velrajc, R. (2011). Review of solar cooling methods and thermal storage options. **Renewable and Sustainable Energy Reviews**, 15, 3220–3228

[15] Fang, G., Wu, S. and Liu, X. (2010). Experimental study on cool storage air-conditioning system with spherical capsules packed bed. **Energy and Buildings,** 42, 1056–1062.

[16] Wildin, M.W. and Truman, C.R. (1989). Performance of stratified vertical cylindrical thermal storage tanks, part I: Scale model tank. **ASHRAE Technical Data Bulletin**, 5(3), 5-15.

[17] Duffie, J. A. and Beckman, W.A. (1991). **Solar engineering of thermal processes**. New York: Wiley.

[18] Kalogirou, S.A. (2004). Solar thermal collectors and applications. **Progress in Energy and Combustion Science,** 30, 231–295

[19] Brienza, B. M., Gandy J. B. and Lackenbach, L. (Eds.). (1983). **Heat exchanger design handbook**. N.P.: Hemisphere Publishing.

[20] Xiao-Hong Han, Li-Qi Cui, Shao-Jie Chen, Guang-Ming Chen and Qin Wang. (2010). A numerical and experimental study of chevron, corrugated-plate heat exchangers. **International Communications in Heat and Mass Transfer,** 37, 1008–1014.

[21] Rafferty, K. D. and Culver, G. (n.d.). **HEAT EXCHANGERS**. N.P.: n.p.

[22] Shah, R.K., Heat exchangers W.M. Rohsenow, J.P. Hartnett and Y.I. Cho (Eds.), (1998). **Handbook of heat transfer.** New York: McGraw-Hill.

[23] Holman, J.P. (2002). **Heat transfer** (9th ed.). New York: McGraw-Hill.

[24] Gut, J.A.W. and Pinto, J. M. (2004). Optimal configuration design for plate heat exchangers. **International Journal of Heat and Mass Transfer,** 47, 4833–4848

[25] Huang, B. J., Chang, J. M., Wang, C. P. and Petrenko, V.A. (1999). A 1-D analysis of ejector performance. **International Journal of Refrigeration**, 22, 354–364.

[26] Huang, B. J. and Chang, J. M. (1999). Empirical correlation for ejector design. **International Journal of Refrigeration**, 22, 379–388.

[27] Yapıcı, R., Ersoy, H. K., Aktoprakoglu, A., Halkacı, H. S. and Yigit, O. (2008). Experimental determination of the optimum performance of ejector refrigeration system depending on ejector area ratio. **International Journal of Refrigeration**, 31, 1183–1189.

[28] Selvaraju, A., Mani, A. (2004). Analysis of a vapour ejector refrigeration system with environment friendly refrigerant. **International Journal of Thermal Science**, 43, 915–921.

[29] Guo, J., Shen H. G. (2009). Modeling solar-driven ejector refrigeration system offering air conditioning for office buildings. **Energy and Buildings**, 41, 175–181.

[30] Pridasawas, W. and Lundqvist P. (2007). A year-round dynamic simulation of a solar-driven ejector refrigeration system with iso-butane as a refrigerant. **International Journal of Refrigeration**, 30, 840 -850.

[31] Aphornratana, S., Eames, I. W. (1997). A small capacity steam-ejector refrigerator: experimental investigation of a system using ejector with movable primary nozzle. **International Journal of Refrigeration,** 20(5), 352–358.

[32] Alexis G. K., Katsanis J. S. (2004). Performance characteristics of a methanol ejector refrigeration unit. **Energy Conversion and Management,** 45, 2729–2744.

[33] Zhu, Y., Li, Y. (2009). Novel ejector model for performance evaluation on both dry and wet vapors ejectors. **International Journal of Refrigeration**, 32, 21–31.

[34] Sun, D. W. (1996). VARIABLE GEOMETRY EJECTORS AND THEIR APPLICATIONS IN EJECTOR REFRIGERATION SYSTEMS. **Energy**, 21(10), 919-929.

[35] Sun, D. W. (1999). Comparative study of the performance of an ejector refrigeration cycle operating with various refrigerants. **Energy Conversion & Management**, 40, 873-884.

[36] Huang, B. J., Chang, J. M., Petrenko, V. A. and Zhuk, K. B. (1998). A SOLAR EJECTOR COOLING SYSTEM USING REFRIGERANT R141b. **Solar Energy**, 64(4–6), 223–226.

[37] Huang B. J., Petrenko V. A., Samofatov I. Y. and Shchetinina N. A. (2001). Collector Selection for Solar Ejector Cooling System. **Solar Energy**, 71(4), 269–274.

[38] Boumaraf, L. and Lallemand, A. (2009). Modeling of an ejector refrigerating system operating in dimensioning and off-dimensioning conditions with the working fluids R142b and R600a. **Applied Thermal Engineering**, 29, 265–274.

[39] Alexis, G. K. and Karayiannis, E. K. (2005). A solar ejector cooling system using refrigerant R134a in the Athens area. **Renewable Energy,** 30, 1457–1469.

[40] Yapıcı, R. (2008). Experimental investigation of performance of vapor ejector refrigeration system using refrigerant R123. **Energy Conversion and Management**, 49, 953–961.

[41] Dessouk, H. E., Ettouney, H., Alatiqi, I. and Nuwaibit, G. A. (2002). Evaluation of steam jet ejectors. **Chemical Engineering and Processing,** 41, 551–561.

[42] Ouzzane, M. and Aidoun, Z. (2003). Model development and numerical procedure for detailed ejector analysis and design. **Applied Thermal Engineering**, 23, 2337–2351.

[43] Yongprayun, S., Ketjoy, N. and Rakwichian, W. (2007). Life Cycle Cost Analysis of Solar Absorption Cooling System. In **5th Conference on Energy Network of Thailand.** Phitsanulok Thailand: Faculty of Science, School of Renewable Energy Technology, Faculty of Engineering, Naresuan University, Phitsanulok, Thailand.

[44] Yapici, R. and Ersoy, H K. (2005). Performance characteristics of the ejector refrigeration system based on the constant area ejector flow model. **Energy Conversion and Management**, 46, 3117-3135.

[45] Pollerberg, C., Heinzel, A. and Weidner, E. (2009). Model of solar driven steam jet ejector chiller and investigation of its dynamic operational behavior. **Solar Energy,** 83, 732-742.

[46] Yen, R H, Huang, B J, Chen, C Y, Shiu, T Y, Cheng, C W, Chen, S S and Shestopalov K. (2013). Performance optimization for a variable throat ejector in a solar refrigeration system. **International Journal of Refrigeration,** 36, 1512-1520.

[47] Petrenko, V.O, Huang, B.J and Shestopalov, K.O. (2011). Innovative solar and waste heat driven ejector air conditioner and chiller. In 2nd **International conference on environmental science and technology IPCBEE** (vol.6). Singapore: International Proceedings of Chemical, Biological and Environmental Engineering.

[48] Department of Alternative Energy Development and Efficiency, Ministry of Energy. (2009). **Final report, study potential production and use of solar cooling systems.** Thailand: Department of Alternative Energy Development and Efficiency, Ministry of Energy.

[49] Bank of Thailand. (n.d.). **Loan Rates of Commercial Banks as of 19 May** Retrieved May 19, 2015, from https://www.bot.or.th/thai/statistics/ _layouts/ application/interest_rate/in_rate.aspx

[50] National Institute of Standards and Technology. (n.d.). **Thermophysical Properties of Fluid Systems.** Retrieved May 15, 2014, from http://webbook.nist.gov/chemistry/fluid/

APPENDIX

APPENDIX A SOURCE CODE PROGRAM AND FUNCTION OF MATHEMATIC DESIGNING MODEL

Parameters Input program

```
clear all;
G = 1.135;          % gas specific heat ratio
Mw=116.95;          % Molecular Weight
Pg=0.465;           % MPa
Pcx=0.087;          % Mpa
Pe=0.040;           % MPa
Tg=357;             % k
Tcx=301;            % k
Te=281;             % k
EN=0.85;            % Nozzle efficiency
ES=0.85;            % Suction efficiency
ED=0.85;            % Diffuser efficiency
R=8314.47/Mw;       % Universal gas constant,J/(kg-mol.k)
dg=0.88;            % The coefficient of primary flow
Cp=1.16;            % R141b Speccific heat capacity ,kJ/kg.k
Cpw=4.186;          % Water Speccific heat capacity ,kJ/kg.k

%//////////////////////////

para{1}=G;
para{2}=Mw;
para{3}=Pg;
para{4}=Pcx;
para{5}=Pe;
para{6}=Tg;
para{7}=Tcx;
para{8}=Te;
para{9}=EN;
para{10}=ES;
para{11}=ED;
para{12}=R;
para{13}=dg;
para{14}=Cp;
para{15}=Cpw;
```

```
%//////////////////////////////
```

```
save parameters para
```

Nozzle throat diameter program

```
clear all;
load parameters;
G=para{1};
Pg=para{3};
EN=para{9};

hg1=337.43;
hg2=340.72;
sg1=1.0366;
sg2=1.0380;
Pg1=0.044157;
Pg2=0.4915;
hg=hg2-(((Pg2-Pg)/(Pg2-Pg1))*(hg2-hg1));
sg=sg2-(((Pg2-Pg)/(Pg2-Pg1))*(sg2-sg1));

Pt=Pg*(1+((G-1)/2))^(-G/(G-1))     % get Pt

Tt1=input('Tempereture at throat 1 => ');
Tt2=input('Tempereture at throat 2 => ');
Pt1=input('Pressure at throat 1 => ');
Pt2=input('Pressure at throat 2 => ');
vt1=input('Volume at throat 1 => ');
vt2=input('Volume at throat 2 => ');
hgt1=input('Enthalpy vapor at throat 1 => ');
hgt2=input('Enthalpy vapor at throat 2 => ');
sgt1=input('Entropy vapor at throat 1 => ');
sgt2=input('Entropy vapor at throat 2 => ');
hft1=input('Enthalpy liquid at throat 1 => ');
hft2=input('Enthalpy liquid at throat 2 => ');
sft1=input('Entropy liquid at throat 1 => ');
sft2=input('Entropy liquid at throat 2 => ');
```

```
% find Entropy and Enthalpy from R141b table property
hft=hft2-(((Pt2-Pt)/(Pt2-Pt1))*(hft2-hft1));
sft=sft2-(((Pt2-Pt)/(Pt2-Pt1))*(sft2-sft1));
hgt=hgt2-(((Pt2-Pt)/(Pt2-Pt1))*(hgt2-hgt1));
sgt=sgt2-(((Pt2-Pt)/(Pt2-Pt1))*(sgt2-sgt1));
Tt=Tt2-(((Pt2-Pt)/(Pt2-Pt1))*(Tt2-Tt1));

x=(sg-sft)/(sgt-sft);
ht_is=hft+(x*(hgt-hft))

Vt=sqrt(2*EN*((hg-ht_is)*1000)); % velocity of the primary flow
ht=hg-(((Vt^2)/2)/1000);

vt=vt2-(((Pt2-Pt)/(Pt2-Pt1))*(vt2-vt1));

Gtx=Vt/vt % kg/m^2.s
```

Nozzle throat diameter program (cont.)

```
clear all;
load parameters;
G=para{1};
Pg=para{3};
EN=para{9};

hg1=337.43;
hg2=340.72;
sg1=1.0366;
sg2=1.0380;
Pg1=0.044157;
Pg2=0.4915;
hg=hg2-(((Pg2-Pg)/(Pg2-Pg1))*(hg2-hg1));
sg=sg2-(((Pg2-Pg)/(Pg2-Pg1))*(sg2-sg1));

Pt=input('Input Delta Pressure at throat => ');
```

```
Tt1=input('Tempereture at throat 1 => ');
Tt2=input('Tempereture at throat 2 => ');
Pt1=input('Pressure at throat 1 => ');
Pt2=input('Pressure at throat 2 => ');
vt1=input('Volume at throat 1 => ');
vt2=input('Volume at throat 2 => ');
hgt1=input('Enthalpy vapor at throat 1 => ');
hgt2=input('Enthalpy vapor at throat 2 => ');
sgt1=input('Entropy vapor at throat 1 => ');
sgt2=input('Entropy vapor at throat 2 => ');
hft1=input('Enthalpy liquid at throat 1 => ');
hft2=input('Enthalpy liquid at throat 2 => ');
sft1=input('Entropy liquid at throat 1 => ');
sft2=input('Entropy liquid at throat 2 => ');

% find Entropy and Enthalpy from R141b table property
hft=hft2-(((Pt2-Pt)/(Pt2-Pt1))*(hft2-hft1));
sft=sft2-(((Pt2-Pt)/(Pt2-Pt1))*(sft2-sft1));
hgt=hgt2-(((Pt2-Pt)/(Pt2-Pt1))*(hgt2-hgt1));
sgt=sgt2-(((Pt2-Pt)/(Pt2-Pt1))*(sgt2-sgt1));
Tt=Tt2-(((Pt2-Pt)/(Pt2-Pt1))*(Tt2-Tt1));

x=(sg-sft)/(sgt-sft);
ht_is=hft+(x*(hgt-hft));
disp(ht_is);

Vt=sqrt(2*EN*((hg-ht_is)*10^3)); % velocity of the primary flow
ht=hg-(((Vt^2)/2)/1000);

vt=vt2-(((Pt2-Pt)/(Pt2-Pt1))*(vt2-vt1));     % Volume of the primary
flow


Gtmax=Vt/vt % kg/m^2.s
```

Throat diameter of the secondary flow program

```
clear all;
load parameters;
G=para{1};
Pe=para{5};
ES=para{10};

he1=286.63;
he2=290.02;
se1=1.0411;
se2=1.0384;
Pe1=0.038053;
Pe2=0.046972;
he=he2-(((Pe2-Pe)/(Pe2-Pe1))*(he2-he1));
se=se2-(((Pe2-Pe)/(Pe2-Pe1))*(se2-se1));

Pey=Pe*(1+((G-1)/2))^(-G/(G-1))     % get Preesure at suction throat


Tey1=input('Tempereture at suction throat 1 => ');
Tey2=input('Tempereture at suction throat 2 => ');
Pey1=input('Pressure at suction throat 1 => ');
Pey2=input('Pressure at suction throat 2 => ');
vey1=input('Volume at suction throat 1 => ');
vey2=input('Volume at suction throat 2 => ');
hgey1=input('Enthalpy vapor at suction throat 1 => ');
hgey2=input('Enthalpy vapor at suction throat 2 => ');
sgey1=input('Entropy vapor at suction throat 1 => ');
sgey2=input('Entropy vapor at suction throat 2 => ');
hfey1=input('Enthalpy liquid at suction throat 1 => ');
hfey2=input('Enthalpy liquid at suction throat 2 => ');
sfey1=input('Entropy liquid at suction throat 1 => ');
sfey2=input('Entropy liquid at suction throat 2 => ');
```

```
% find Entropy and Enthalpy from R141b table property
hfey=hfey2-(((Pey2-Pey)/(Pey2-Pey1))*(hfey2-hfey1));
sfey=sfey2-(((Pey2-Pey)/(Pey2-Pey1))*(sfey2-sfey1));
hgey=hgey2-(((Pey2-Pey)/(Pey2-Pey1))*(hgey2-hgey1));
sgey=sgey2-(((Pey2-Pey)/(Pey2-Pey1))*(sgey2-sgey1));
Tey=Tey2-(((Pey2-Pey)/(Pey2-Pey1))*(Tey2-Tey1));

xe=(se-sfey)/(sgey-sfey);
hey_is=hfey+(xe*(hgey-hfey));
disp(hey_is);

Vey=sqrt(2*ES*((he-hey_is)*1000)); % velocity of the secondary flow
hey=he-(((Vey^2)/2)/1000);

vey=vey2-(((Pey2-Pey)/(Pey2-Pey1))*(vey2-vey1));

Geyx=Vey/vey
```

Throat diameter of the secondary flow program (cont.)

```
load parameters;
G=para{1};
Pe=para{5};
ES=para{10};

he1=286.63;
he2=290.02;
se1=1.0411;
se2=1.0384;
Pe1=0.038053;
Pe2=0.046972;
he=he2-(((Pe2-Pe)/(Pe2-Pe1))*(he2-he1));
se=se2-(((Pe2-Pe)/(Pe2-Pe1))*(se2-se1));

Pey=input('Input Delta Pressure at suction throat => ');     % get
Preesure at suction throat
```

```
Tey1=input('Tempereture at suction throat 1 => ');
Tey2=input('Tempereture at suction throat 2 => ');
Pey1=input('Pressure at suction throat 1 => ');
Pey2=input('Pressure at suction throat 2 => ');
vey1=input('Volume at suction throat 1 => ');
vey2=input('Volume at suction throat 2 => ');
hgey1=input('Enthalpy vapor at suction throat 1 => ');
hgey2=input('Enthalpy vapor at suction throat 2 => ');
sgey1=input('Entropy vapor at suction throat 1 => ');
sgey2=input('Entropy vapor at suction throat 2 => ');
hfey1=input('Enthalpy liquid at suction throat 1 => ');
hfey2=input('Enthalpy liquid at suction throat 2 => ');
sfey1=input('Entropy liquid at suction throat 1 => ');
sfey2=input('Entropy liquid at suction throat 2 => ');

% find Entropy and Enthalpy from R141b table property
hfey=hfey2-(((Pey2-Pey)/(Pey2-Pey1))*(hfey2-hfey1));
sfey=sfey2-(((Pey2-Pey)/(Pey2-Pey1))*(sfey2-sfey1));
hgey=hgey2-(((Pey2-Pey)/(Pey2-Pey1))*(hgey2-hgey1));
sgey=sgey2-(((Pey2-Pey)/(Pey2-Pey1))*(sgey2-sgey1));
Tey=Tey2-(((Pey2-Pey)/(Pey2-Pey1))*(Tey2-Tey1));

xe=(se-sfey)/(sgey-sfey);
hey_is=hfey+(xe*(hgey-hfey));
disp(hey_is);

Vey=sqrt(2*ES*((he-hey_is)*1000)); % velocity of the secondary flow
hey=he-(((Vey^2)/2)/1000);

vey=vey2-(((Pey2-Pey)/(Pey2-Pey1))*(vey2-vey1));    % Volume of the
secondary flow

Geymax=Vey/vey
```

Ejector Geometry program

```
clear all;
load parameters;
G=para{1};
```

```
Pg=para{3}*1000;
Pcx=para{4}*1000;
Pe=para{5}*1000;
Tg=para{6};
Tcx=para{7};
Te=para{8};
EN=para{9};
ES=para{10};
ED=para{11};
R=para{12};
dg=para{13};
Cp=para{14};
Cpw=para{15};

%%%%%%%%%%%%%%%%%%%%%%%%%%%%%%%%%%%%%%%%%%%%%%%%%%%%%%%%%%%%%%%%%%%%%%%
Gt_max=1.8737*10^3;  % kg/m^2.s
Gey_max=163.0101;    % kg/m^2.s
Pey=0.0243*10^3;     % kPa
Vey=126.8748;        % m/s
Tey=270.0072;        % k
Maey=1;

%%%%%%%%%%%%%%%%%%%%%%%%%%%%%%%%%%%%%%%%%%%%%%%%%%%%%%%%%%%%%%%%%%%%%%%
Dt=2.0;             % mm
Dt=Dt/1000;         % m
At=(pi/4)*Dt^2;     % m^2
mg=At*Gt_max;       % kg/s

%%%%%%%%%%%%%%%%%%%%%%%%%%%%%%%%%%%%%%%%%%%%%%%%%%%%%%%%%%%%%%%%%%%%%%%
Dg1=8;                 % mm
Dg1=Dg1/1000;          % m0
Ag1=(pi/4)*Dg1^2;      % m^2

%%%%%%%%%%%%%%%%%%%%%%%%%%%%%%%%%%%%%%%%%%%%%%%%%%%%%%%%%%%%%%%%%%%%%%%
a=1;
a1=(At/Ag1)*(((1+((G-1)/2)*a^2)/((G+1)/2))^((G+1)/((2*(G-1)))));
while    (a-a1)>=0.00001;
         a=a+0.00001;
```

มหาวิทยาลัยนเรศวร

```
        a1=(At/Ag1)*(((1+((G-1)/2)*a^2)/((G+1)/2))^((G+1)/((2*(G-
1)))));
end
Mag1=a1;

%%%%%%%%%%%%%%%%%%%%%%%%%%%%%%%%%%%%%%%%%%%%%%%%%%%%%%%%%%%%%%%%%%%%%%%%%%%%%%%%%%%%%%%%
Pg1=Pg*(1+(((G-1)/(2*EN))*Mag1^2))^(-G/(G-1));


%%%%%%%%%%%%%%%%%%%%%%%%%%%%%%%%%%%%%%%%%%%%%%%%%%%%%%%%%%%%%%%%%%%%%%%%%%%%%%%%%%%%%%%%
Pgy=Pey;
a3=((((Mag1^2)*((G-1)/2))+1)^(G/(G-1)))*(Pg1/Pgy);
Magy=sqrt(((2)/(G-1))*((a3^((G-1)/G))-1));

%%%%%%%%%%%%%%%%%%%%%%%%%%%%%%%%%%%%%%%%%%%%%%%%%%%%%%%%%%%%%%%%%%%%%%%%%%%%%%%%%%%%%%%%
a=(dg/Magy)*((1+(((G-1)/2)*Magy^2))/((G+1)/2))^((G+1)/(2*(G-1)));
b=(1/Mag1)*((1+(((G-1)/2)*Mag1^2))/((G+1)/2))^((G+1)/(2*(G-1)));
Agy=Ag1*(a/b);

%%%%%%%%%%%%%%%%%%%%%%%%%%%%%%%%%%%%%%%%%%%%%%%%%%%%%%%%%%%%%%%%%%%%%%%%%%%%%%%%%%%%%%%%
Tgy=Tg*(1+((G-1)/2)*Magy^2)^(-1);

%%%%%%%%%%%%%%%%%%%%%%%%%%%%%%%%%%%%%%%%%%%%%%%%%%%%%%%%%%%%%%%%%%%%%%%%%%%%%%%%%%%%%%%%
Vgy=(Magy*sqrt(G*R*Tgy));

%%%%%%%%%%%%%%%%%%%%%%%%%%%%%%%%%%%%%%%%%%%%%%%%%%%%%%%%%%%%%%%%%%%%%%%%%%%%%%%%%%%%%%%%
Aey=input('Aey =>');
me=Aey*Gey_max;  % kg/s
mc=mg+me;        % kg/s

A3=Aey+Agy;
D3=sqrt(A3*(4/pi));
AR=A3/At   %Area ratio

%%%%%%%%%%%%%%%%%%%%%%%%%%%%%%%%%%%%%%%%%%%%%%%%%%%%%%%%%%%%%%%%%%%%%%%%%%%%%%%%%%%%%%%%
dm=input('dm =>');  % 0.80>8.3, 0.82<=8.3, 0.84<=6.9
Vm=(dm*((mg*Vgy)+(me*Vey)))/(mg+me);
```

```
%%%%%%%%%%%%%%%%%%%%%%%%%%%%%%%%%%%%%%%%%%%%%%%%%%%%%%%%%%%%%%%%%%%%%%%%
Tm=(((mg*((Cp*Tgy)+(((Vgy/1000)^2)/2))+me*(Cp*Tey)+(((Vey/1000)^2)/2)
)/mc)-((Vm/1000)^2))/Cp;

%%%%%%%%%%%%%%%%%%%%%%%%%%%%%%%%%%%%%%%%%%%%%%%%%%%%%%%%%%%%%%%%%%%%%%%%
Mam=Vm/(sqrt(G*R*Tm));

%%%%%%%%%%%%%%%%%%%%%%%%%%%%%%%%%%%%%%%%%%%%%%%%%%%%%%%%%%%%%%%%%%%%%%%%
Pm=Pgy;
P3=Pm*(1+(((2*G)/(G+1))*((Mam^2)-1)));

Ma3=sqrt((1+((G-1)/2)*Mam^2)/((G*Mam^2)-((G-1)/2)));

%%%%%%%%%%%%%%%%%%%%%%%%%%%%%%%%%%%%%%%%%%%%%%%%%%%%%%%%%%%%%%%%%%%%%%%%
Pc=P3*(ED*((G-1)/2)*(Ma3^2)+1)^(G/(G-1))


%%%%%%%%%%%%%%%%%%%%%%%%%%%%%%%%%%%%%%%%%%%%%%%%%%%%%%%%%%%%%%%%%%%%%%%%
OMEGA=me/mg

%%%%%%%%%%%%%%%%%%%%%%%%%% Find Ejector Geometry %%%%%%%%%%%%%%%%%%%%%%%%
Pg_1=0.44157*1000;
Pg_2=0.49915*1000;
Pe1=0.038053*1000;
Pe2=0.046972*1000;
Pc1=0.084108*1000;
Pc2=0.10063*1000;
vg1=0.051173;
vg2=0.045445;
ve1=0.51260;
ve2=0.42136;
vg_c1=0.24486;
vg_c2=0.20711;
vf_c1=0.00081288;
vf_c2=0.00081939;
```

```
vg=vg2-(((Pg_2-Pg)/(Pg_2-Pg_1))*(vg2-vg1));
ve=ve2-(((Pe2-Pe)/(Pe2-Pe1))*(ve2-ve1));
Vg=sqrt(G*R*Tg);
Ve=sqrt(G*R*Te);

Ani=((mg*vg)/Vg);
Asi=((me*ve)/Ve);

Dni=sqrt((Ani*4)/pi);    % Nozzle inlet diameter
Dsi=sqrt((Asi*4)/pi);    % Suction inlet diameter
Dc=2.4*D3;               % Diffuser exit diameter xxz

Lm=5*D3;     % Mixing section Length
Lc=5*D3;     % Constant section Length
Ld=7*D3;     % Diffuser section Length
Lx=1.5*D3;   % Nozzle exit to Mixing section Length
```

Plate heat exchanger sizing program

```
%%%%%%%%%%%%%%%%%% Find Heat load, Q (KW) %%%%%%%%%%%%%%%%%%%%%%%%%%%%
hggen1=337.43;
hggen2=340.72;
hgev1=286.63;
hgev2=290.02;
hfcond1=75.037;
hfcond2=80.843;
vfcond1=0.00081288;
vfcond2=0.00081939;

hggen=hggen2-(((Pg_2-Pg)/(Pg_2-Pg_1))*(hggen2-hggen1));
hgev=hgev2-(((Pe2-Pe)/(Pe2-Pe1))*(hgev2-hgev1));
hfcond=hfcond2-(((Pc2-Pcx)/(Pc2-Pc1))*(hfcond2-hfcond1));
vfcond=vfcond2-(((Pc2-Pcx)/(Pc2-Pc1))*(vfcond2-vfcond1));

hfgen=hfcond+(Pg-Pc)*vfcond;
hcond=(hggen+(OMEGA*hgev))/(1+OMEGA);

Cr=Pc/Pe
Qg=mg*(hggen-hfgen)
Qe=me*(hgev-hfcond)
Qc=mc*(hcond-hfcond)

Wp=mg*vfcond*(Pg-Pc);
COP_ejc=Qe/Qg
COP=Qe/(Qg+Wp)

%%%%%%%%%%%%%%%%%%%%%%%%%%%%%%%%%%%%%%%%%%%%%%%%%%%%%%%%%%%%%%%%%%%%%%%
% Fine Outlet cooling water Temp
mwg=0.49; %kg/s
mwe=0.49;
mwc=0.49;
Twe_i=30;    %c
Twe_o=Twe_i-(Qe/(mwe*Cpw))    % Evaparature Water Temparature outlet

Twc_i=30;
```

```
Twc_o=Twc_i+(Qc/(mwc*Cpw))    % Condenser Water Temparature outlet

Twg_i=94;
Twg_o=Twg_i-(Qg/(mwg*Cpw))    % Genarater Water Temparature outlet
```

Storage tank sizing program

```
clear all;
load parameters;
G=para{1};
Pg=para{3}*1000;
Pcx=para{4}*1000;
Pe=para{5}*1000;
Tg=para{6};
Tcx=para{7};
Te=para{8};
EN=para{9};
ES=para{10};
ED=para{11};
R=para{12};
dg=para{13};
Cp=para{14};
Cpw=para{15};
Qg=11942.49; %3.5 kw = 11942.49 BTU/h
T=6;
Et=Qg*T %BTU
% 1 w = 3412 BTU/h , 1 w = 1 j/s
% 1 kJ = 0.9478 Btu
Eg=Et/0.9478;
Wv=Eg/(Cpw*55)%liter

%%%%%%%%%%%%%%%%%%%%%%%%%%%%%%%%%%%%%%%%%%%%%%%%%%%%%%%%%%%%%%%%%%%%%%%%%%%%%%%
```

Solar collector sizing program

```
clear all;
Gt=585; % w/m2
Ta=35;
Ti=80;
```

```
To=90;
Tm=((Ti+To)/2);
a1=1.58;
a2=0.0057;
Fr=0.77;
FrUl=1.5;
Qg=3.5;
Ecoll=Fr-(a1*((Tm-Ta)/Gt))-(a2*(Gt*((Tm-Ta)/Gt)))^2;
Asc=Qg/(Ecoll*Gt)*1000
```

APPENDIX B TABLE OF SOLAR RADITION

Table 10 Average of solar radiation at School of Renewable Energy Technology, Naresuan Uinversity, Thailand

Time	Solar Radiation
9:00	445.04
9:15	477.34
9:30	533.87
9:45	581.58
10:00	630.54
10:15	680.21
10:30	718.25
10:45	753.23
11:00	795.44
11:15	769.43
11:30	819.87
11:45	848.14
12:00	854.69
12:15	857.30
12:30	853.72
12:45	848.43
13:00	835.88
13:15	819.31
13:30	804.87
13:45	777.53
14:00	755.49
14:15	725.80
14:30	688.54
14:45	649.57
15:00	610.72
15:15	557.83
15:30	505.91
15:45	465.61
16:00	409.63
Average	692.20

APPENDIX C ECONOMIC ANALYSIS

Table 11 Net Present Value

Periods	Cash Outflow or Investment	Cash Inflow	Expected Net Cash Flow	Time t Calculation
0	158,158.3	25,200.00	25,200.00	23,387.47
1	0	25,200.00	25,200.00	21,705.31
2	0	25,200.00	25,200.00	20,144.14
3	0	25,200.00	25,200.00	18,695.26
4	0	25,200.00	25,200.00	17,350.59
5	0	25,200.00	25,200.00	16,102.63
6	0	25,200.00	25,200.00	14,944.44
7	0	25,200.00	25,200.00	13,869.55
8	0	25,200.00	25,200.00	12,871.97
9	0	25,200.00	25,200.00	11,946.14
10	0	25,200.00	25,200.00	11,086.91
11	0	25,200.00	25,200.00	10,289.47
12	0	25,200.00	25,200.00	9,549.40
13	0	25,200.00	25,200.00	8,862.55
14	0	25,200.00	25,200.00	8,225.10
15	0	25,200.00	25,200.00	23,387.47
Discount rate (r)			8.75%	
Net Present Value (NPV)				**60,872.63 Baht**

Table 12 Internal Rate of Return

Periods	Cash Outflow or Investment	Cash Inflow	Expected Net Cash Flow	Time t Calculation
0	158,158.30	0.00	-158,158.30	-158,158.30
1	0.00	25,200.00	25,200.00	22,188.67
2	0.00	25,200.00	25,200.00	19,537.19
3	0.00	25,200.00	25,200.00	17,202.56
4	0.00	25,200.00	25,200.00	15,146.90
5	0.00	25,200.00	25,200.00	13,336.89
6	0.00	25,200.00	25,200.00	11,743.17
7	0.00	25,200.00	25,200.00	10,339.90
8	0.00	25,200.00	25,200.00	9,104.31
9	0.00	25,200.00	25,200.00	8,016.37
10	0.00	25,200.00	25,200.00	7,058.44
11	0.00	25,200.00	25,200.00	6,214.98
12	0.00	25,200.00	25,200.00	5,472.31
13	0.00	25,200.00	25,200.00	4,818.38
14	0.00	25,200.00	25,200.00	4,242.60
15	0.00	25,200.00	25,200.00	3,735.62
Net Present Value (NPV)			0.00	
Internal Rate of Return (r)			13.57%	

APPENDIX D THERMO DYNAMIC TABLE PROPOTIES OF R141b

Table 13 Thermodynamic table properties of R141b (liquid phase data)

Temperature (C)	Pressure (MPa)	Density (kg/m3)	Volume (m3/kg)	Internal Energy (kJ/kg)	Enthalpy (kJ/kg)	Entropy (J/g*K)	Cv (J/g*K)	Cp (J/g*K)	Sound Spd. (m/s)	Joule-Thomson (K/MPa)	Viscosity (uPa*s)	Therm. Cond. (W/m*K)	Surf. Tension (N/m)
-100	0.0000	1462.4000	0.0007	-66.7860	-66.7860	-0.3315	0.8020	1.1521	1345.2000	-0.4633	4675.9000	0.1254	0.0349
-95	0.0000	1453.2000	0.0007	-61.0550	-61.0550	-0.2989	0.7939	1.1407	1320.9000	-0.4672	3895.6000	0.1242	0.0342
-90	0.0000	1444.0000	0.0007	-55.3760	-55.3760	-0.2675	0.7872	1.1310	1297.0000	-0.4703	3290.1000	0.1229	0.0335
-85	0.0001	1434.9000	0.0007	-49.7410	-49.7410	-0.2371	0.7818	1.1230	1273.4000	-0.4726	2812.7000	0.1216	0.0328
-80	0.0001	1425.8000	0.0007	-44.1440	-44.1440	-0.2078	0.7774	1.1164	1250.1000	-0.4741	2431.0000	0.1203	0.0321
-75	0.0002	1416.8000	0.0007	-38.5760	-38.5760	-0.1793	0.7739	1.1110	1227.2000	-0.4750	2121.7000	0.1190	0.0314
-70	0.0003	1407.8000	0.0007	-33.0320	-33.0320	-0.1517	0.7713	1.1067	1204.5000	-0.4752	1868.2000	0.1177	0.0307
-65	0.0005	1398.8000	0.0007	-27.5070	-27.5060	-0.1248	0.7694	1.1035	1182.2000	-0.4748	1658.1000	0.1163	0.0300
-60	0.0007	1389.8000	0.0007	-21.9950	-21.9950	-0.0986	0.7682	1.1013	1160.2000	-0.4737	1482.2000	0.1149	0.0293
-55	0.0011	1380.9000	0.0007	-16.4930	-16.4920	-0.0731	0.7676	1.0998	1138.4000	-0.4721	1333.6000	0.1135	0.0286
-50	0.0015	1371.9000	0.0007	-10.9960	-10.9950	-0.0482	0.7675	1.0992	1117.0000	-0.4699	1206.9000	0.1121	0.0280
-45	0.0022	1362.9000	0.0007	-5.5000	-5.4983	-0.0238	0.7680	1.0993	1095.8000	-0.4671	1097.9000	0.1107	0.0273
-40	0.0031	1354.0000	0.0007	-0.0023	0.0000	0.0000	0.7688	1.1000	1074.8000	-0.4638	1003.5000	0.1093	0.0266
-35	0.0043	1345.0000	0.0007	5.5005	5.5037	0.0234	0.7701	1.1013	1054.1000	-0.4600	921.1300	0.1078	0.0259
-30	0.0058	1336.0000	0.0007	11.0110	11.0160	0.0463	0.7717	1.1033	1033.6000	-0.4556	848.7700	0.1064	0.0253
-25	0.0078	1326.9000	0.0008	16.5330	16.5390	0.0687	0.7737	1.1057	1013.4000	-0.4508	784.7900	0.1049	0.0246
-20	0.0104	1317.9000	0.0008	22.0680	22.0760	0.0908	0.7759	1.1087	993.3000	-0.4454	727.9000	0.1035	0.0239

Table 13 (cont.)

Temperature (C)	Pressure (MPa)	Density (kg/m3)	Volume (m3/kg)	Internal Energy (kJ/kg)	Enthalpy (kJ/kg)	Entropy (J/g*K)	Cv (J/g*K)	Cp (J/g*K)	Sound Spd. (m/s)	Joule-Thomson (K/MPa)	Viscosity (uPa*s)	Therm. Cond. (W/m*K)	Surf. Tension (N/m)
-15	0.0135	1308.8000	0.0008	27.6190	27.6290	0.1125	0.7785	1.1121	973.4500	-0.4395	677.0400	0.1021	0.0233
-10	0.0174	1299.6000	0.0008	33.1870	33.2010	0.1339	0.7813	1.1159	953.7900	-0.4331	631.3400	0.1006	0.0226
-5	0.0223	1290.4000	0.0008	38.7760	38.7930	0.1549	0.7843	1.1202	934.3100	-0.4262	590.0700	0.0992	0.0220
0	0.0281	1281.1000	0.0008	44.3870	44.4090	0.1757	0.7875	1.1249	914.9900	-0.4187	552.6600	0.0977	0.0213
5	0.0351	1271.8000	0.0008	50.0220	50.0490	0.1961	0.7909	1.1300	895.8400	-0.4107	518.6000	0.0963	0.0207
10	0.0435	1262.4000	0.0008	55.6820	55.7160	0.2163	0.7945	1.1354	876.8300	-0.4021	487.4800	0.0949	0.0201
15	0.0534	1253.0000	0.0008	61.3700	61.4120	0.2362	0.7982	1.1412	857.9700	-0.3929	458.9500	0.0935	0.0194
20	0.0650	1243.4000	0.0008	67.0870	67.1390	0.2559	0.8021	1.1474	839.2400	-0.3831	432.7000	0.0920	0.0188
25	0.0786	1233.8000	0.0008	72.8340	72.8980	0.2753	0.8061	1.1539	820.6200	-0.3726	408.4900	0.0906	0.0182
30	0.0942	1224.1000	0.0008	78.6140	78.6910	0.2945	0.8102	1.1607	802.1200	-0.3615	386.1000	0.0893	0.0175
35	0.1123	1214.2000	0.0008	84.4270	84.5200	0.3136	0.8144	1.1679	783.7300	-0.3496	365.3400	0.0879	0.0169
40	0.1329	1204.3000	0.0008	90.2760	90.3870	0.3324	0.8187	1.1754	765.4300	-0.3368	346.0400	0.0865	0.0163
45	0.1564	1194.2000	0.0008	96.1620	96.2920	0.3510	0.8231	1.1833	747.2100	-0.3233	328.0600	0.0852	0.0157
50	0.1829	1184.0000	0.0008	102.0800	102.2400	0.3695	0.8276	1.1916	729.0700	-0.3088	311.2700	0.0838	0.0151
55	0.2127	1173.7000	0.0009	108.0500	108.2300	0.3878	0.8322	1.2002	711.0000	-0.2932	295.5700	0.0825	0.0145
60	0.2462	1163.2000	0.0009	114.0500	114.2600	0.4060	0.8368	1.2091	692.9900	-0.2766	280.8600	0.0812	0.0139
65	0.2835	1152.5000	0.0009	120.1000	120.3400	0.4240	0.8414	1.2185	675.0200	-0.2588	267.0500	0.0799	0.0133
70	0.3250	1141.7000	0.0009	126.1900	126.4700	0.4419	0.8462	1.2283	657.1000	-0.2396	254.0600	0.0786	0.0127
75	0.3709	1130.7000	0.0009	132.3300	132.6500	0.4597	0.8509	1.2386	639.2200	-0.2189	241.8200	0.0773	0.0121
80	0.4216	1119.6000	0.0009	138.5100	138.8900	0.4773	0.8557	1.2493	621.3500	-0.1966	230.2700	0.0761	0.0116

Table 13 (cont.)

Temperature (C)	Pressure (MPa)	Density (kg/m3)	Volume (m3/kg)	Internal Energy (kJ/kg)	Enthalpy (kJ/kg)	Entropy (J/g*K)	Cv (J/g*K)	Cp (J/g*K)	Sound Spd. (m/s)	Joule-Thomson (K/MPa)	Viscosity (uPa*s)	Therm. Cond. (W/m*K)	Surf. Tension (N/m)
85	0.4772	1108.2000	0.0009	144.7400	145.1700	0.4949	0.8606	1.2606	603.5000	-0.1724	219.3600	0.0749	0.0110
90	0.5382	1096.5000	0.0009	151.0300	151.5200	0.5123	0.8655	1.2725	585.6500	-0.1462	209.0200	0.0737	0.0104
95	0.6048	1084.7000	0.0009	157.3700	157.9200	0.5296	0.8704	1.2851	567.7900	-0.1176	199.2200	0.0725	0.0099
100	0.6773	1072.5000	0.0009	163.7600	164.3900	0.5469	0.8754	1.2983	549.9100	-0.0863	189.9100	0.0713	0.0093
105	0.7561	1060.1000	0.0009	170.2100	170.9300	0.5641	0.8804	1.3124	531.9900	-0.0520	181.0500	0.0702	0.0088
110	0.8414	1047.4000	0.0010	176.7300	177.5300	0.5812	0.8854	1.3274	514.0400	-0.0142	172.6000	0.0691	0.0082
115	0.9336	1034.3000	0.0010	183.3000	184.2000	0.5983	0.8905	1.3435	496.0200	0.0277	164.5300	0.0680	0.0077
120	1.0331	1020.9000	0.0010	189.9500	190.9600	0.6154	0.8956	1.3609	477.9200	0.0742	156.8100	0.0669	0.0072
125	1.1401	1007.0000	0.0010	196.6600	197.7900	0.6324	0.9008	1.3797	459.7300	0.1263	149.4100	0.0659	0.0066
130	1.2550	992.7300	0.0010	203.4500	204.7200	0.6494	0.9060	1.4003	441.4200	0.1850	142.2900	0.0649	0.0061
135	1.3782	977.9400	0.0010	210.3300	211.7400	0.6664	0.9114	1.4229	422.9600	0.2515	135.4400	0.0639	0.0056
140	1.5101	962.5900	0.0010	217.2900	218.8600	0.6834	0.9168	1.4481	404.3300	0.3274	128.8200	0.0629	0.0051
145	1.6509	946.6100	0.0011	224.3500	226.0900	0.7004	0.9223	1.4764	385.4900	0.4150	122.4100	0.0620	0.0046
150	1.8013	929.9200	0.0011	231.5100	233.4500	0.7175	0.9279	1.5088	366.3900	0.5171	116.1800	0.0611	0.0042
155	1.9615	912.4100	0.0011	238.7900	240.9400	0.7347	0.9337	1.5462	346.9700	0.6375	110.1100	0.0602	0.0037
160	2.1320	893.9400	0.0011	246.2100	248.5900	0.7520	0.9397	1.5905	327.1800	0.7816	104.1700	0.0593	0.0032
165	2.3134	874.3300	0.0011	253.7700	256.4200	0.7695	0.9460	1.6441	306.9100	0.9570	98.3150	0.0585	0.0028
170	2.5061	853.3400	0.0012	261.5200	264.4600	0.7873	0.9526	1.7110	286.0600	1.1752	92.5220	0.0577	0.0024
175	2.7109	830.6200	0.0012	269.4900	272.7500	0.8053	0.9598	1.7977	264.4700	1.4540	86.7420	0.0570	0.0019
180	2.9284	805.6600	0.0012	277.7200	281.3600	0.8239	0.9677	1.9164	241.9300	1.8227	80.9140	0.0563	0.0015

Table 13 (cont.)

Temperature (C)	Pressure (MPa)	Density (kg/m3)	Volume (m3/kg)	Internal Energy (kJ/kg)	Enthalpy (kJ/kg)	Entropy (J/g*K)	Cv (J/g*K)	Cp (J/g*K)	Sound Spd. (m/s)	Joule-Thomson (K/MPa)	Viscosity (uPa*s)	Therm. Cond. (W/m*K)	Surf. Tension (N/m)
185	3.1595	777.6300	0.0013	286.3300	290.3900	0.8430	0.9766	2.0916	218.1300	2.3334	74.9490	0.0557	0.0012
190	3.4053	745.0500	0.0013	295.4600	300.0300	0.8633	0.9873	2.3823	192.6000	3.0891	68.6970	0.0554	0.0008
195	3.6673	704.8000	0.0014	305.4700	310.6700	0.8853	1.0011	2.9766	164.5300	4.3275	61.8430	0.0557	0.0005
200	3.9479	647.3600	0.0015	317.4100	323.5100	0.9117	1.0225	4.9755	132.1900	6.7751	53.4520	0.0582	0.0002

Table 14 Thermodynamic table properties of R141b (vapor phase data)

Temperature (C)	Pressure (MPa)	Density (kg/m3)	Volume (m3/kg)	Internal Energy (kJ/kg)	Enthalpy (kJ/kg)	Entropy (J/g*K)	Cv (J/g*K)	Cp (J/g*K)	Sound Spd. (m/s)	Joule-Thomson (K/MPa)	Viscosity (uPa*s)	Therm. Cond. (W/m*K)
-100.0000	0.0000	0.0009	1175.2000	207.6600	219.9700	1.3246	0.4728	0.5440	119.0000	775.4800	5.3386	0.0034
-95.0000	0.0000	0.0016	630.9400	210.0500	222.7200	1.2940	0.4829	0.5541	120.5400	649.5000	5.4889	0.0036
-90.0000	0.0000	0.0028	352.9100	212.4900	225.5100	1.2661	0.4928	0.5640	122.0600	548.0500	5.6398	0.0038
-85.0000	0.0001	0.0049	204.9100	214.9700	228.3400	1.2409	0.5025	0.5737	123.5600	465.7800	5.7914	0.0040
-80.0000	0.0001	0.0081	123.1000	217.5000	231.2200	1.2179	0.5120	0.5833	125.0400	398.6100	5.9436	0.0042
-75.0000	0.0002	0.0131	76.2940	220.0700	234.1500	1.1971	0.5214	0.5928	126.5000	343.4100	6.0965	0.0044
-70.0000	0.0003	0.0206	48.6570	222.6800	237.1100	1.1781	0.5307	0.6022	127.9300	297.7600	6.2498	0.0046
-65.0000	0.0005	0.0314	31.8580	225.3300	240.1200	1.1609	0.5398	0.6115	129.3500	259.7800	6.4036	0.0048
-60.0000	0.0007	0.0468	21.3690	228.0300	243.1600	1.1454	0.5490	0.6208	130.7400	228.0000	6.5579	0.0051

Table 14 (cont.)

Temperature (C)	Pressure (MPa)	Density (kg/m3)	Volume (m3/kg)	Internal Energy (kJ/kg)	Enthalpy (kJ/kg)	Entropy (J/g*K)	Cv (J/g*K)	Cp (J/g*K)	Sound Spd. (m/s)	Joule-Thomson (K/MPa)	Viscosity (uPa*s)	Therm. Cond. (W/m*K)
-55.0000	0.0011	0.0682	14.6570	230.7600	246.2400	1.1313	0.5580	0.6301	132.1100	201.2500	6.7124	0.0053
-50.0000	0.0015	0.0974	10.2620	233.5300	249.3600	1.1185	0.5671	0.6394	133.4600	178.6000	6.8673	0.0055
-45.0000	0.0022	0.1366	7.3228	236.3300	252.5100	1.1070	0.5761	0.6488	134.7700	159.3200	7.0223	0.0058
-40.0000	0.0031	0.1880	5.3186	239.1700	255.6900	1.0967	0.5852	0.6583	136.0600	142.8200	7.1775	0.0060
-35.0000	0.0043	0.2547	3.9265	242.0400	258.9000	1.0874	0.5942	0.6678	137.3200	128.6200	7.3328	0.0063
-30.0000	0.0058	0.3398	2.9431	244.9400	262.1300	1.0790	0.6033	0.6774	138.5400	116.3500	7.4881	0.0065
-25.0000	0.0078	0.4470	2.2374	247.8700	265.3900	1.0716	0.6124	0.6872	139.7300	105.6700	7.6434	0.0068
-20.0000	0.0104	0.5803	1.7233	250.8300	268.6800	1.0649	0.6216	0.6971	140.8800	96.3550	7.7986	0.0071
-15.0000	0.0135	0.7442	1.3436	253.8100	271.9800	1.0591	0.6309	0.7072	141.9900	88.1800	7.9536	0.0074
-10.0000	0.0174	0.9437	1.0596	256.8200	275.3100	1.0539	0.6402	0.7174	143.0500	80.9770	8.1085	0.0076
-5.0000	0.0223	1.1841	0.8446	259.8500	278.6500	1.0494	0.6495	0.7278	144.0800	74.6070	8.2632	0.0079
0.0000	0.0281	1.4709	0.6798	262.9100	282.0100	1.0455	0.6589	0.7384	145.0500	68.9510	8.4178	0.0082
5.0000	0.0351	1.8105	0.5523	265.9800	285.3800	1.0422	0.6684	0.7491	145.9700	63.9120	8.5722	0.0086

Table 15 Vapor Phase Data

Temperature (C)	Pressure (MPa)	Density (kg/m3)	Volume (m3/kg)	Internal Energy (kJ/kg)	Enthalpy (kJ/kg)	Entropy (J/g*K)	Cv (J/g*K)	Cp (J/g*K)	Sound Spd. (m/s)	Joule-Thomson (K/MPa)	Viscosity (uPa*s)	Therm. Cond. (W/m*K)
10.0000	0.0435	2.2093	0.4526	269.0800	288.7700	1.0393	0.6779	0.7601	146.8400	59.4090	8.7264	0.0089
15.0000	0.0534	2.6743	0.3739	272.1900	292.1600	1.0370	0.6875	0.7712	147.6500	55.3740	8.8806	0.0092
20.0000	0.0650	3.2128	0.3113	275.3200	295.5600	1.0351	0.6971	0.7826	148.4000	51.7480	9.0347	0.0095
25.0000	0.0786	3.8325	0.2609	278.4700	298.9700	1.0335	0.7068	0.7941	149.0900	48.4830	9.1890	0.0099
30.0000	0.0942	4.5416	0.2202	281.6300	302.3800	1.0324	0.7164	0.8059	149.7200	45.5360	9.3434	0.0102
35.0000	0.1123	5.3487	0.1870	284.8000	305.7900	1.0316	0.7261	0.8179	150.2700	42.8710	9.4981	0.0106
40.0000	0.1329	6.2628	0.1597	287.9800	309.2100	1.0311	0.7358	0.8300	150.7600	40.4590	9.6533	0.0109
45.0000	0.1564	7.2933	0.1371	291.1800	312.6200	1.0310	0.7455	0.8424	151.1700	38.2720	9.8092	0.0113
50.0000	0.1829	8.4504	0.1183	294.3800	316.0200	1.0311	0.7551	0.8551	151.5100	36.2860	9.9660	0.0117
55.0000	0.2127	9.7445	0.1026	297.5900	319.4200	1.0314	0.7648	0.8680	151.7600	34.4820	10.1240	0.0121
60.0000	0.2462	11.1870	0.0894	300.8000	322.8100	1.0320	0.7744	0.8811	151.9300	32.8430	10.2830	0.0125
65.0000	0.2835	12.7890	0.0782	304.0100	326.1800	1.0327	0.7840	0.8946	152.0200	31.3510	10.4440	0.0129
70.0000	0.3250	14.5640	0.0687	307.2300	329.5400	1.0337	0.7936	0.9084	152.0100	29.9950	10.6080	0.0134
75.0000	0.3709	16.5260	0.0605	310.4400	332.8900	1.0348	0.8031	0.9225	151.9100	28.7620	10.7730	0.0138
80.0000	0.4216	18.6880	0.0535	313.6500	336.2100	1.0361	0.8126	0.9371	151.7100	27.6420	10.9420	0.0143
85.0000	0.4772	21.0660	0.0475	316.8500	339.5100	1.0374	0.8220	0.9521	151.4100	26.6250	11.1140	0.0147
90.0000	0.5382	23.6780	0.0422	320.0400	342.7700	1.0389	0.8314	0.9676	151.0100	25.7030	11.2900	0.0152
95.0000	0.6048	26.5420	0.0377	323.2200	346.0100	1.0405	0.8408	0.9838	150.4900	24.8690	11.4710	0.0157
100.0000	0.6773	29.6780	0.0337	326.3900	349.2100	1.0422	0.8501	1.0007	149.8500	24.1170	11.6570	0.0163
105.0000	0.7561	33.1090	0.0302	329.5300	352.3700	1.0439	0.8594	1.0184	149.1000	23.4420	11.8490	0.0168

Table 15 (cont.)

Temperature (C)	Pressure (MPa)	Density (kg/m3)	Volume (m3/kg)	Internal Energy (kJ/kg)	Enthalpy (kJ/kg)	Entropy (J/g*K)	Cv (J/g*K)	Cp (J/g*K)	Sound Spd. (m/s)	Joule-Thomson (K/MPa)	Viscosity (uPa*s)	Therm. Cond. (W/m*K)
110.0000	0.8414	36.8610	0.0271	332.6500	355.4800	1.0457	0.8686	1.0371	148.2100	22.8390	12.0490	0.0174
115.0000	0.9336	40.9620	0.0244	335.7400	358.5300	1.0474	0.8778	1.0570	147.1900	22.3030	12.2560	0.0180
120.0000	1.0331	45.4430	0.0220	338.8000	361.5300	1.0492	0.8871	1.0782	146.0300	21.8330	12.4740	0.0186
125.0000	1.1401	50.3440	0.0199	341.8100	364.4500	1.0510	0.8963	1.1012	144.7200	21.4250	12.7020	0.0193
130.0000	1.2550	55.7060	0.0180	344.7700	367.3000	1.0526	0.9055	1.1262	143.2400	21.0770	12.9430	0.0200
135.0000	1.3782	61.5810	0.0162	347.6800	370.0600	1.0543	0.9148	1.1537	141.6000	20.7890	13.1980	0.0208
140.0000	1.5101	68.0280	0.0147	350.5200	372.7200	1.0558	0.9241	1.1844	139.7700	20.5590	13.4710	0.0216
145.0000	1.6509	75.1190	0.0133	353.2900	375.2600	1.0572	0.9335	1.2191	137.7400	20.3890	13.7650	0.0225
150.0000	1.8013	82.9460	0.0121	355.9500	377.6700	1.0584	0.9430	1.2590	135.5100	20.2790	14.0830	0.0234
155.0000	1.9615	91.6170	0.0109	358.5100	379.9200	1.0593	0.9527	1.3055	133.0400	20.2310	14.4300	0.0245
160.0000	2.1320	101.2800	0.0099	360.9300	381.9800	1.0600	0.9626	1.3612	130.3200	20.2470	14.8130	0.0256
165.0000	2.3134	112.1100	0.0089	363.1900	383.8200	1.0603	0.9728	1.4294	127.3300	20.3310	15.2410	0.0269
170.0000	2.5061	124.3700	0.0080	365.2400	385.3900	1.0602	0.9834	1.5159	124.0400	20.4860	15.7250	0.0283
175.0000	2.7109	138.4100	0.0072	367.0300	386.6200	1.0594	0.9945	1.6299	120.4200	20.7160	16.2830	0.0300
180.0000	2.9284	154.7600	0.0065	368.4800	387.4000	1.0579	1.0063	1.7887	116.4200	21.0210	16.9410	0.0319
185.0000	3.1595	174.2700	0.0057	369.4500	387.5800	1.0552	1.0190	2.0270	112.0000	21.3940	17.7430	0.0343
190.0000	3.4053	198.4300	0.0050	369.7300	386.8900	1.0508	1.0332	2.4287	107.1100	21.8020	18.7660	0.0373
195.0000	3.6673	230.4200	0.0043	368.8200	384.7400	1.0435	1.0498	3.2579	101.6800	22.1330	20.1840	0.0415
200.0000	3.9479	279.7000	0.0036	365.3600	379.4700	1.0300	1.0708	6.0173	95.6680	21.9300	22.5420	0.0493